Appendix A: SPIRE colors vs. galactocentric distance

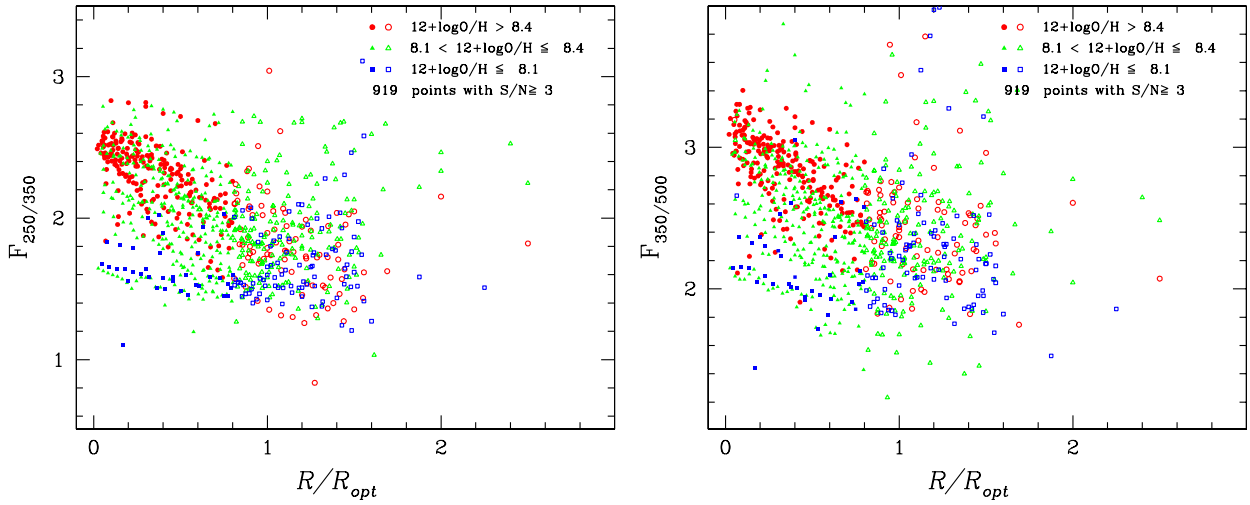

Fig. A.1. SPIRE colors F_{250}/F_{350} (*left panel*) and F_{350}/F_{500} (*right*) vs. galactocentric distance $R_{\rm opt}$. As in Fig. 8, points are coded by their oxygen abundance, with filled symbols corresponding to $R/R_{\rm opt} \leq 0.8$ and open ones to larger radii.

Appendix B: Radial surface brightness profiles with exponential fits

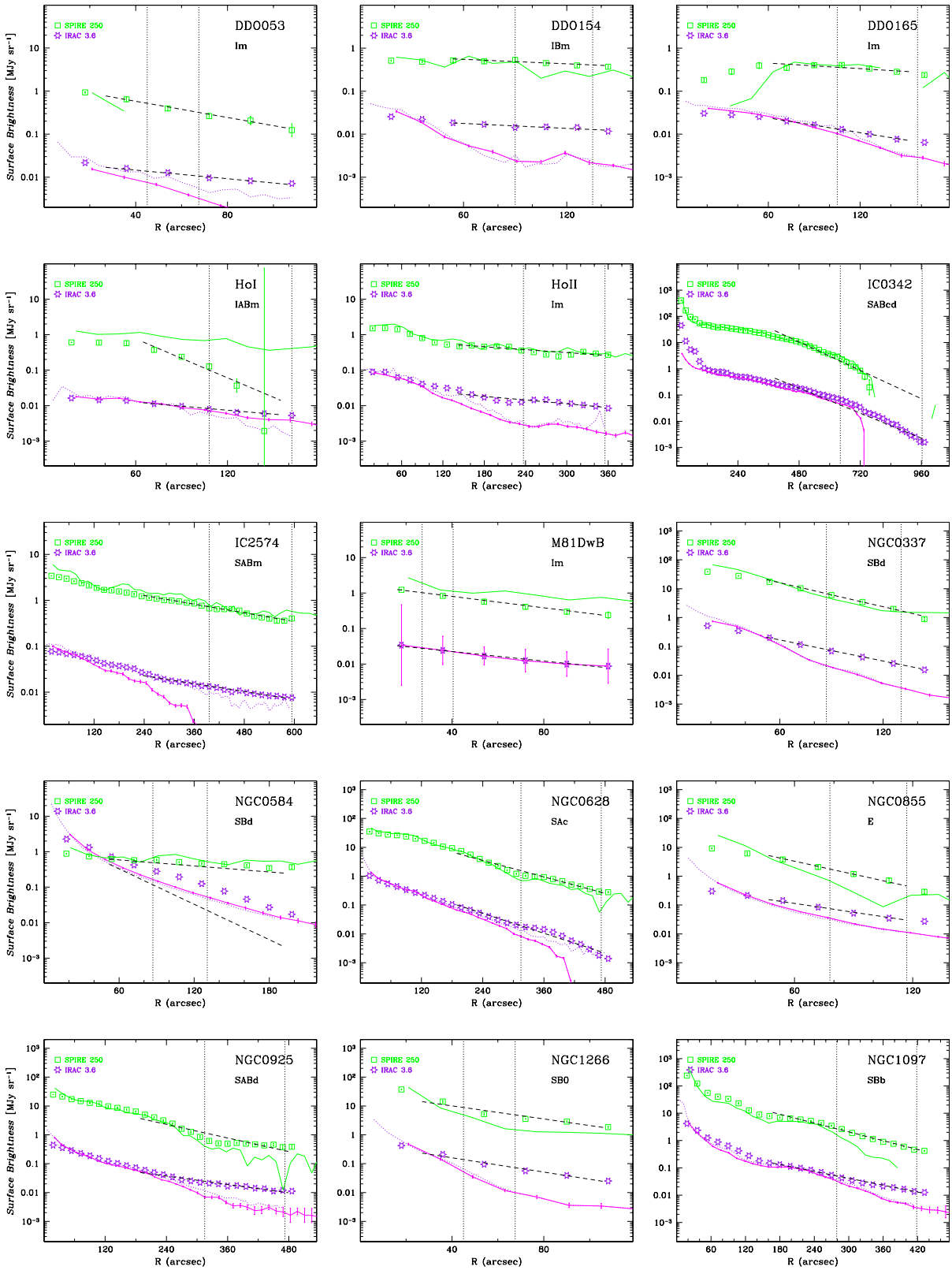

Fig. B.1. Surface brightness profiles at SPIRE 250 μm and IRAC 3.6 μm. The profiles with convolution (see Aniano et al. 2012) are shown by symbols (green) open squares, 250 μm, and ((purple) open stars, 3.6 μm). The Muñoz-Mateos et al. (2009a) IRAC profiles are shown by a dotted curve, and the IRAC and 250 μm profiles extracted without convolution (and with different methods of sky subtraction) are shown by solid curves. The dashed lines indicate the best-fit disk model fitted from 0.6*$R_{\rm opt}$. The vertical dotted lines indicate the optical radius, $R_{\rm opt}$, and 1.5 $R_{\rm opt}$.

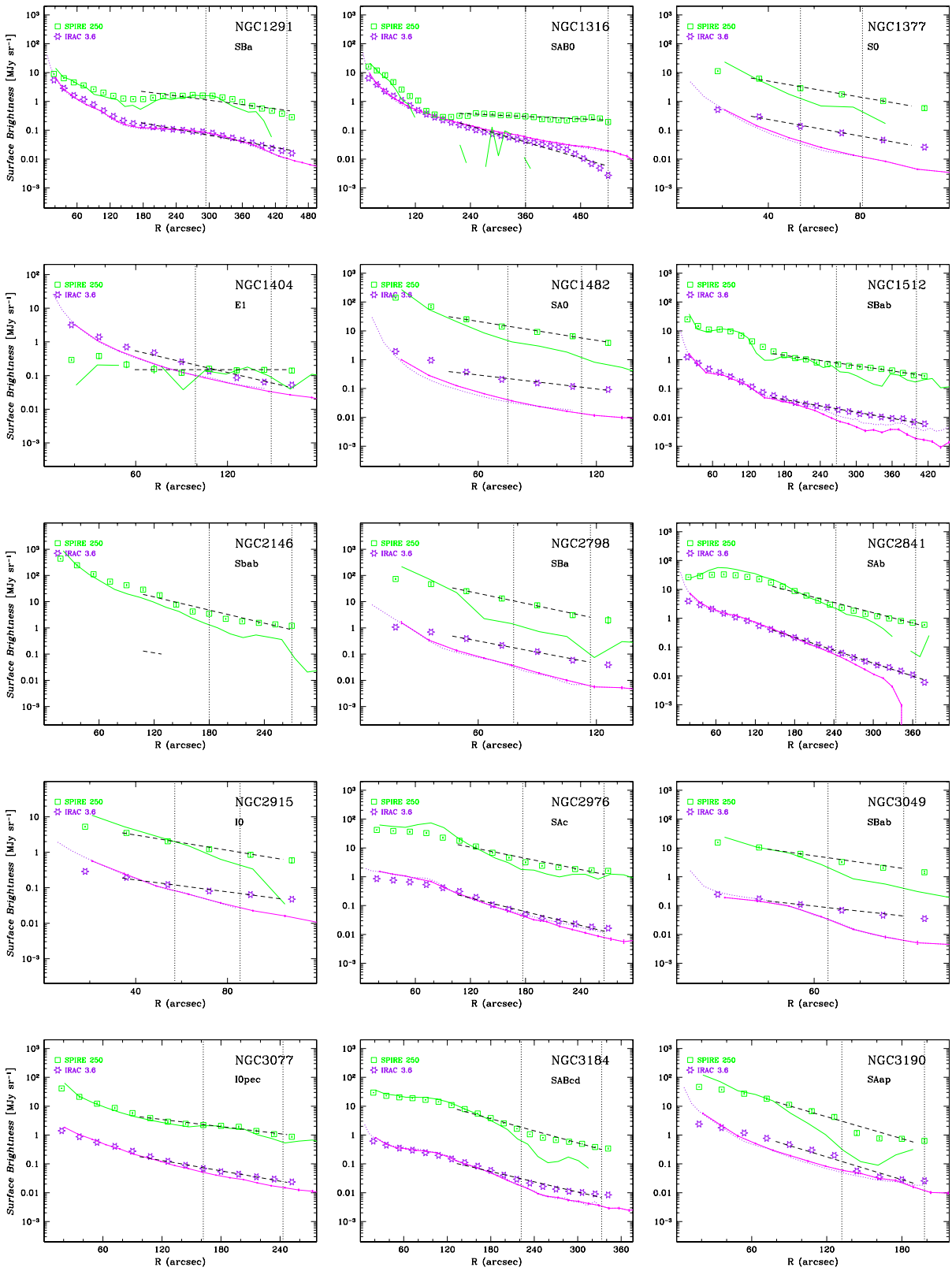

Fig. B.1. continued.

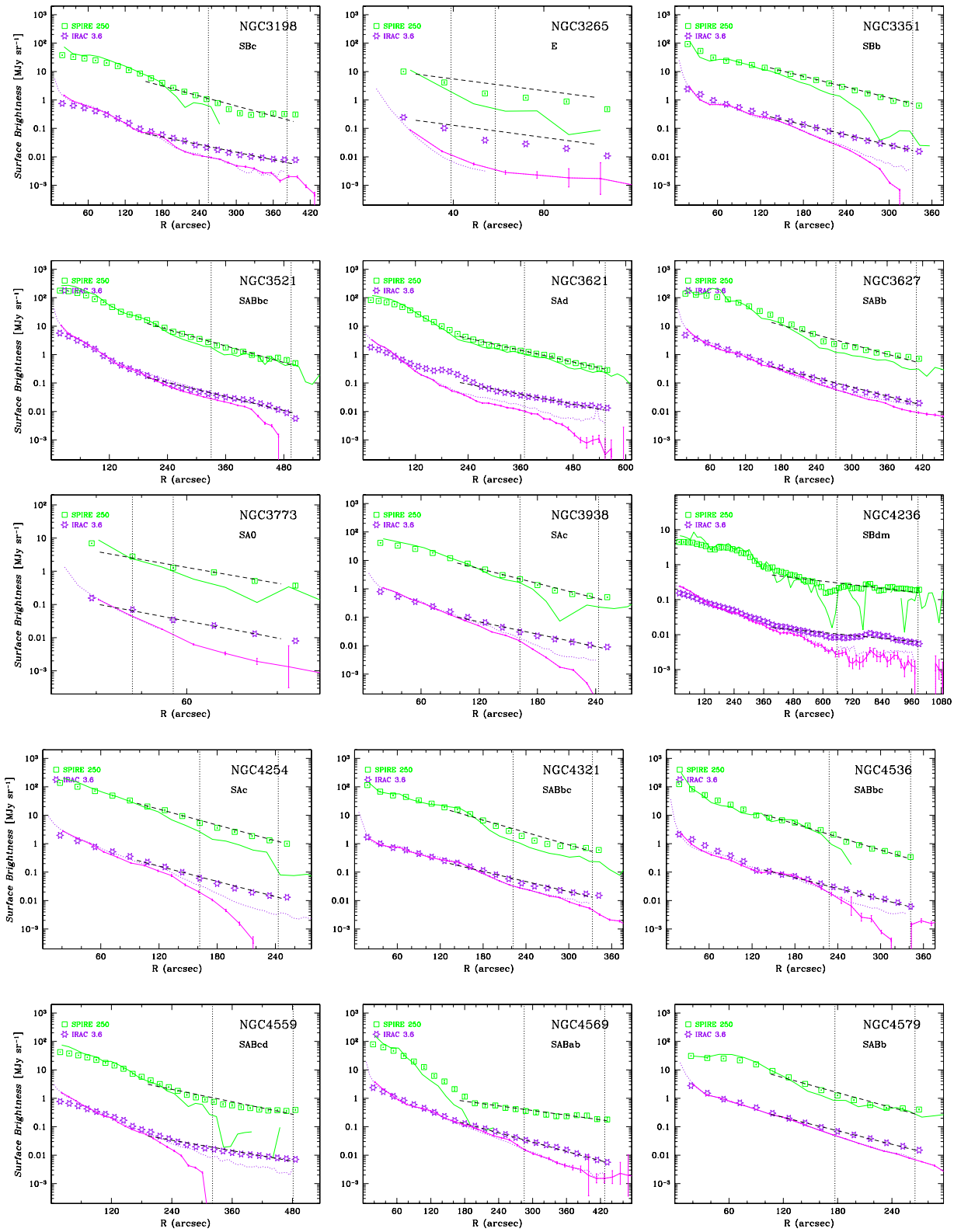

Fig. B.1. continued.

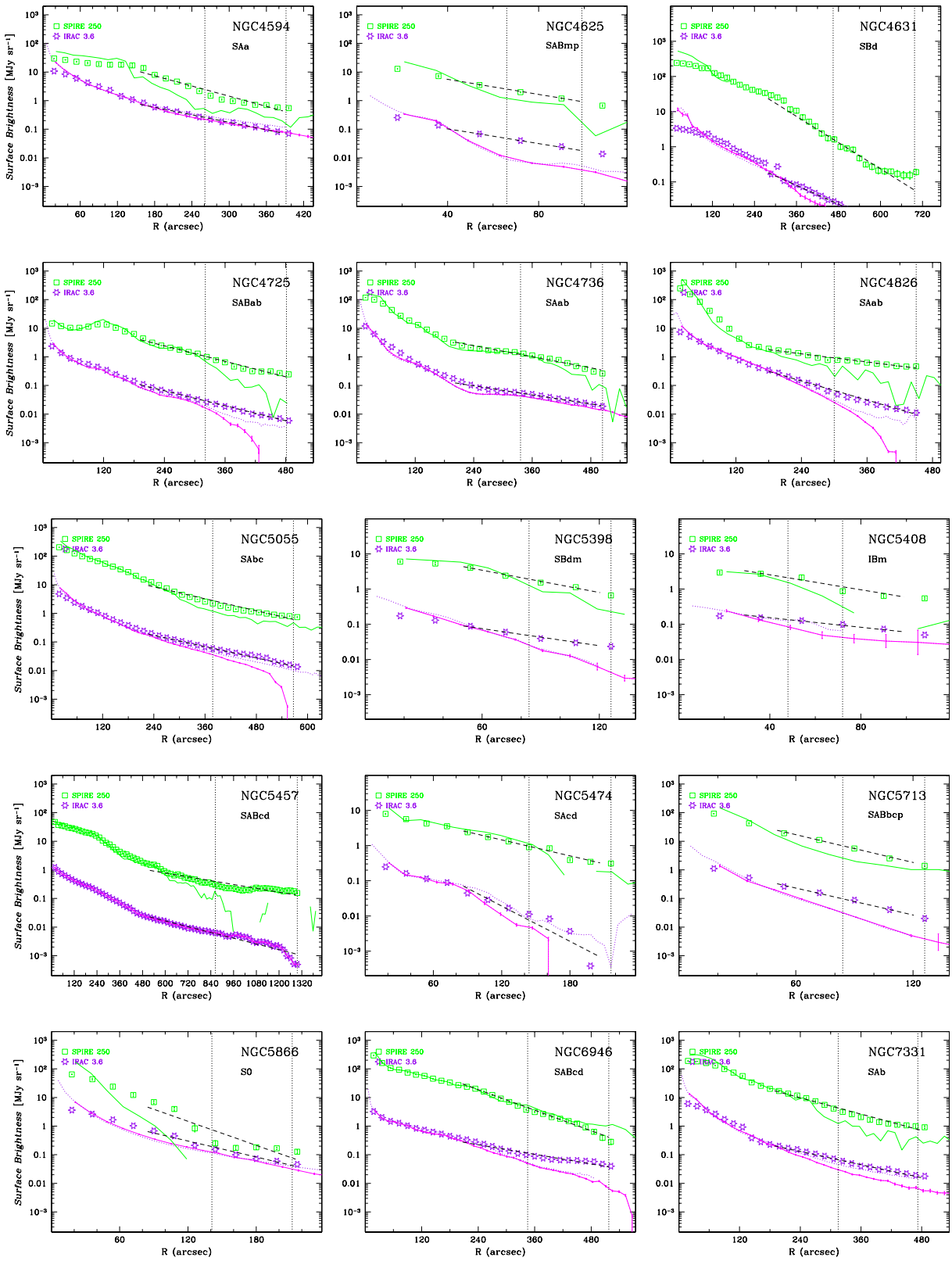

Fig. B.1. continued.

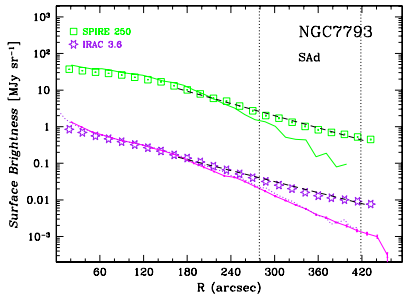

Fig. B.1. continued.

Appendix C: Radial surface brightness profiles with MBBV and DL07 fits

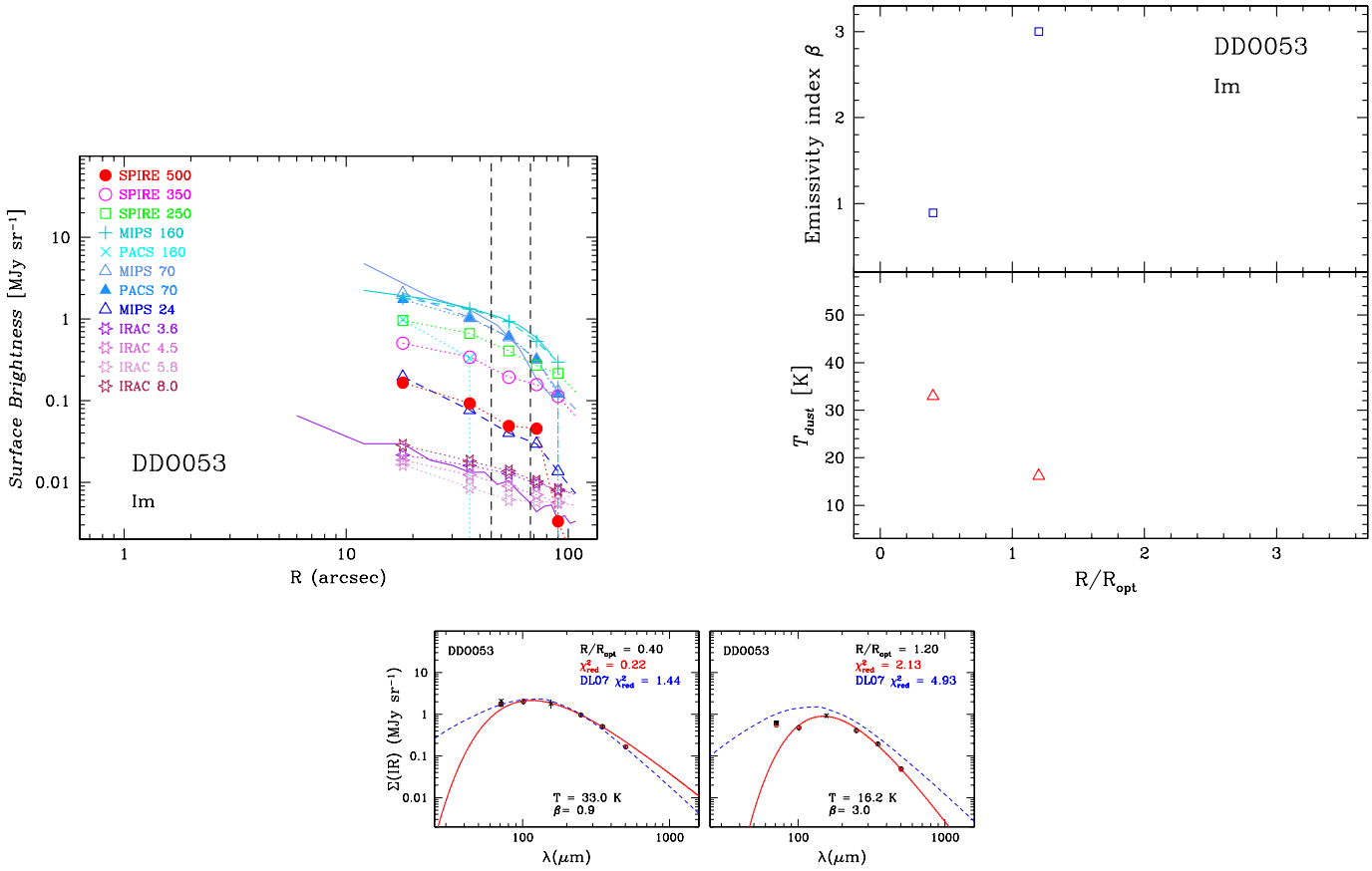

Fig. C.1. *Top left panel*: surface brightness profiles, $\Sigma_{\rm IR}$, for PACS, MIPS, SPIRE, and IRAC 3.6 μm. *Top right panel*: radial temperature trends $T_{\rm dust}$ and emissivity index trends β vs. normalized radii, $R/R_{\rm opt}$. Sets of fluxes are defined over ≥4 wavelengths. *The bottom panels* show each individual SED fit, $\Sigma_{\rm IR}$ vs. wavelength, with best-fit temperature and emissivity index β. The DL07 best-fit models are shown as a (blue) dashed line, and the MBBV fits as a (red) solid one. S/N lower limit = 3.0. The 70 μm (PACS+MIPS) and 500 μm points are excluded from the fits.

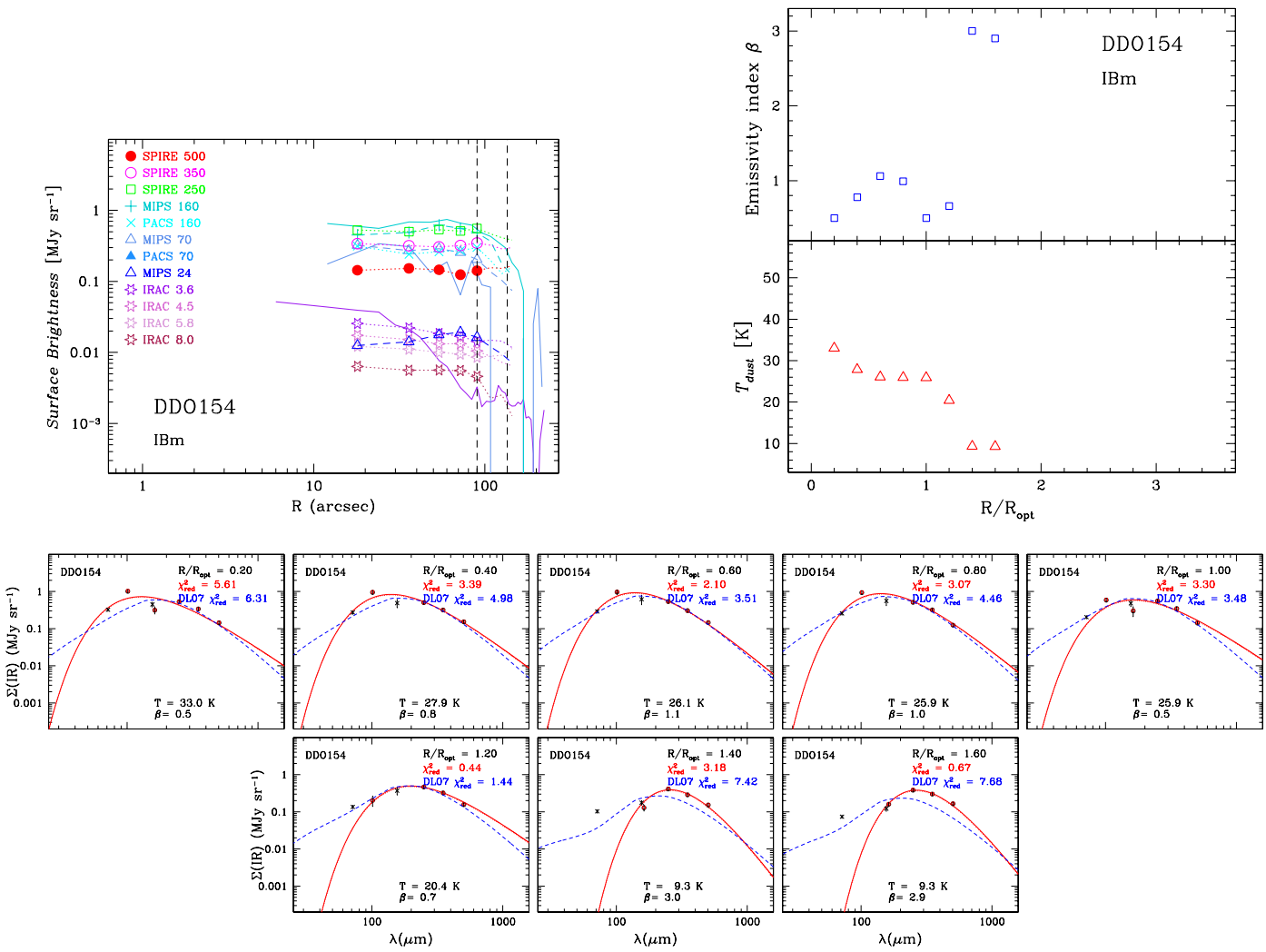

Fig. C.2. *Top left panel*: surface brightness profiles, $\Sigma_{\rm IR}$, for PACS, MIPS, SPIRE, and IRAC 3.6 μm. *Top right panel*: radial temperature trends $T_{\rm dust}$ and emissivity index trends β vs. normalized radii, $R/R_{\rm opt}$. Sets of fluxes are defined over ≥4 wavelengths. The *bottom panels* show each individual SED fit, $\Sigma_{\rm IR}$ vs. wavelength, with best-fit temperature and emissivity index β. The DL07 best-fit models are shown as a (blue) dashed line, and the MBBV fits as a (red) solid one. S/N lower limit = 3.0. The 70 μm (PACS+MIPS) and 500 μm points are excluded from the fits.

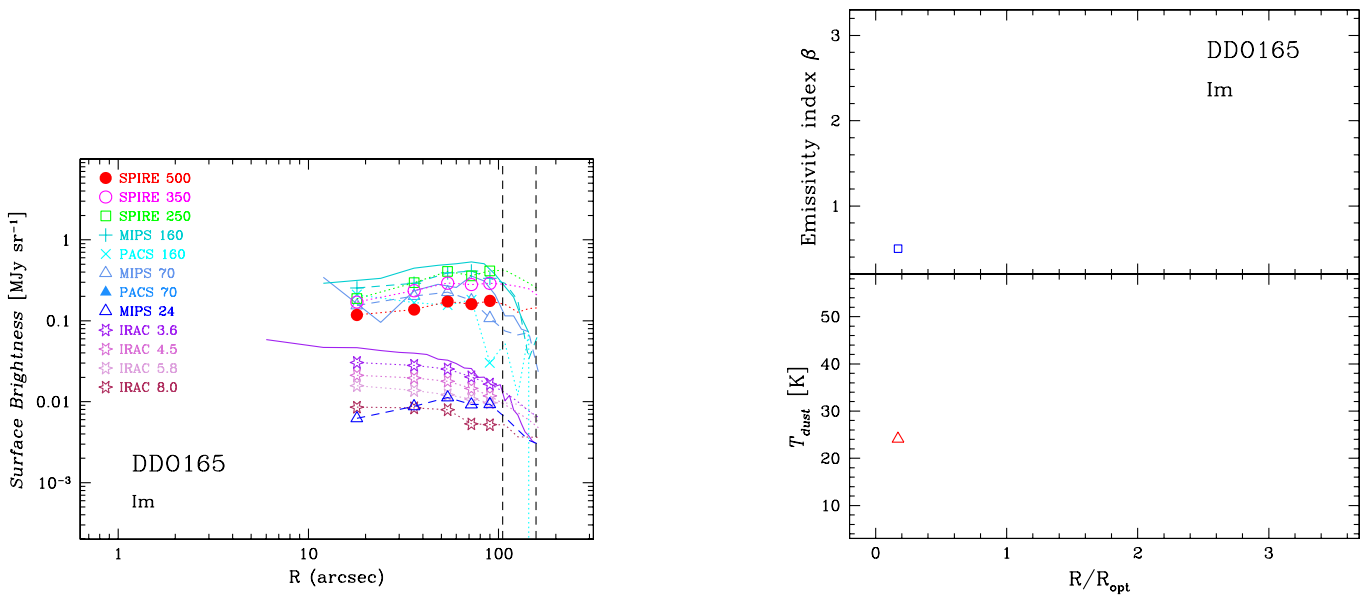

Fig. C.3. *Left panel*: surface brightness profiles for PACS, MIPS, SPIRE, and IRAC 3.6 μm. Profiles are extracted as in Munoz-Mateos et al. (2009); those profiles are shown by solid lines, while the profiles presented here extend beyond the symbols as dashed lines. The vertical dashed lines indicate the optical radius, $R_{\rm opt}$ and 1.5 $R_{\rm opt}$. *Right panel*: radial temperature trends $T_{\rm dust}$ vs. R/$R_{\rm opt}$. For this galaxy, there are no radial bins having data with sufficient signal-to-noise to fit.

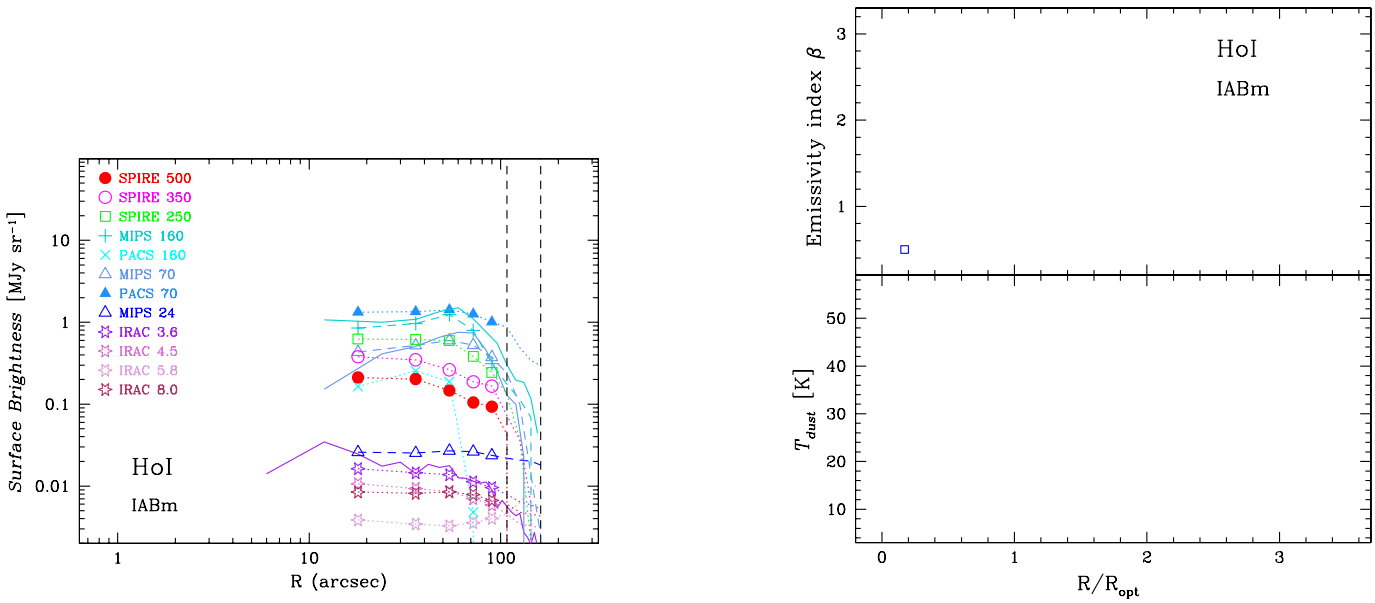

Fig. C.4. *Left panel*: surface brightness profiles for PACS, MIPS, SPIRE, and IRAC 3.6 μm. Profiles are extracted as in Munoz-Mateos et al. (2009); those profiles are shown by solid lines, while the profiles presented here extend beyond the symbols as dashed lines. The vertical dashed lines indicate the optical radius, $R_{\rm opt}$ and 1.5 $R_{\rm opt}$. *Right panel*: radial temperature trends $T_{\rm dust}$ vs. $R/R_{\rm opt}$. For this galaxy, there are no radial bins having data with sufficient signal-to-noise to fit.

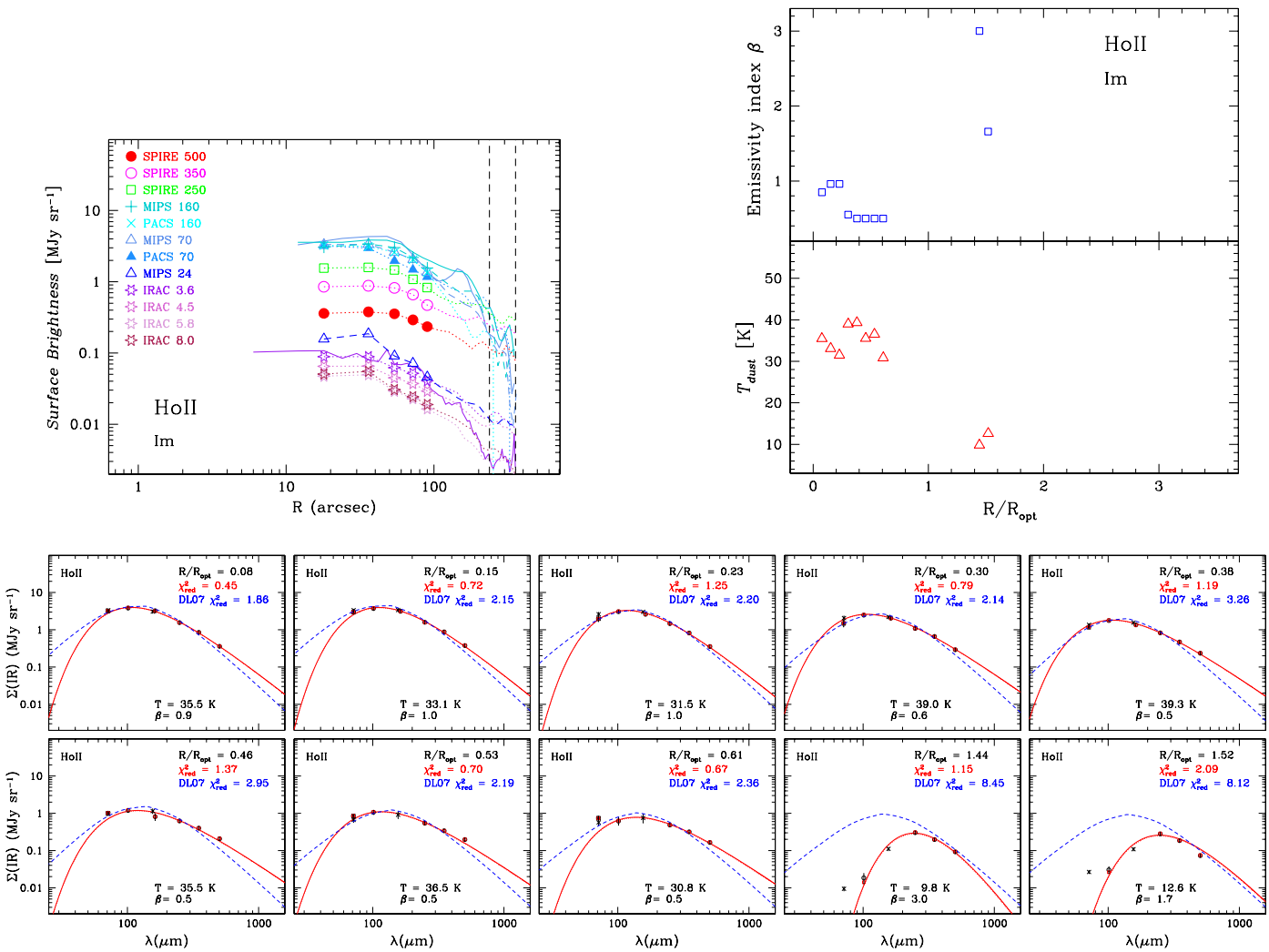

Fig. C.5. *Top left panel*: surface brightness profiles, $\Sigma_{\rm IR}$, for PACS, MIPS, SPIRE, and IRAC 3.6 μm. *Top right panel*: radial temperature trends $T_{\rm dust}$ and emissivity index trends β vs. normalized radii, $R/R_{\rm opt}$. Sets of fluxes are defined over ≥4 wavelengths. The *bottom panels* show each individual SED fit, $\Sigma_{\rm IR}$ vs. wavelength, with best-fit temperature and emissivity index β. The DL07 best-fit models are shown as a (blue) dashed line, and the MBBV fits as a (red) solid one. S/N lower limit = 3.0. The 70 μm (PACS+MIPS) and 500 μm points are excluded from the fits.

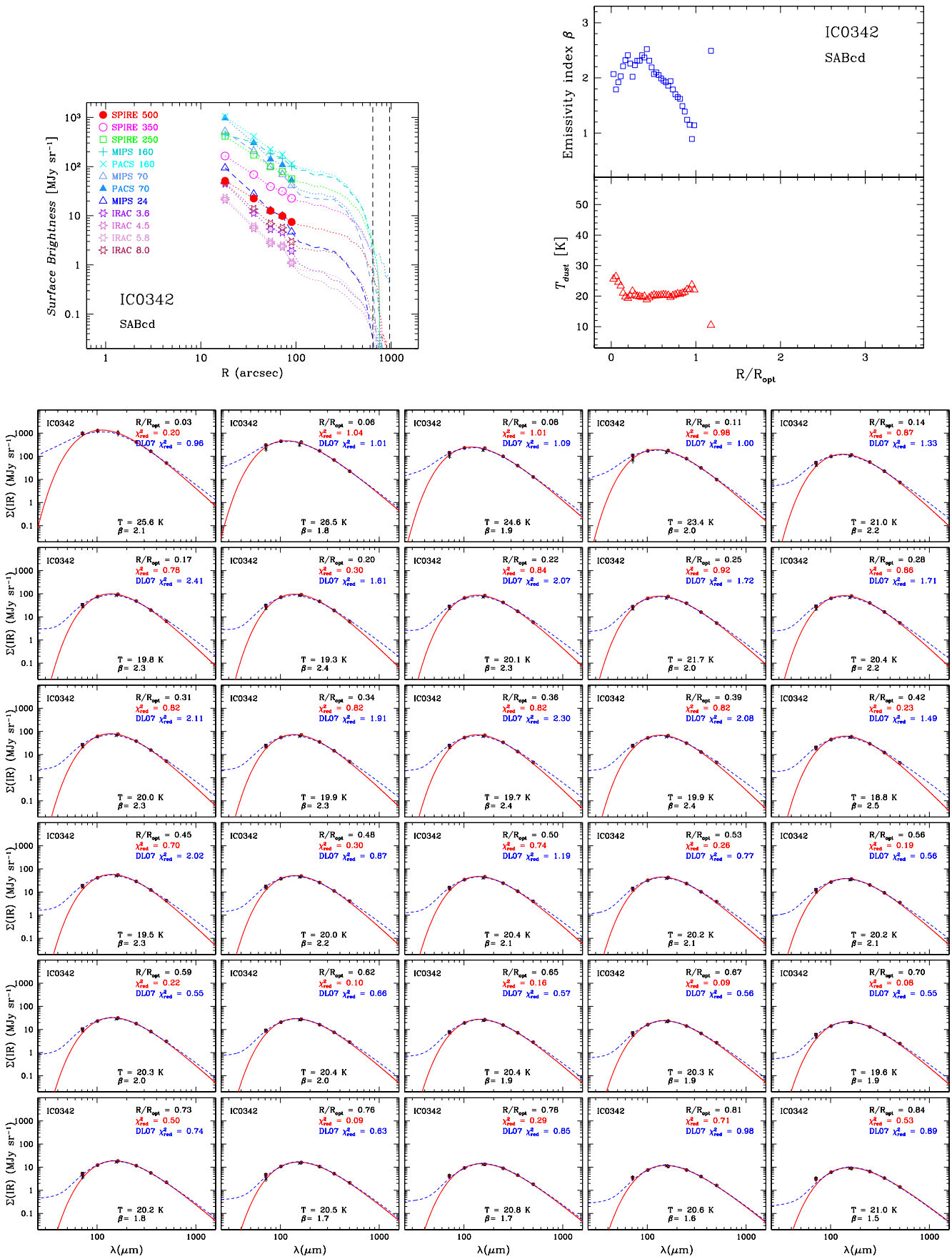

Fig. C.6. *Top left panel*: surface brightness profiles, Σ_{IR}, for PACS, MIPS, SPIRE, and IRAC 3.6 μm. *Top right panel*: radial temperature trends T_{dust} and emissivity index trends β vs. normalized radii, R/R_{opt}. Sets of fluxes are defined over ≥4 wavelengths. The *bottom panels* show each individual SED fit, Σ_{IR} vs. wavelength, with best-fit temperature and emissivity index β. The DL07 best-fit models are shown as a (blue) dashed line, and the MBBV fits as a (red) solid one. S/N lower limit = 3.0. The 70 μm (PACS+MIPS) and 500 μm points are excluded from the fits.

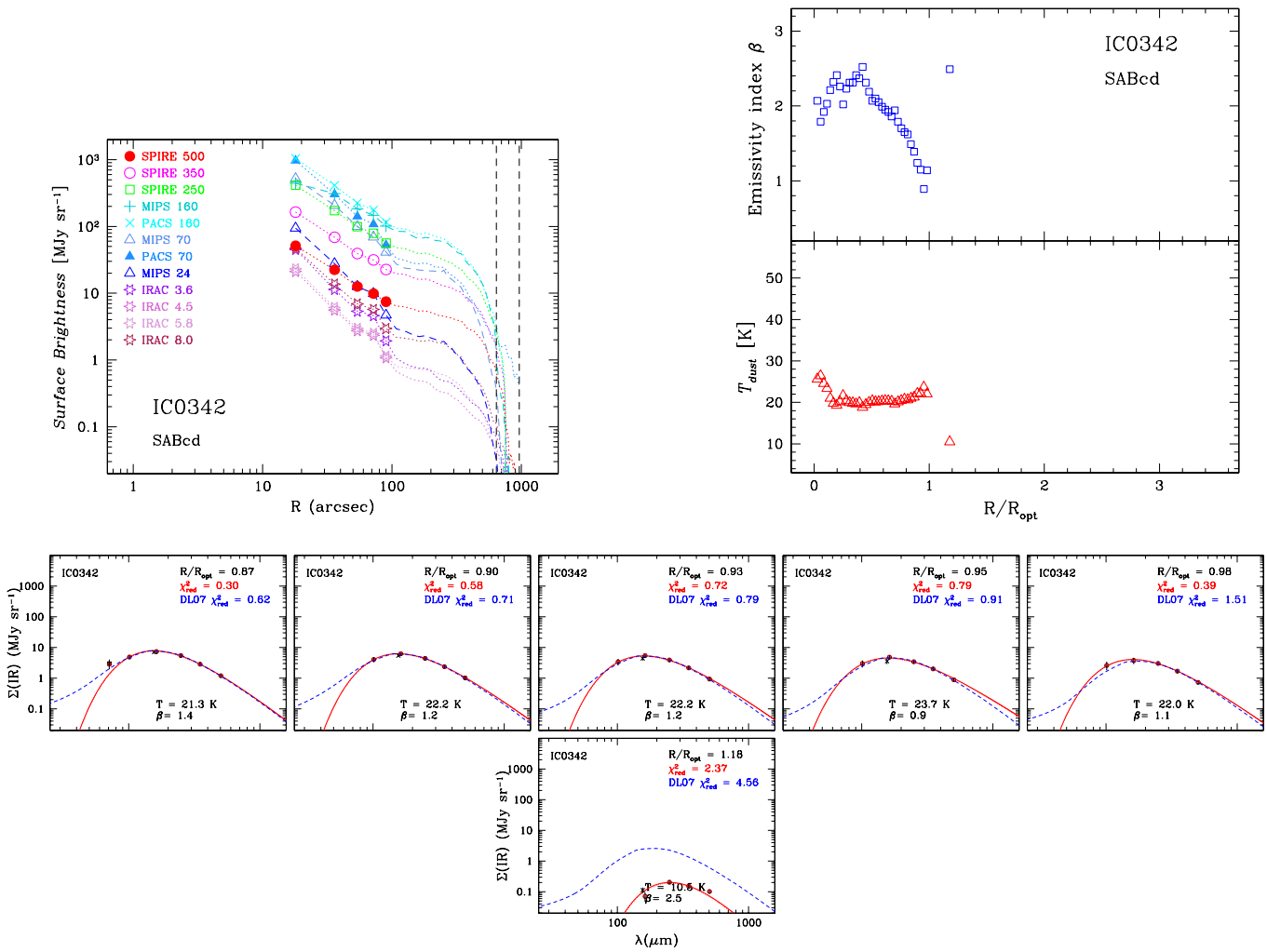

Fig. C.6. continued.

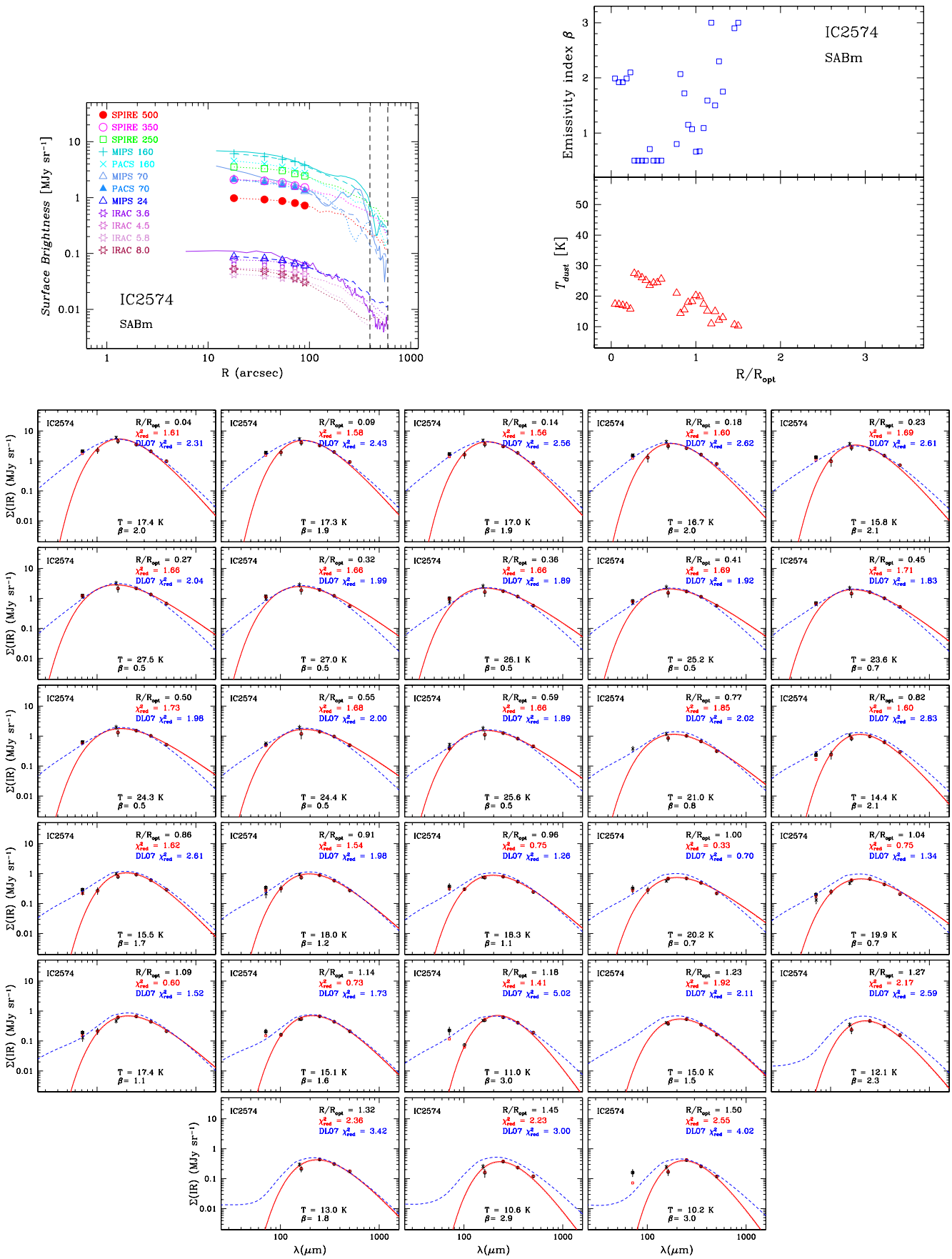

Fig. C.7. *Top left panel*: surface brightness profiles, Σ_{IR}, for PACS, MIPS, SPIRE, and IRAC 3.6 μm. *Top right panel*: radial temperature trends T_{dust} and emissivity index trends β vs. normalized radii, R/R_{opt}. Sets of fluxes are defined over ≥4 wavelengths. The *bottom panels* show each individual SED fit, Σ_{IR} vs. wavelength, with best-fit temperature and emissivity index β. The DL07 best-fit models are shown as a (blue) dashed line, and the MBBV fits as a (red) solid one. S/N lower limit = 3.0. The 70 μm (PACS+MIPS) and 500 μm points are excluded from the fits.

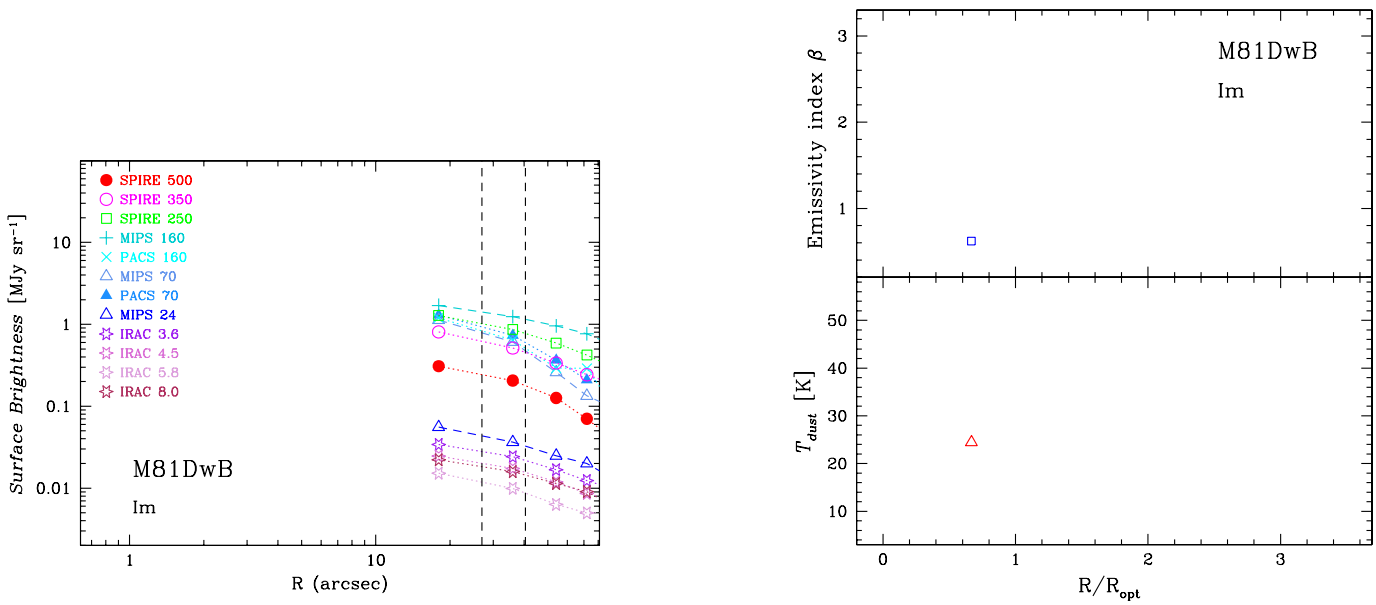

Fig. C.8. *Left panel*: surface brightness profiles for PACS, MIPS, SPIRE, and IRAC 3.6 μm. Profiles are extracted as in Munoz-Mateos et al. (2009); those profiles are shown by solid lines, while the profiles presented here extend beyond the symbols as dashed lines. The vertical dashed lines indicate the optical radius, $R_{\rm opt}$ and 1.5 $R_{\rm opt}$. *Right panel*: radial temperature trends $T_{\rm dust}$ vs. $R/R_{\rm opt}$. For this galaxy, there are no radial bins having data with sufficient signal-to-noise to fit.

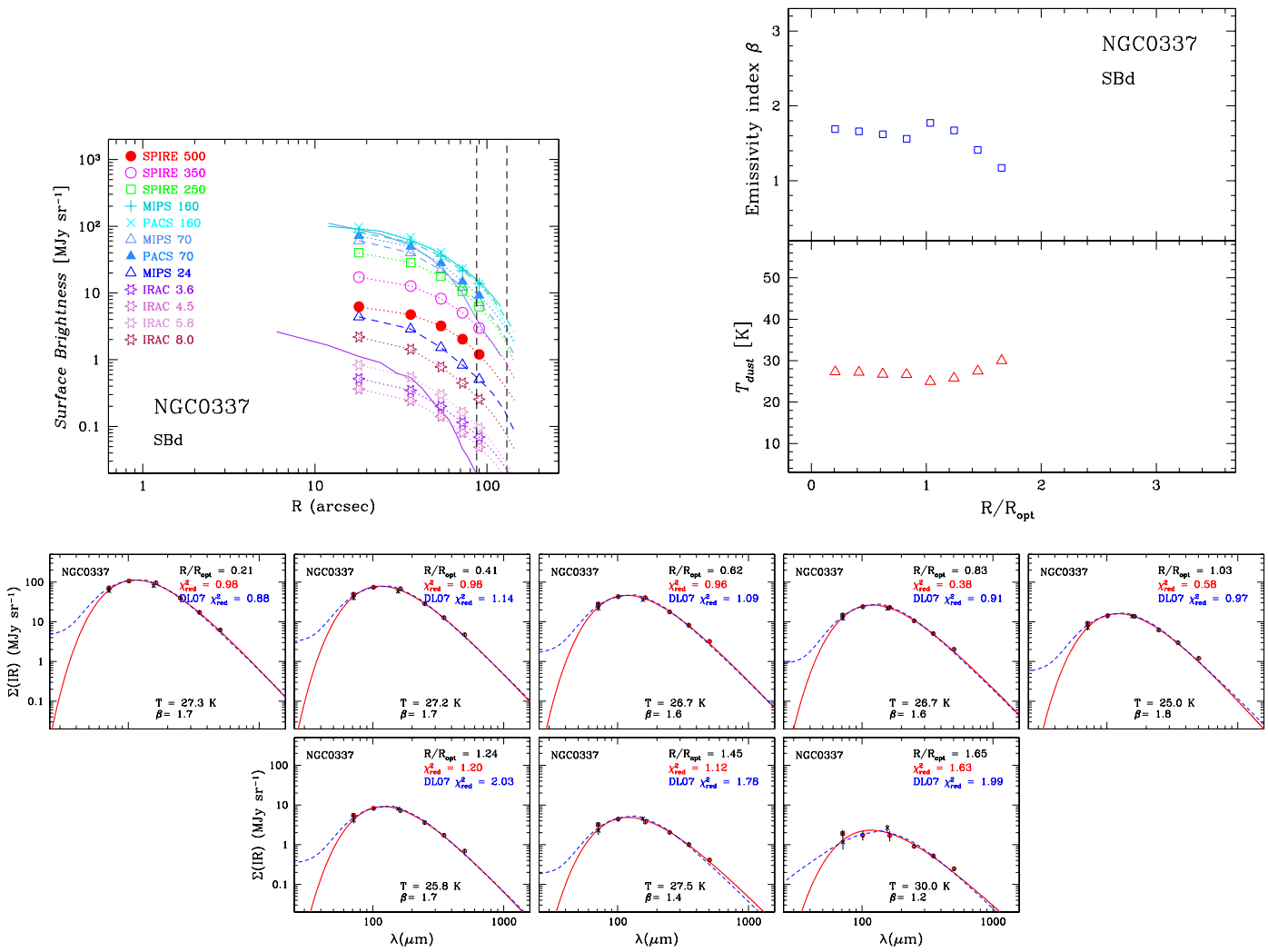

Fig. C.9. *Top left panel*: surface brightness profiles, $\Sigma_{\rm IR}$, for PACS, MIPS, SPIRE, and IRAC 3.6 μm. *Top right panel*: radial temperature trends $T_{\rm dust}$ and emissivity index trends β vs. normalized radii, $R/R_{\rm opt}$. Sets of fluxes are defined over ≥4 wavelengths. The *bottom panels* show each individual SED fit, $\Sigma_{\rm IR}$ vs. wavelength, with best-fit temperature and emissivity index β. The DL07 best-fit models are shown as a (blue) dashed line, and the MBBV fits as a (red) solid one. S/N lower limit = 3.0. The 70 μm (PACS+MIPS) and 500 μm points are excluded from the fits.

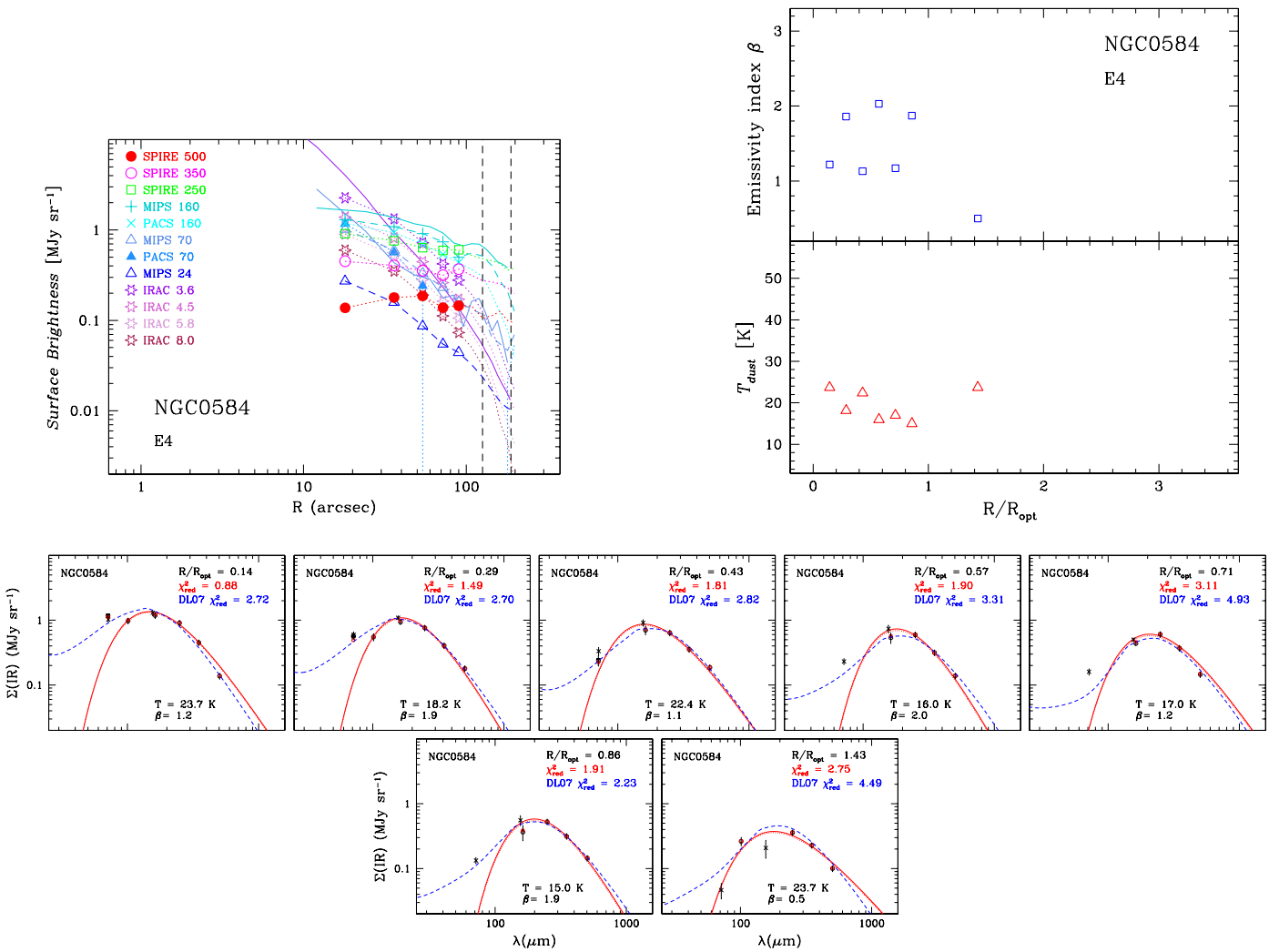

Fig. C.10. *Top left panel*: surface brightness profiles, $\Sigma_{\rm IR}$, for PACS, MIPS, SPIRE, and IRAC 3.6 μm. *Top right panel*: radial temperature trends $T_{\rm dust}$ and emissivity index trends β vs. normalized radii, $R/R_{\rm opt}$. Sets of fluxes are defined over ≥4 wavelengths. The *bottom panels* show each individual SED fit, $\Sigma_{\rm IR}$ vs. wavelength, with best-fit temperature and emissivity index β. The DL07 best-fit models are shown as a (blue) dashed line, and the MBBV fits as a (red) solid one. S/N lower limit = 3.0. The 70 μm (PACS+MIPS) and 500 μm points are excluded from the fits.

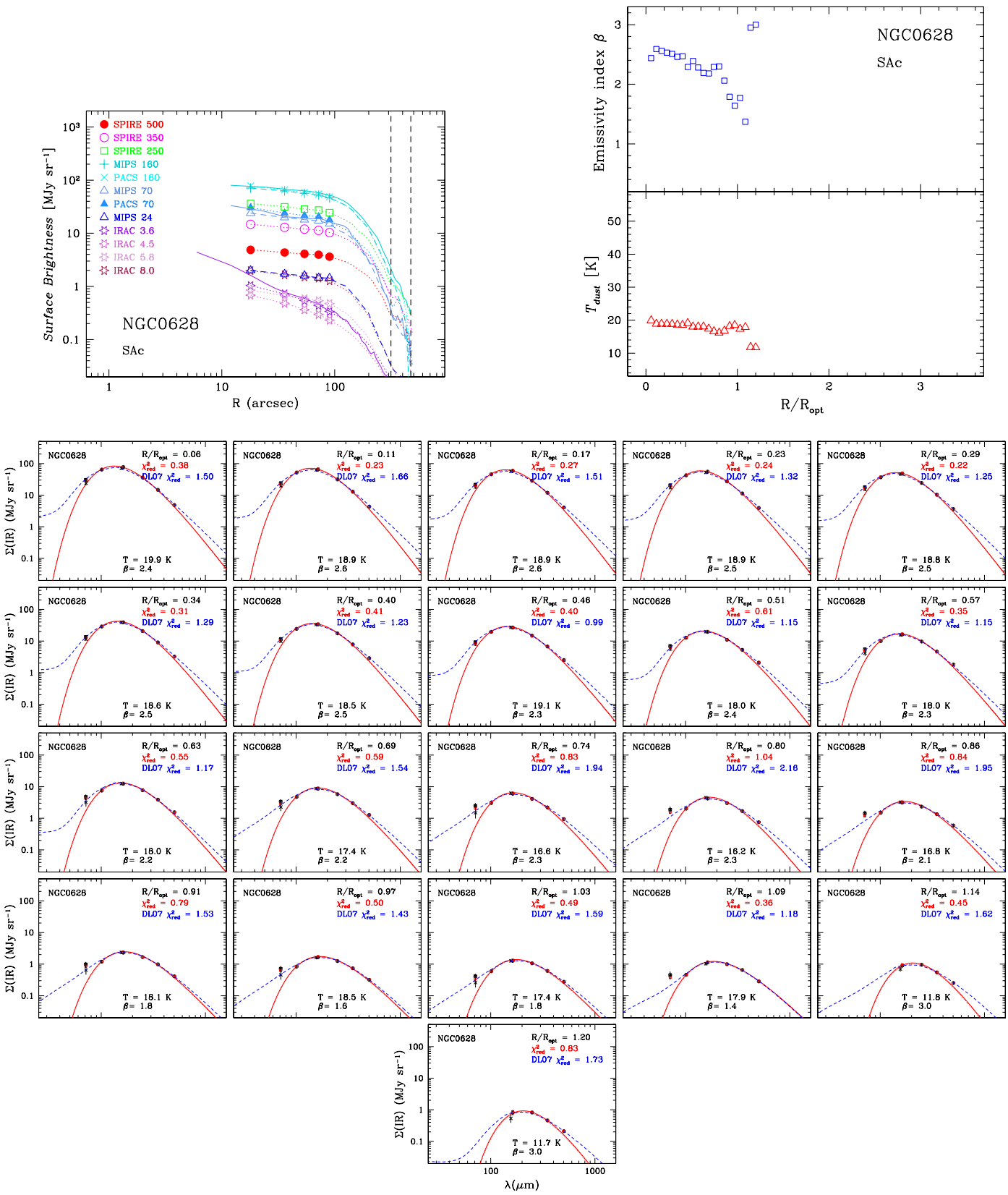

Fig. C.11. *Top left panel*: surface brightness profiles, $\Sigma_{\rm IR}$, for PACS, MIPS, SPIRE, and IRAC 3.6 μm. *Top right panel*: radial temperature trends $T_{\rm dust}$ and emissivity index trends β vs. normalized radii, $R/R_{\rm opt}$. Sets of fluxes are defined over ≥4 wavelengths. The *bottom panels* show each individual SED fit, $\Sigma_{\rm IR}$ vs. wavelength, with best-fit temperature and emissivity index β. The DL07 best-fit models are shown as a (blue) dashed line, and the MBBV fits as a (red) solid one. S/N lower limit = 3.0. The 70 μm (PACS+MIPS) and 500 μm points are excluded from the fits.

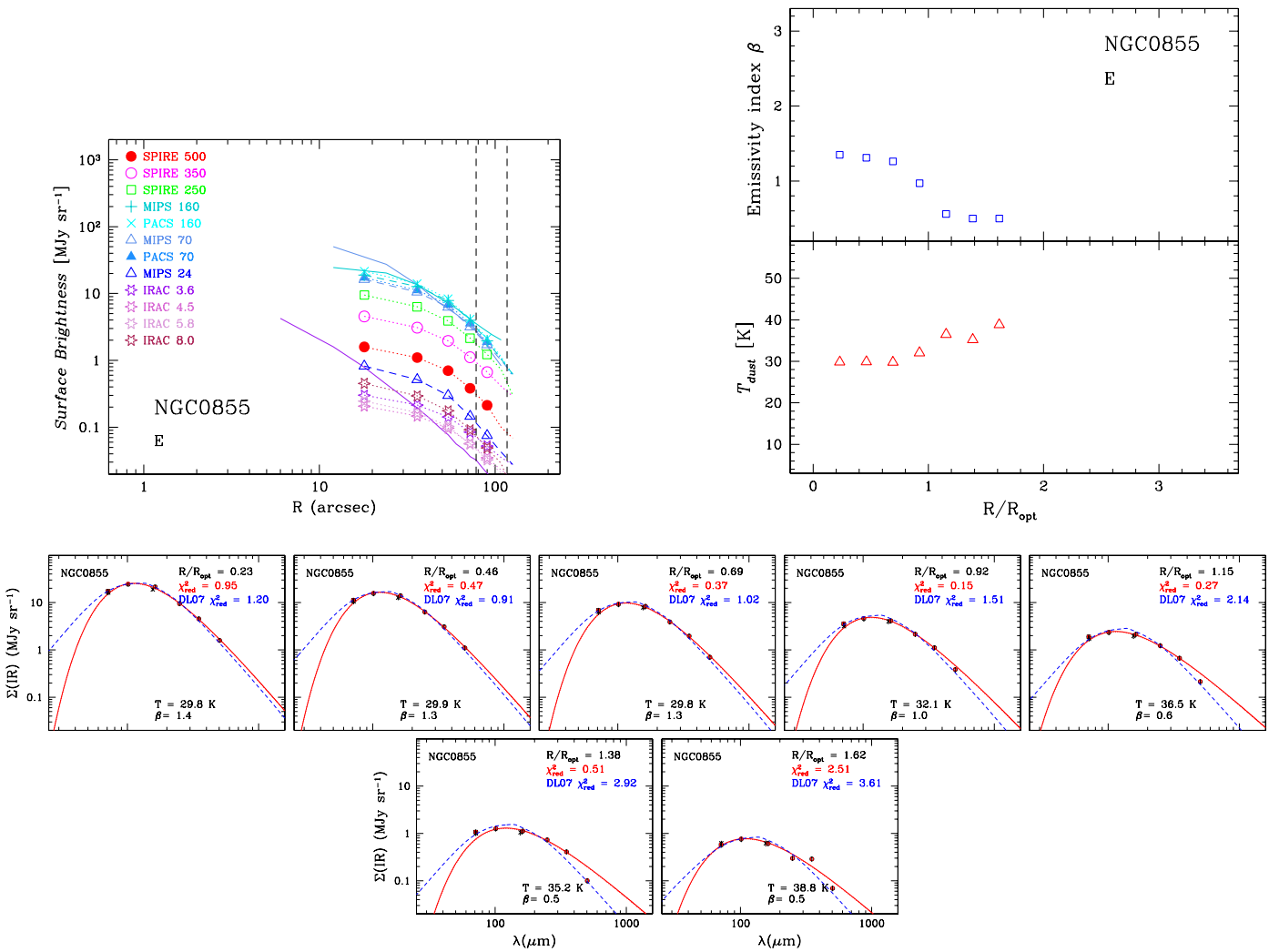

Fig. C.12. *Top left panel*: surface brightness profiles, $\Sigma_{\rm IR}$, for PACS, MIPS, SPIRE, and IRAC 3.6 μm. *Top right panel*: radial temperature trends $T_{\rm dust}$ and emissivity index trends β vs. normalized radii, $R/R_{\rm opt}$. Sets of fluxes are defined over ≥4 wavelengths. The *bottom panels* show each individual SED fit, $\Sigma_{\rm IR}$ vs. wavelength, with best-fit temperature and emissivity index β. The DL07 best-fit models are shown as a (blue) dashed line, and the MBBV fits as a (red) solid one. S/N lower limit = 3.0. The 70 ,μm (PACS+MIPS) and 500 μm points are excluded from the fits.

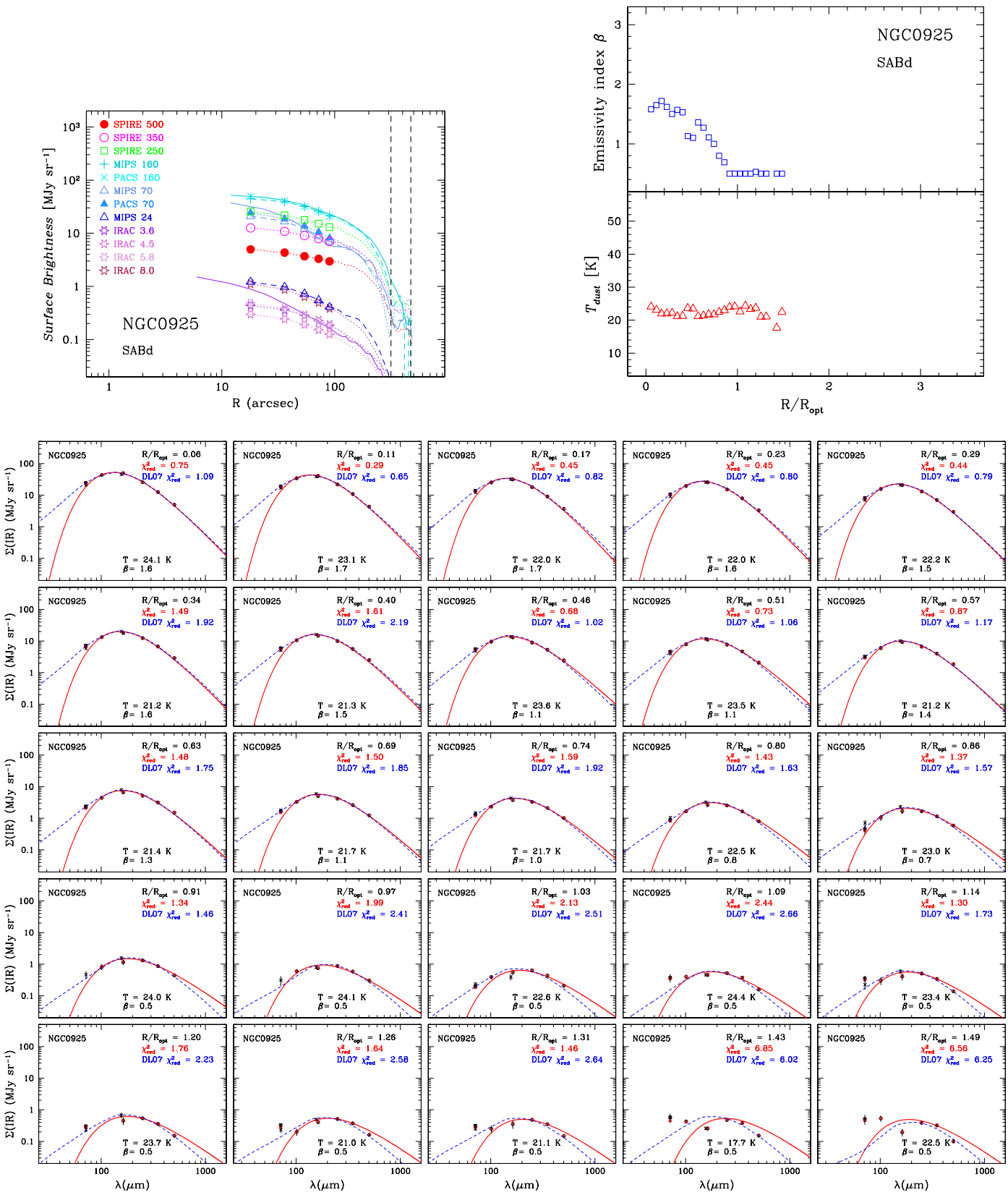

Fig. C.13. *Top left panel*: surface brightness profiles, $\Sigma_{\rm IR}$, for PACS, MIPS, SPIRE, and IRAC 3.6 μm. *Top right panel*: radial temperature trends $T_{\rm dust}$ and emissivity index trends β vs. normalized radii, $R/R_{\rm opt}$. Sets of fluxes are defined over ≥4 wavelengths. The *bottom panels* show each individual SED fit, $\Sigma_{\rm IR}$ vs. wavelength, with best-fit temperature and emissivity index β. The DL07 best-fit models are shown as a (blue) dashed line, and the MBBV fits as a (red) solid one. S/N lower limit = 3.0. The 70 μm (PACS+MIPS) and 500 μm points are excluded from the fits.

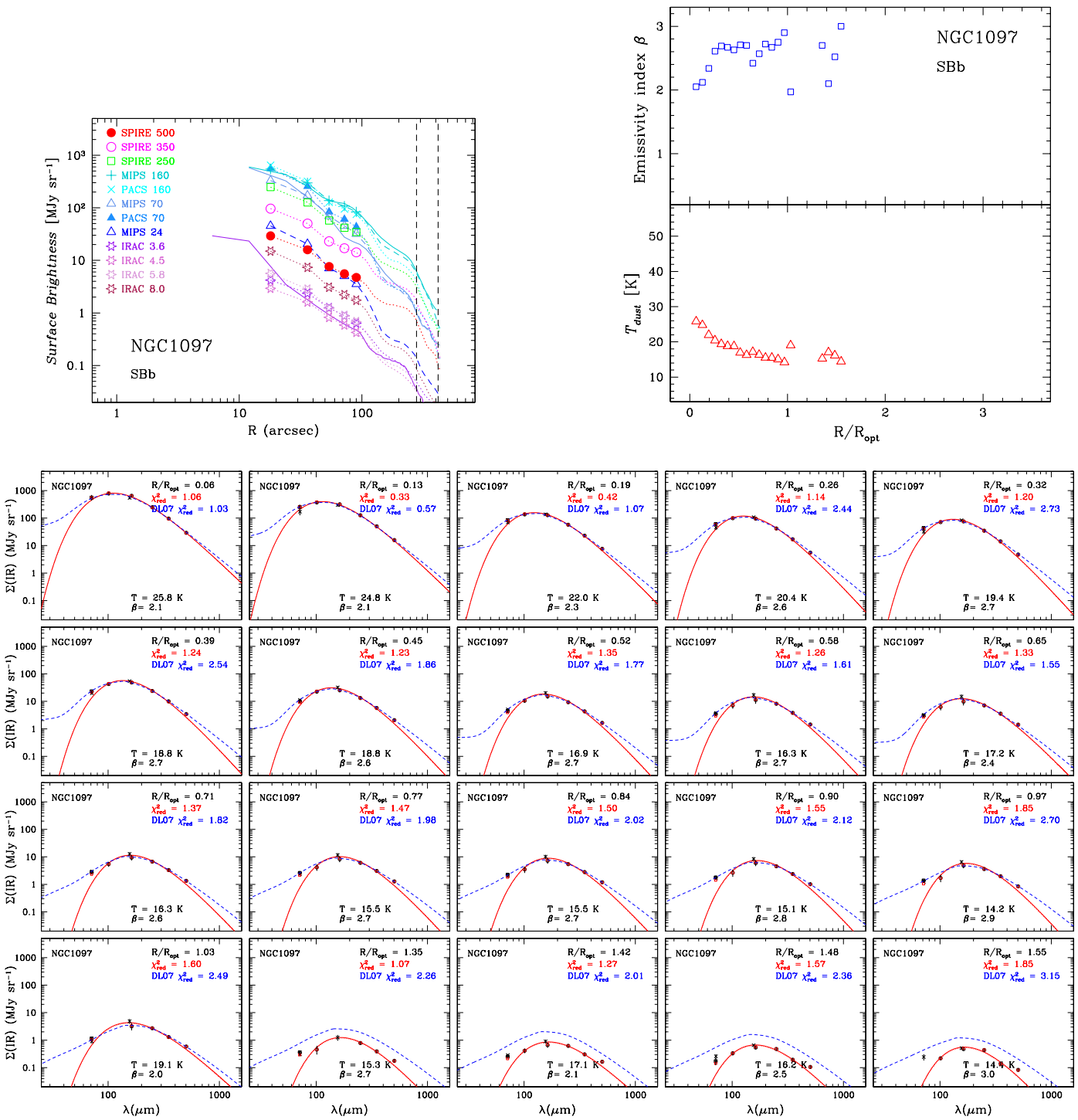

Fig. C.14. *Top left panel*: surface brightness profiles, $\Sigma_{\rm IR}$, for PACS, MIPS, SPIRE, and IRAC 3.6 μm. *Top right panel*: radial temperature trends $T_{\rm dust}$ and emissivity index trends β vs. normalized radii, $R/R_{\rm opt}$. Sets of fluxes are defined over ≥4 wavelengths. The *bottom panels* show each individual SED fit, $\Sigma_{\rm IR}$ vs. wavelength, with best-fit temperature and emissivity index β. The DL07 best-fit models are shown as a (blue) dashed line, and the MBBV fits as a (red) solid one. S/N lower limit = 3.0. The 70 μm (PACS+MIPS) and 500 μm points are excluded from the fits.

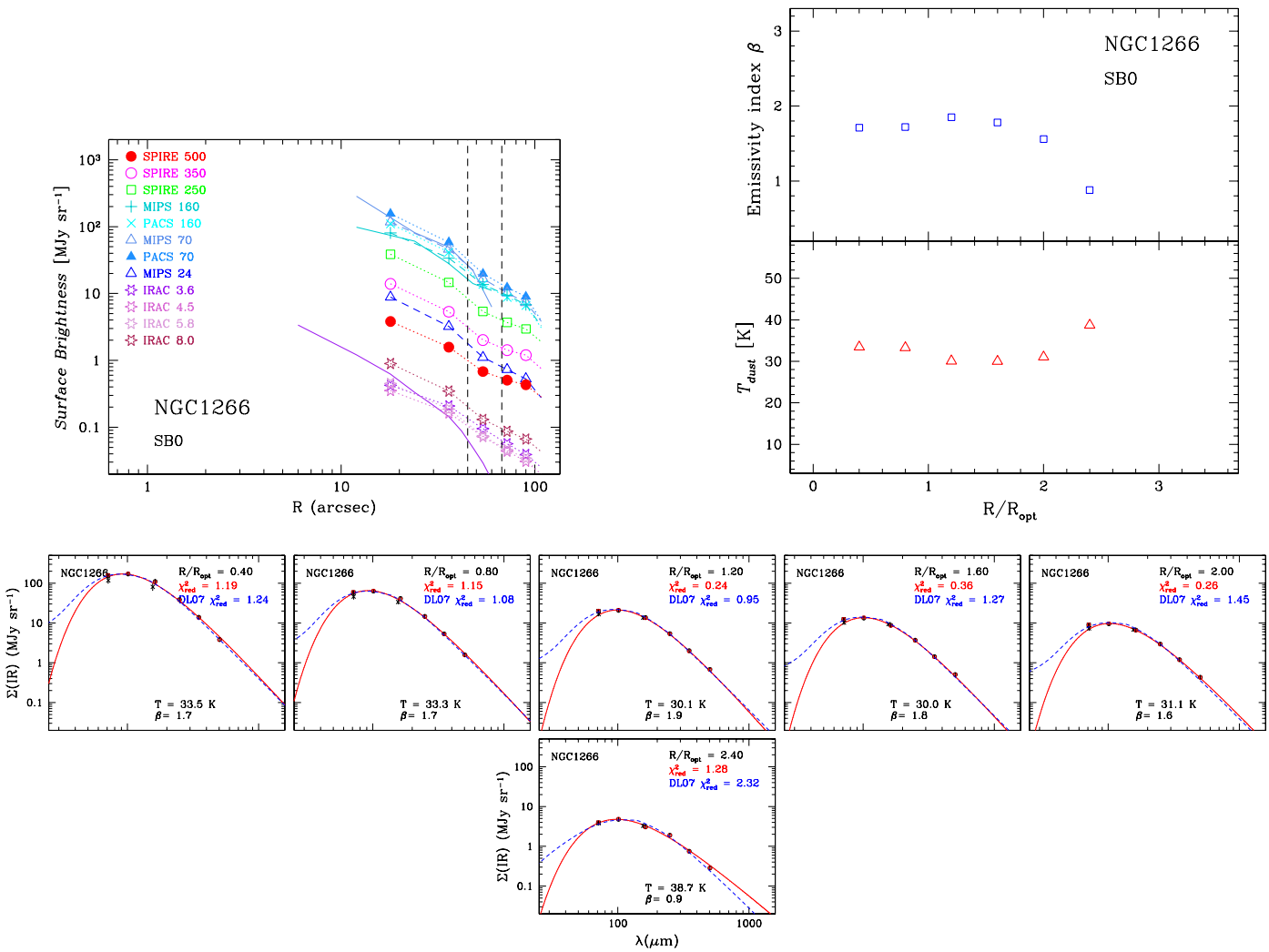

Fig. C.15. *Top left panel*: surface brightness profiles, $\Sigma_{\rm IR}$, for PACS, MIPS, SPIRE, and IRAC 3.6 μm. *Top right panel*: radial temperature trends $T_{\rm dust}$ and emissivity index trends β vs. normalized radii, $R/R_{\rm opt}$. Sets of fluxes are defined over ≥4 wavelengths. The *bottom panels* show each individual SED fit, $\Sigma_{\rm IR}$ vs. wavelength, with best-fit temperature and emissivity index β. The DL07 best-fit models are shown as a (blue) dashed line, and the MBBV fits as a (red) solid one. S/N lower limit = 3.0. The 70 μm (PACS+MIPS) and 500 μm points are excluded from the fits.

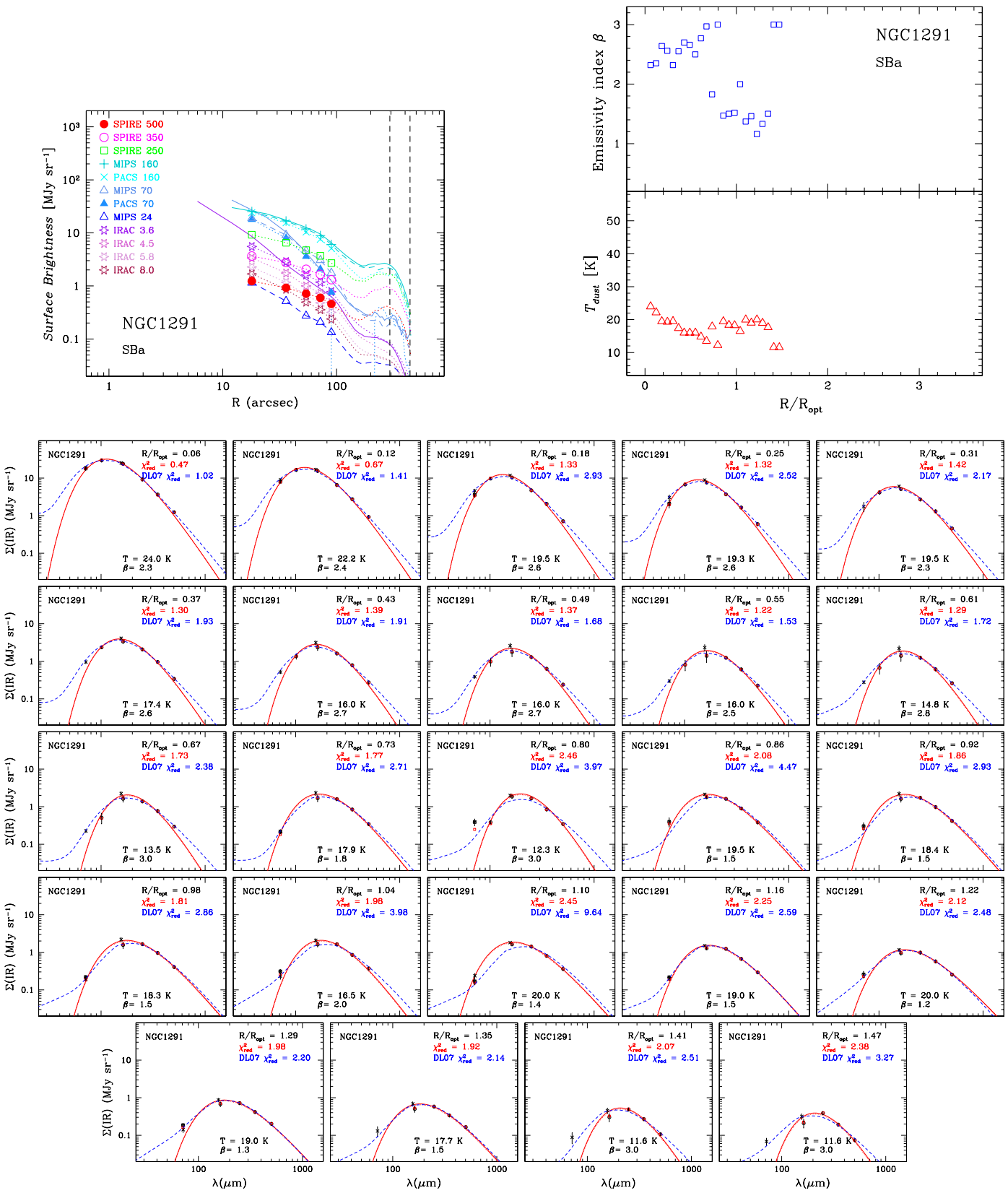

Fig. C.16. *Top left panel*: surface brightness profiles, $\Sigma_{\rm IR}$, for PACS, MIPS, SPIRE, and IRAC 3.6 μm. *Top right panel*: radial temperature trends $T_{\rm dust}$ and emissivity index trends β vs. normalized radii, $R/R_{\rm opt}$. Sets of fluxes are defined over ≥4 wavelengths. The *bottom panels* show each individual SED fit, $\Sigma_{\rm IR}$ vs. wavelength, with best-fit temperature and emissivity index β. The DL07 best-fit models are shown as a (blue) dashed line, and the MBBV fits as a (red) solid one. S/N lower limit = 3.0. The 70 μm (PACS+MIPS) and 500 μm points are excluded from the fits.

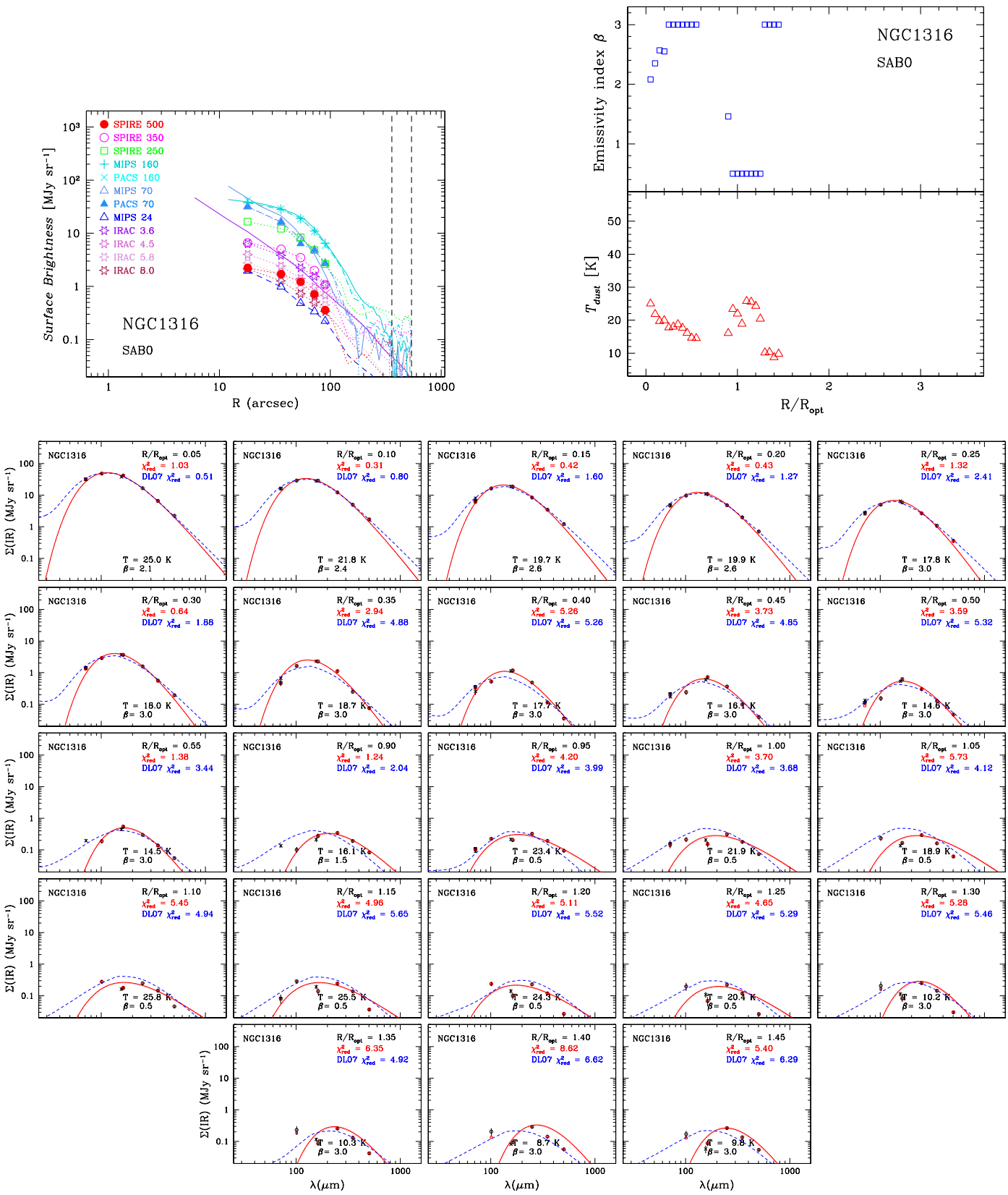

Fig. C.17. *Top left panel*: surface brightness profiles, Σ_{IR}, for PACS, MIPS, SPIRE, and IRAC 3.6 μm. *Top right panel*: radial temperature trends T_{dust} and emissivity index trends β vs. normalized radii, R/R_{opt}. Sets of fluxes are defined over ≥4 wavelengths. The *bottom panels* show each individual SED fit, Σ_{IR} vs. wavelength, with best-fit temperature and emissivity index β. The DL07 best-fit models are shown as a (blue) dashed line, and the MBBV fits as a (red) solid one. S/N lower limit = 3.0. The 70 μm (PACS+MIPS) and 500 μm points are excluded from the fits.

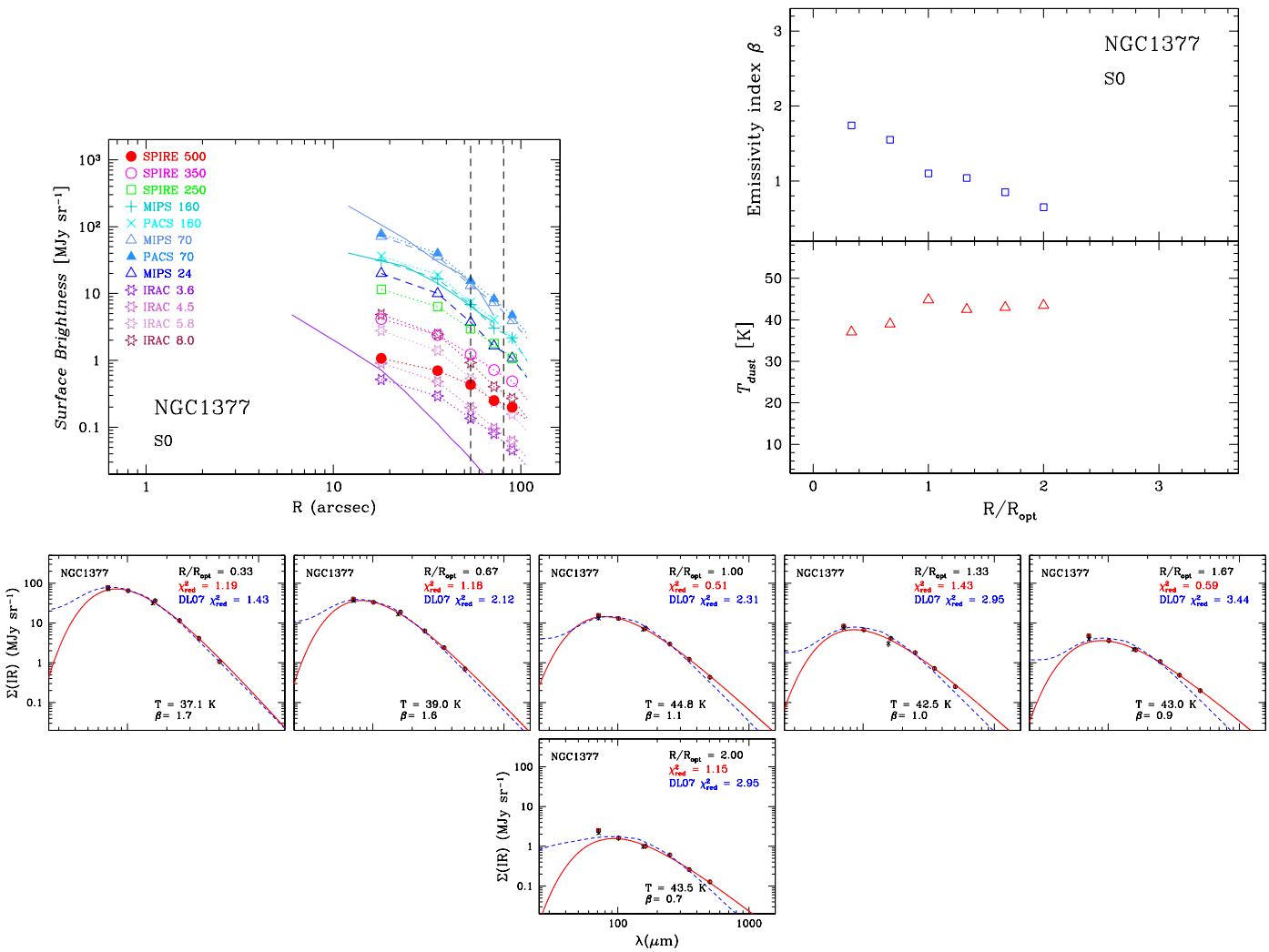

Fig. C.18. *Top left panel*: surface brightness profiles, $\Sigma_{\rm IR}$, for PACS, MIPS, SPIRE, and IRAC 3.6 μm. *Top right panel*: radial temperature trends $T_{\rm dust}$ and emissivity index trends β vs. normalized radii, $R/R_{\rm opt}$. Sets of fluxes are defined over ≥4 wavelengths. The *bottom panels* show each individual SED fit, $\Sigma_{\rm IR}$ vs. wavelength, with best-fit temperature and emissivity index β. The DL07 best-fit models are shown as a (blue) dashed line, and the MBBV fits as a (red) solid one. S/N lower limit = 3.0. The 70 μm (PACS+MIPS) and 500 μm points are excluded from the fits.

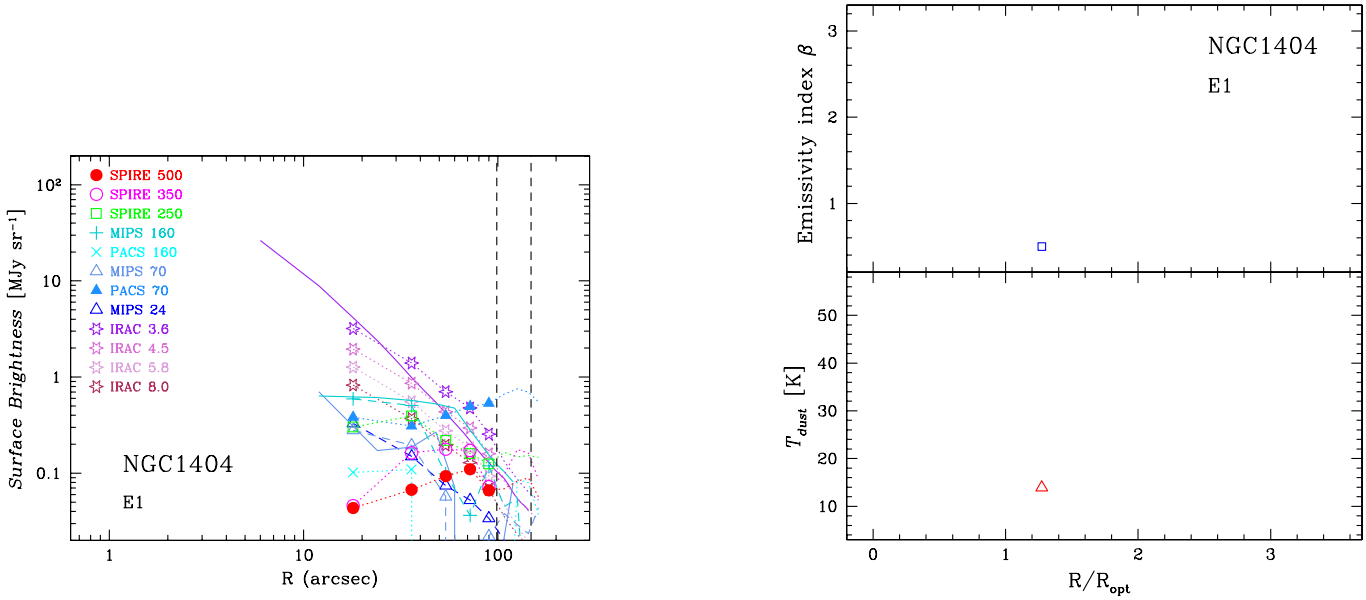

Fig. C.19. *Left panel*: surface brightness profiles for PACS, MIPS, SPIRE, and IRAC 3.6 μm. Profiles are extracted as in Munoz-Mateos et al. (2009); those profiles are shown by solid lines, while the profiles presented here extend beyond the symbols as dashed lines. The vertical dashed lines indicate the optical radius, $R_{\rm opt}$ and 1.5 $R_{\rm opt}$. *Right panel*: radial temperature trends $T_{\rm dust}$ vs. $R/R_{\rm opt}$. For this galaxy, there are no radial bins having data with sufficient signal-to-noise to fit.

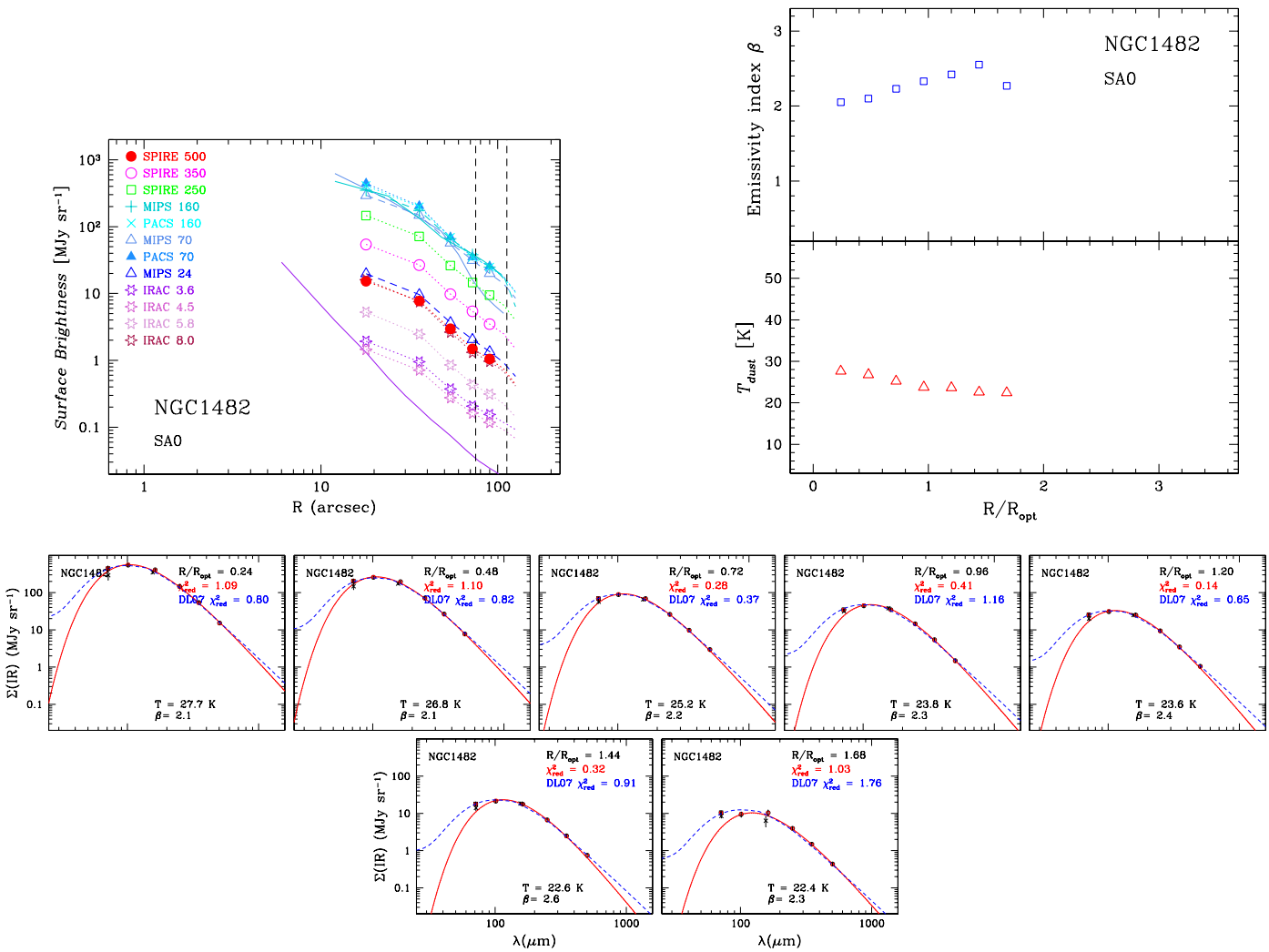

Fig. C.20. *Top left panel*: surface brightness profiles, $\Sigma_{\rm IR}$, for PACS, MIPS, SPIRE, and IRAC 3.6 μm. *Top right panel*: radial temperature trends $T_{\rm dust}$ and emissivity index trends β vs. normalized radii, $R/R_{\rm opt}$. Sets of fluxes are defined over ≥4 wavelengths. The *bottom panels* show each individual SED fit, $\Sigma_{\rm IR}$ vs. wavelength, with best-fit temperature and emissivity index β. The DL07 best-fit models are shown as a (blue) dashed line, and the MBBV fits as a (red) solid one. S/N lower limit = 3.0. The 70 μm (PACS+MIPS) and 500 μm points are excluded from the fits.

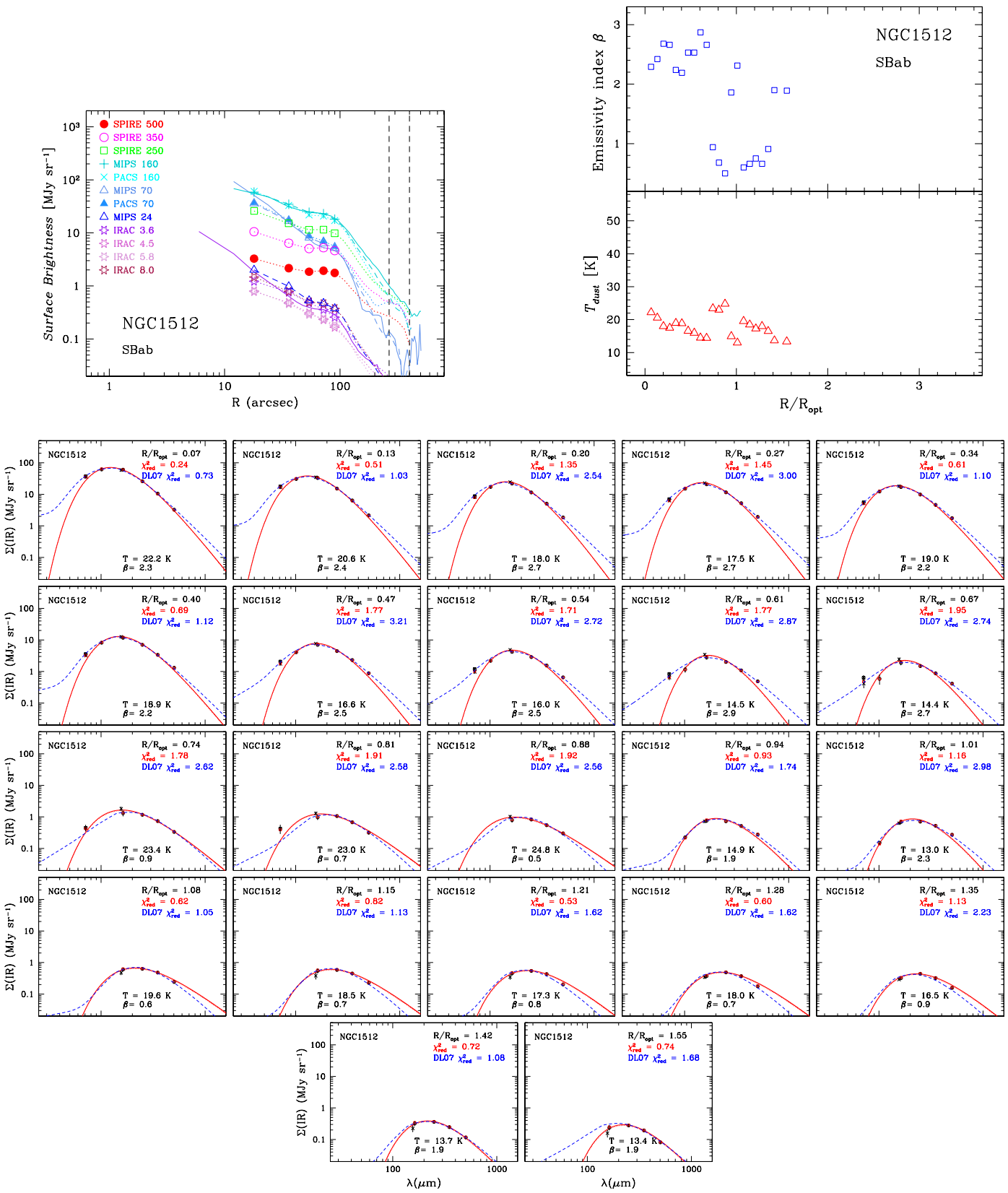

Fig. C.21. *Top left panel*: surface brightness profiles, $\Sigma_{\rm IR}$, for PACS, MIPS, SPIRE, and IRAC 3.6 μm. *Top right panel*: radial temperature trends $T_{\rm dust}$ and emissivity index trends β vs. normalized radii, $R/R_{\rm opt}$. Sets of fluxes are defined over ≥4 wavelengths. The *bottom panels* show each individual SED fit, $\Sigma_{\rm IR}$ vs. wavelength, with best-fit temperature and emissivity index β. The DL07 best-fit models are shown as a (blue) dashed line, and the MBBV fits as a (red) solid one. S/N lower limit = 3.0. The 70 μm (PACS+MIPS) and 500 μm points are excluded from the fits.

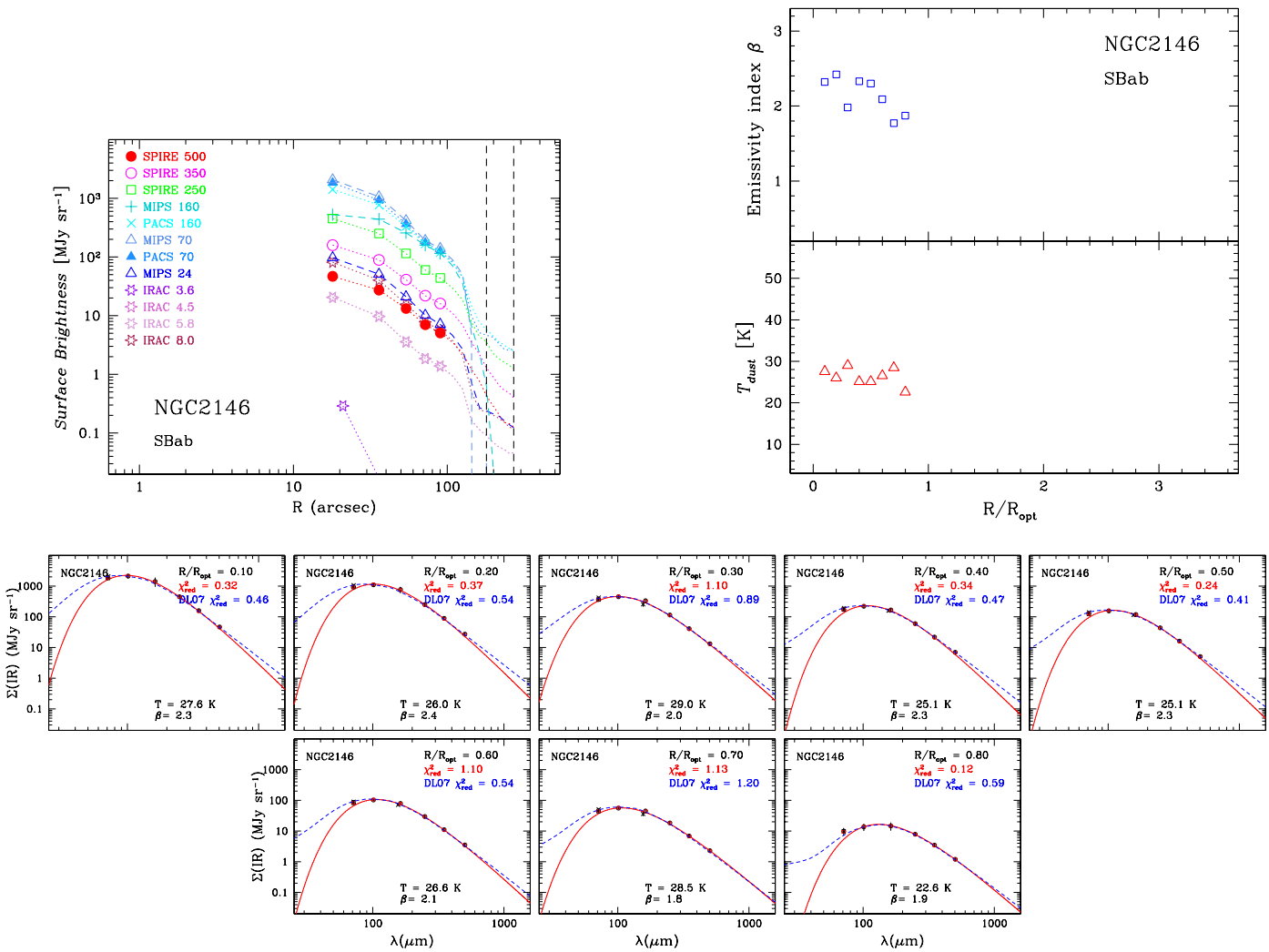

Fig. C.22. *Top left panel*: surface brightness profiles, $\Sigma_{\rm IR}$, for PACS, MIPS, SPIRE, and IRAC 3.6 μm. *Top right panel*: radial temperature trends $T_{\rm dust}$ and emissivity index trends β vs. normalized radii, $R/R_{\rm opt}$. Sets of fluxes are defined over ≥4 wavelengths. The *bottom panels* show each individual SED fit, $\Sigma_{\rm IR}$ vs. wavelength, with best-fit temperature and emissivity index β. The DL07 best-fit models are shown as a (blue) dashed line, and the MBBV fits as a (red) solid one. S/N lower limit = 3.0. The 70 μm (PACS+MIPS) and 500 μm points are excluded from the fits.

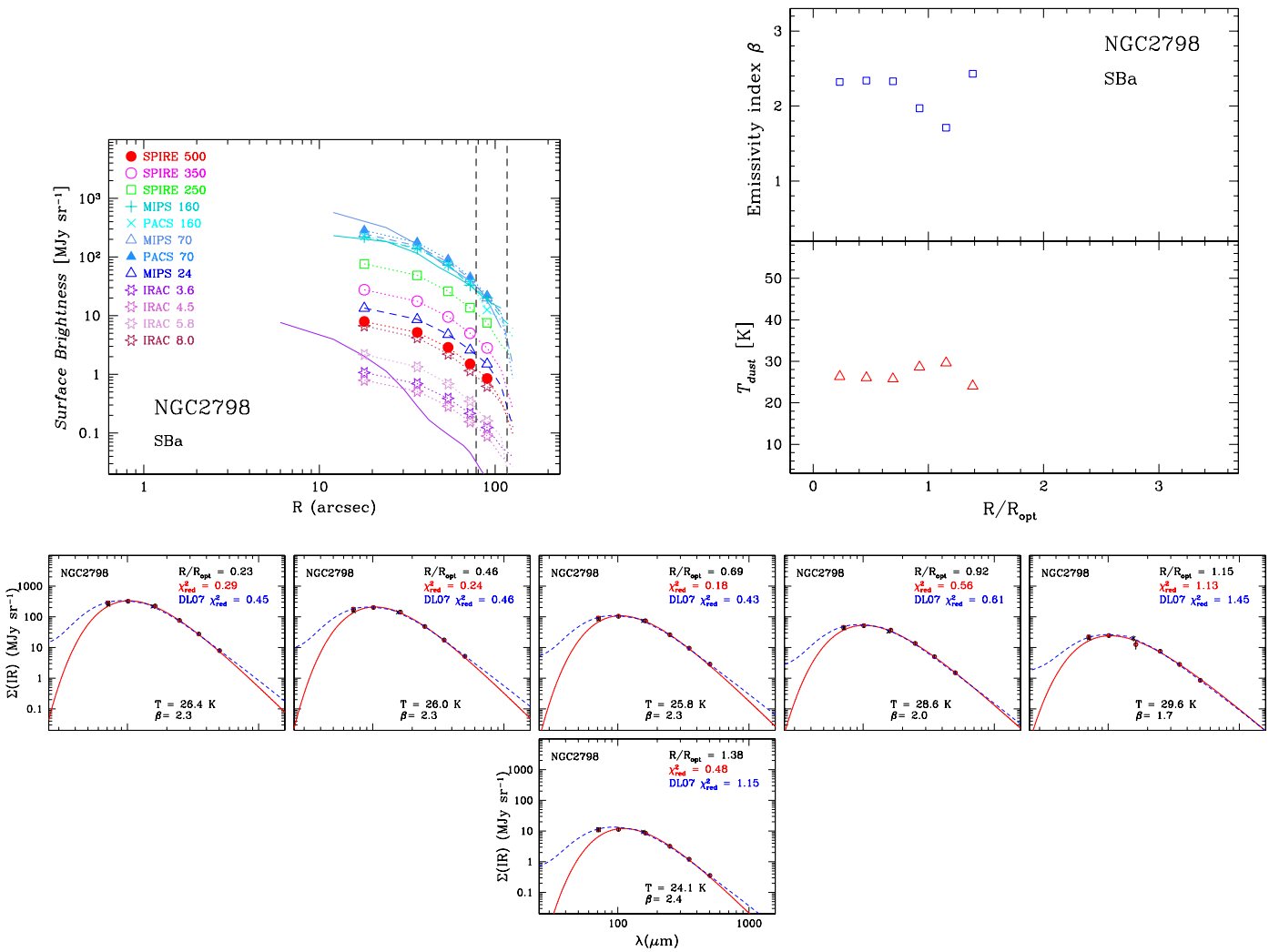

Fig. C.23. *Top left panel*: surface brightness profiles, $\Sigma_{\rm IR}$, for PACS, MIPS, SPIRE, and IRAC 3.6 μm. *Top right panel*: radial temperature trends $T_{\rm dust}$ and emissivity index trends β vs. normalized radii, $R/R_{\rm opt}$. Sets of fluxes are defined over ≥4 wavelengths. The *bottom panels* show each individual SED fit, $\Sigma_{\rm IR}$ vs. wavelength, with best-fit temperature and emissivity index β. The DL07 best-fit models are shown as a (blue) dashed line, and the MBBV fits as a (red) solid one. S/N lower limit = 3.0. The 70 μm (PACS+MIPS) and 500 μm points are excluded from the fits.

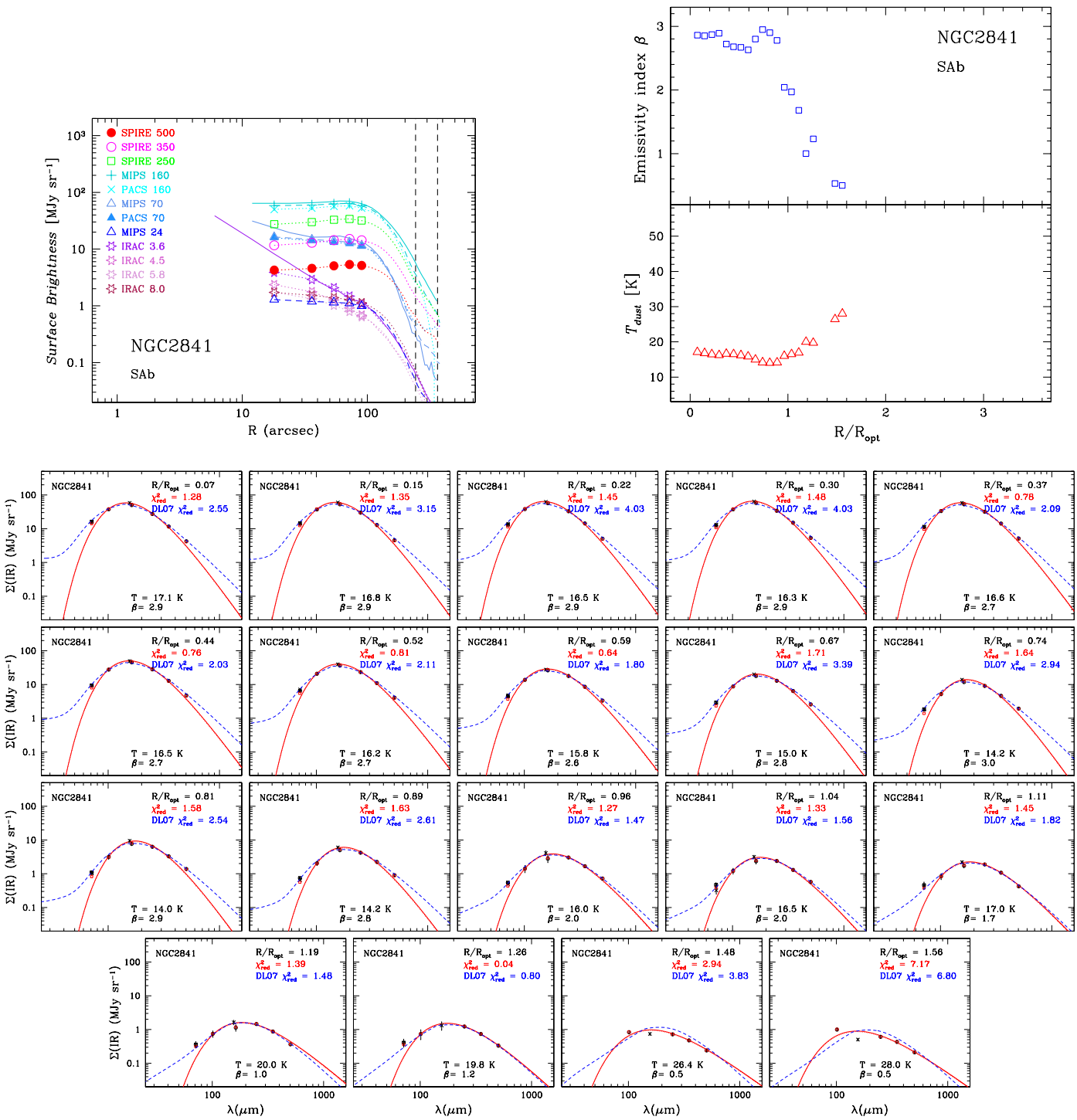

Fig. C.24. *Top left panel*: surface brightness profiles, $\Sigma_{\rm IR}$, for PACS, MIPS, SPIRE, and IRAC 3.6 μm. *Top right panel*: radial temperature trends $T_{\rm dust}$ and emissivity index trends β vs. normalized radii, $R/R_{\rm opt}$. Sets of fluxes are defined over ≥4 wavelengths. The *bottom panels* show each individual SED fit, $\Sigma_{\rm IR}$ vs. wavelength, with best-fit temperature and emissivity index β. The DL07 best-fit models are shown as a (blue) dashed line, and the MBBV fits as a (red) solid one. S/N lower limit = 3.0. The 70 μm (PACS+MIPS) and 500 μm points are excluded from the fits.

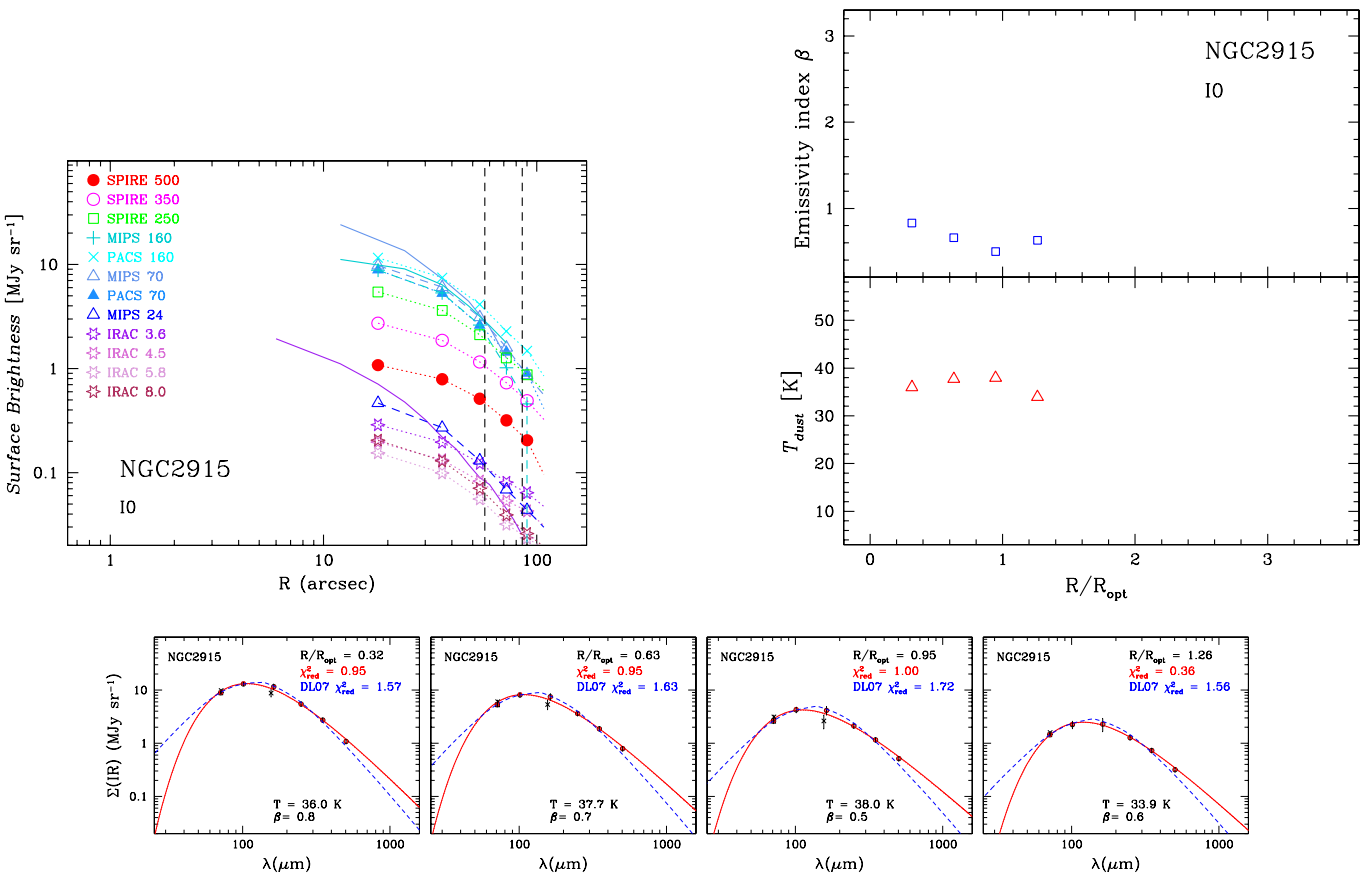

Fig. C.25. *Top left panel*: surface brightness profiles, Σ_{IR}, for PACS, MIPS, SPIRE, and IRAC 3.6 μm. *Top right panel*: radial temperature trends T_{dust} and emissivity index trends β vs. normalized radii, R/R_{opt}. Sets of fluxes are defined over ≥4 wavelengths. The *bottom panels* show each individual SED fit, Σ_{IR} vs. wavelength, with best-fit temperature and emissivity index β. The DL07 best-fit models are shown as a (blue) dashed line, and the MBBV fits as a (red) solid one. S/N lower limit = 3.0. The 70 μm (PACS+MIPS) and 500 μm points are excluded from the fits.

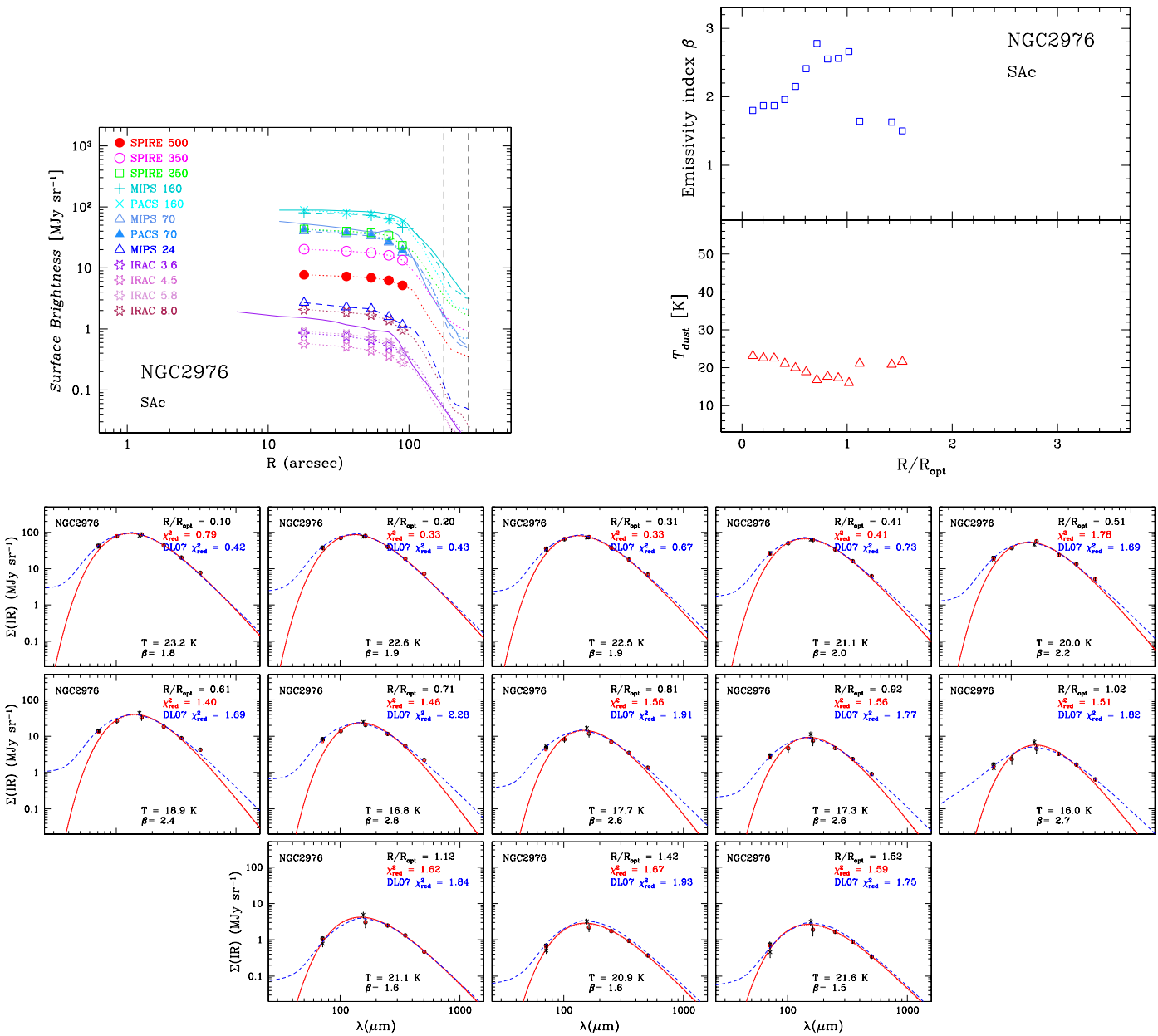

Fig. C.26. *Top left panel*: surface brightness profiles, $\Sigma_{\rm IR}$, for PACS, MIPS, SPIRE, and IRAC 3.6 μm. *Top right panel*: radial temperature trends $T_{\rm dust}$ and emissivity index trends β vs. normalized radii, $R/R_{\rm opt}$. Sets of fluxes are defined over ≥4 wavelengths. The *bottom panels* show each individual SED fit, $\Sigma_{\rm IR}$ vs. wavelength, with best-fit temperature and emissivity index β. The DL07 best-fit models are shown as a (blue) dashed line, and the MBBV fits as a (red) solid one. S/N lower limit = 3.0. The 70 μm (PACS+MIPS) and 500 μm points are excluded from the fits.

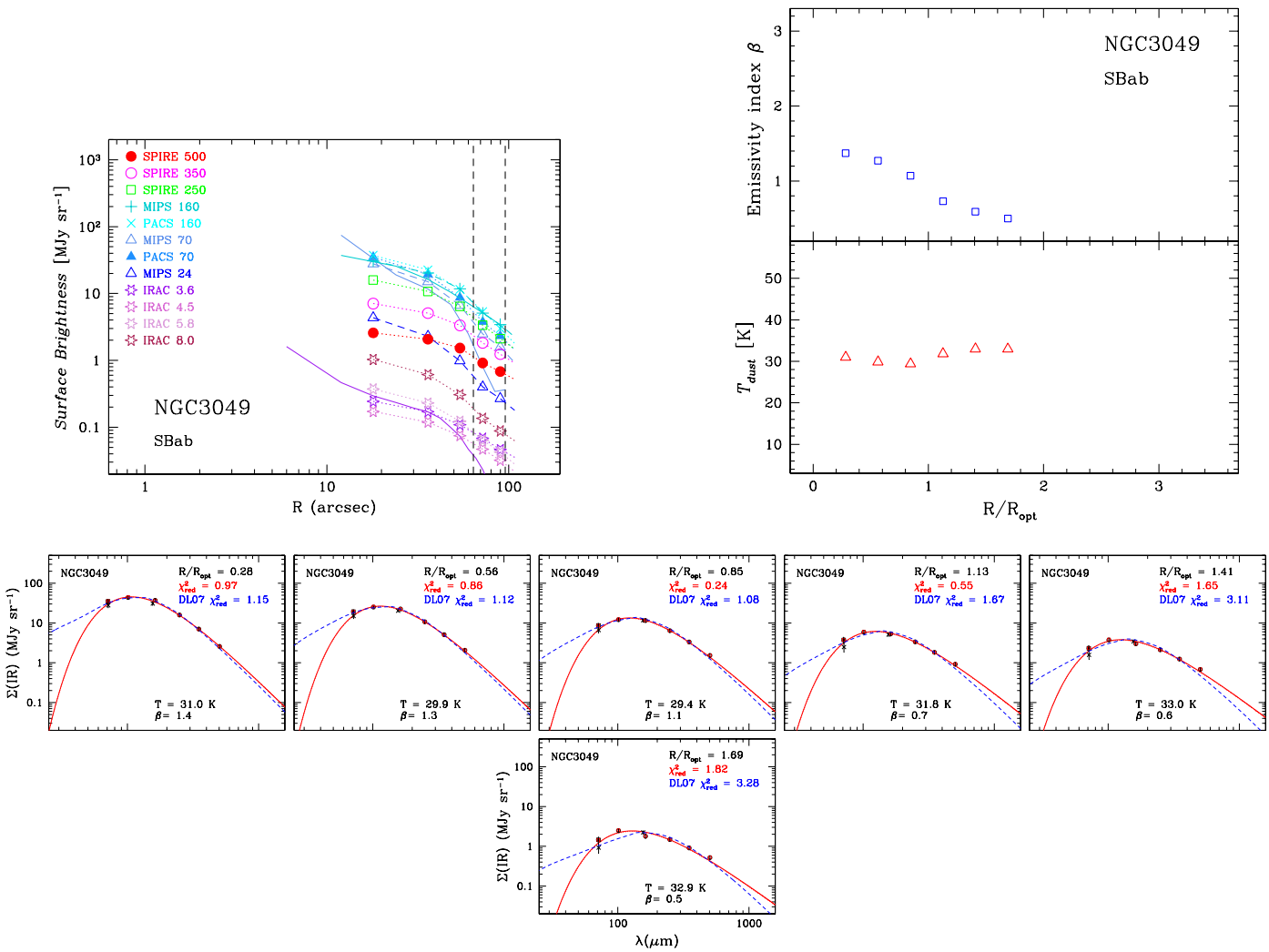

Fig. C.27. *Top left panel*: surface brightness profiles, $\Sigma_{\rm IR}$, for PACS, MIPS, SPIRE, and IRAC 3.6 μm. *Top right panel*: radial temperature trends $T_{\rm dust}$ and emissivity index trends β vs. normalized radii, $R/R_{\rm opt}$. Sets of fluxes are defined over ≥4 wavelengths. The *bottom panels* show each individual SED fit, $\Sigma_{\rm IR}$ vs. wavelength, with best-fit temperature and emissivity index β. The DL07 best-fit models are shown as a (blue) dashed line, and the MBBV fits as a (red) solid one. S/N lower limit = 3.0. The 70 μm (PACS+MIPS) and 500 μm points are excluded from the fits.

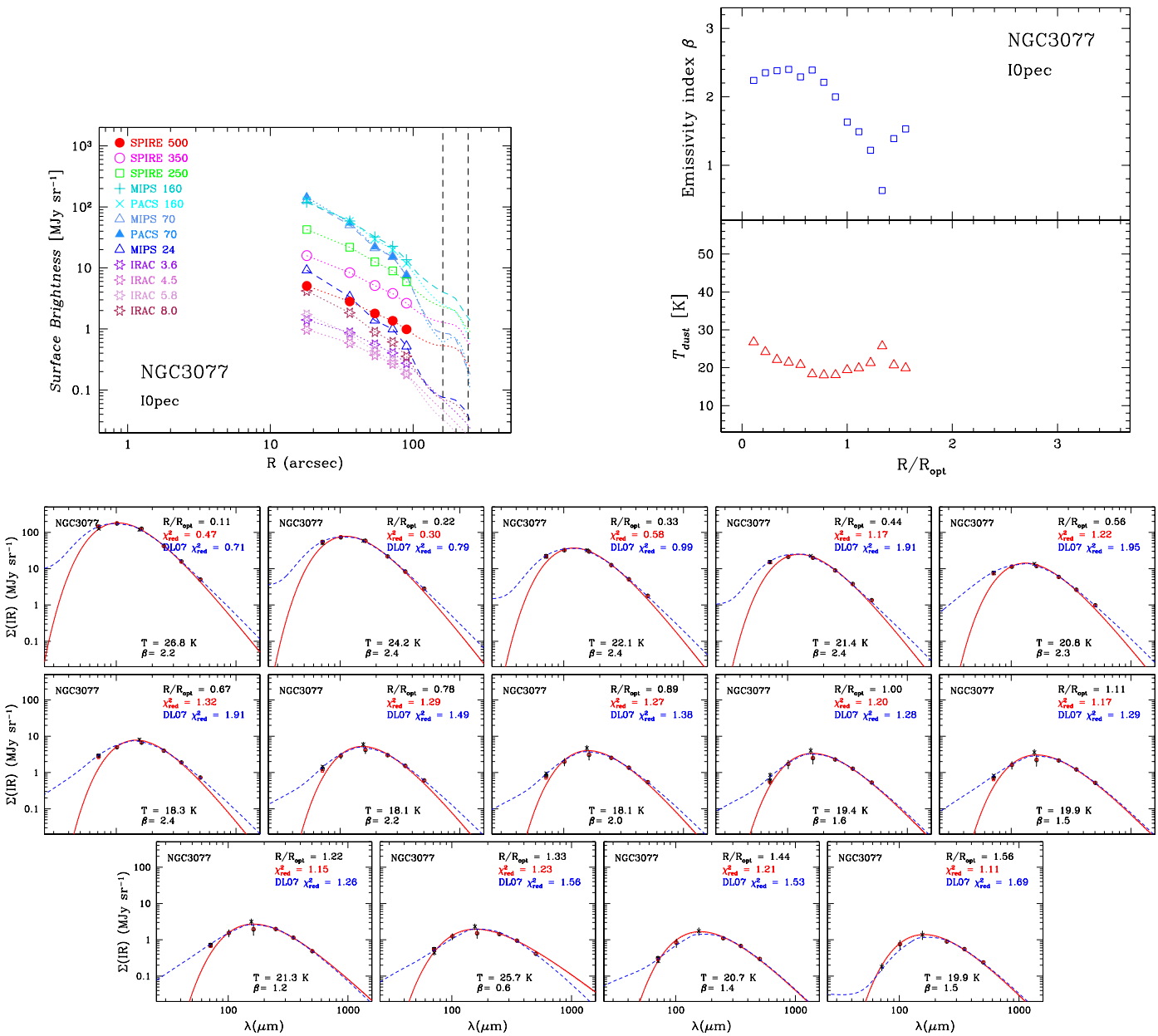

Fig. C.28. *Top left panel*: surface brightness profiles, $\Sigma_{\rm IR}$, for PACS, MIPS, SPIRE, and IRAC 3.6 μm. *Top right panel*: radial temperature trends $T_{\rm dust}$ and emissivity index trends β vs. normalized radii, $R/R_{\rm opt}$. Sets of fluxes are defined over ≥4 wavelengths. The *bottom panels* show each individual SED fit, $\Sigma_{\rm IR}$ vs. wavelength, with best-fit temperature and emissivity index β. The DL07 best-fit models are shown as a (blue) dashed line, and the MBBV fits as a (red) solid one. S/N lower limit = 3.0. The 70 μm (PACS+MIPS) and 500 μm points are excluded from the fits.

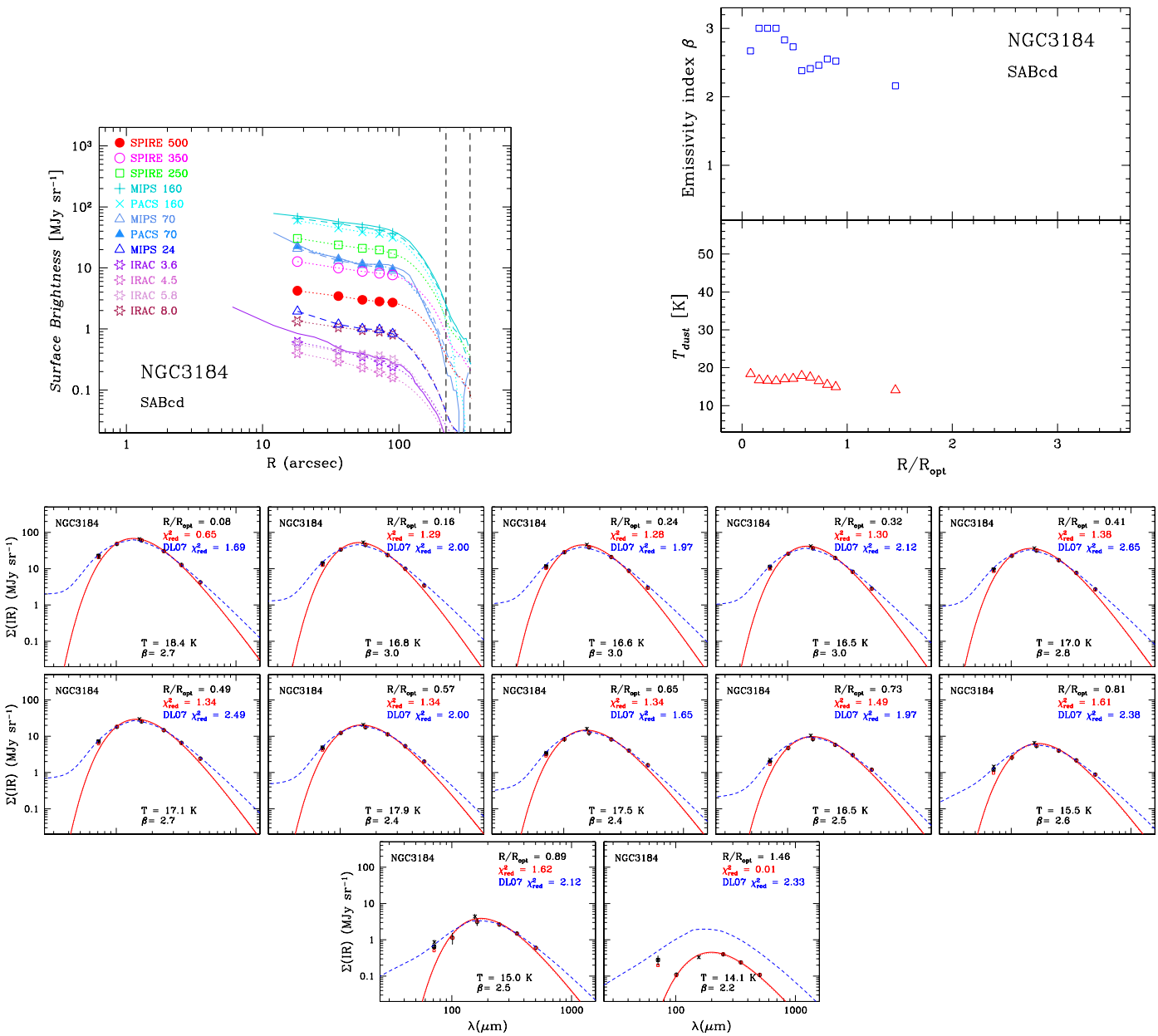

Fig. C.29. *Top left panel*: surface brightness profiles, $\Sigma_{\rm IR}$, for PACS, MIPS, SPIRE, and IRAC 3.6 μm. *Top right panel*: radial temperature trends $T_{\rm dust}$ and emissivity index trends β vs. normalized radii, $R/R_{\rm opt}$. Sets of fluxes are defined over ≥4 wavelengths. The *bottom panels* show each individual SED fit, $\Sigma_{\rm IR}$ vs. wavelength, with best-fit temperature and emissivity index β. The DL07 best-fit models are shown as a (blue) dashed line, and the MBBV fits as a (red) solid one. S/N lower limit = 3.0. The 70 μm (PACS+MIPS) and 500 μm points are excluded from the fits.

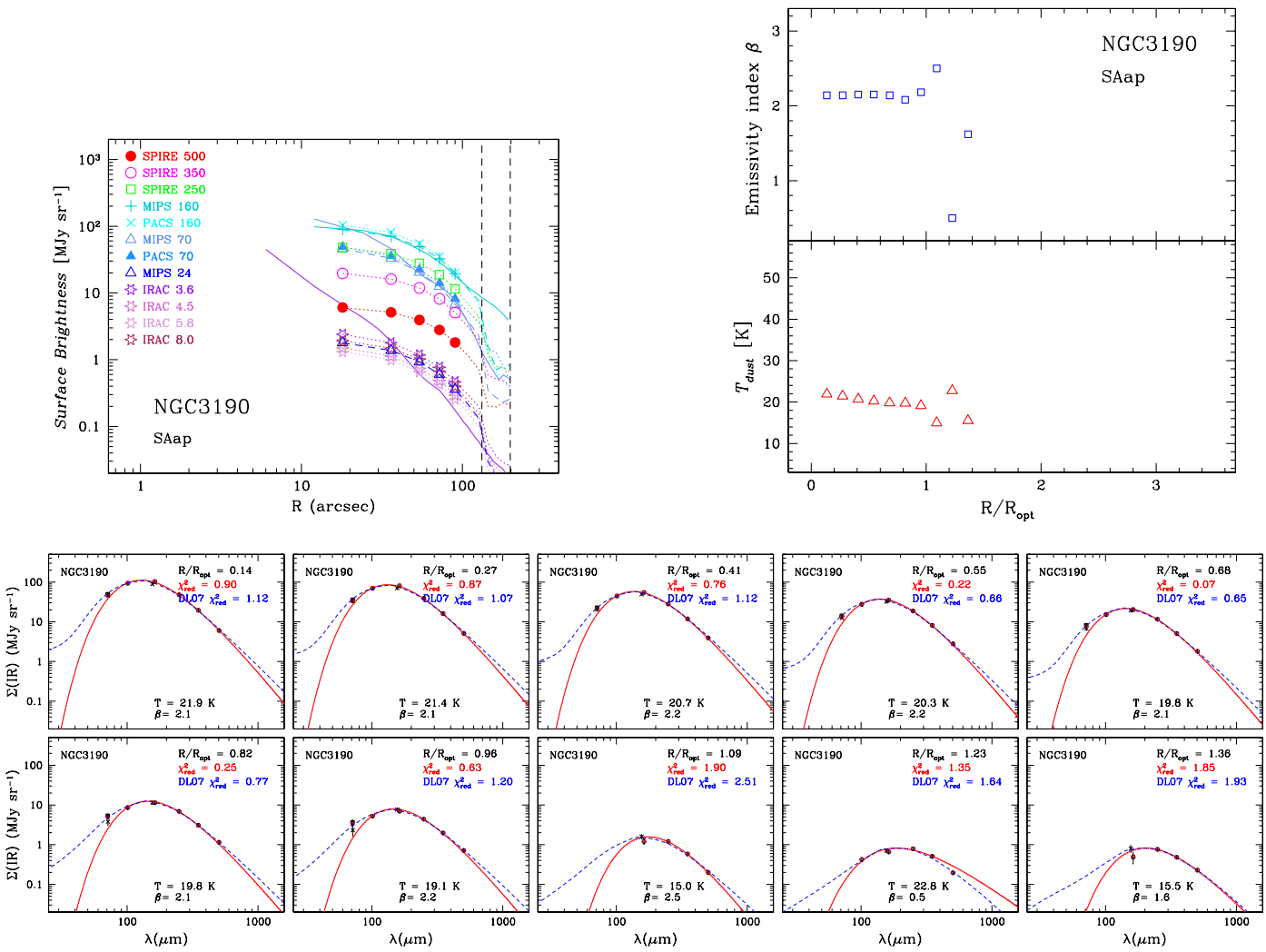

Fig. C.30. *Top left panel*: surface brightness profiles, $\Sigma_{\rm IR}$, for PACS, MIPS, SPIRE, and IRAC 3.6 μm. *Top right panel*: radial temperature trends $T_{\rm dust}$ and emissivity index trends β vs. normalized radii, $R/R_{\rm opt}$. Sets of fluxes are defined over ≥4 wavelengths. The *bottom panels* show each individual SED fit, $\Sigma_{\rm IR}$ vs. wavelength, with best-fit temperature and emissivity index β. The DL07 best-fit models are shown as a (blue) dashed line, and the MBBV fits as a (red) solid one. S/N lower limit = 3.0. The 70 μm (PACS+MIPS) and 500 μm points are excluded from the fits.

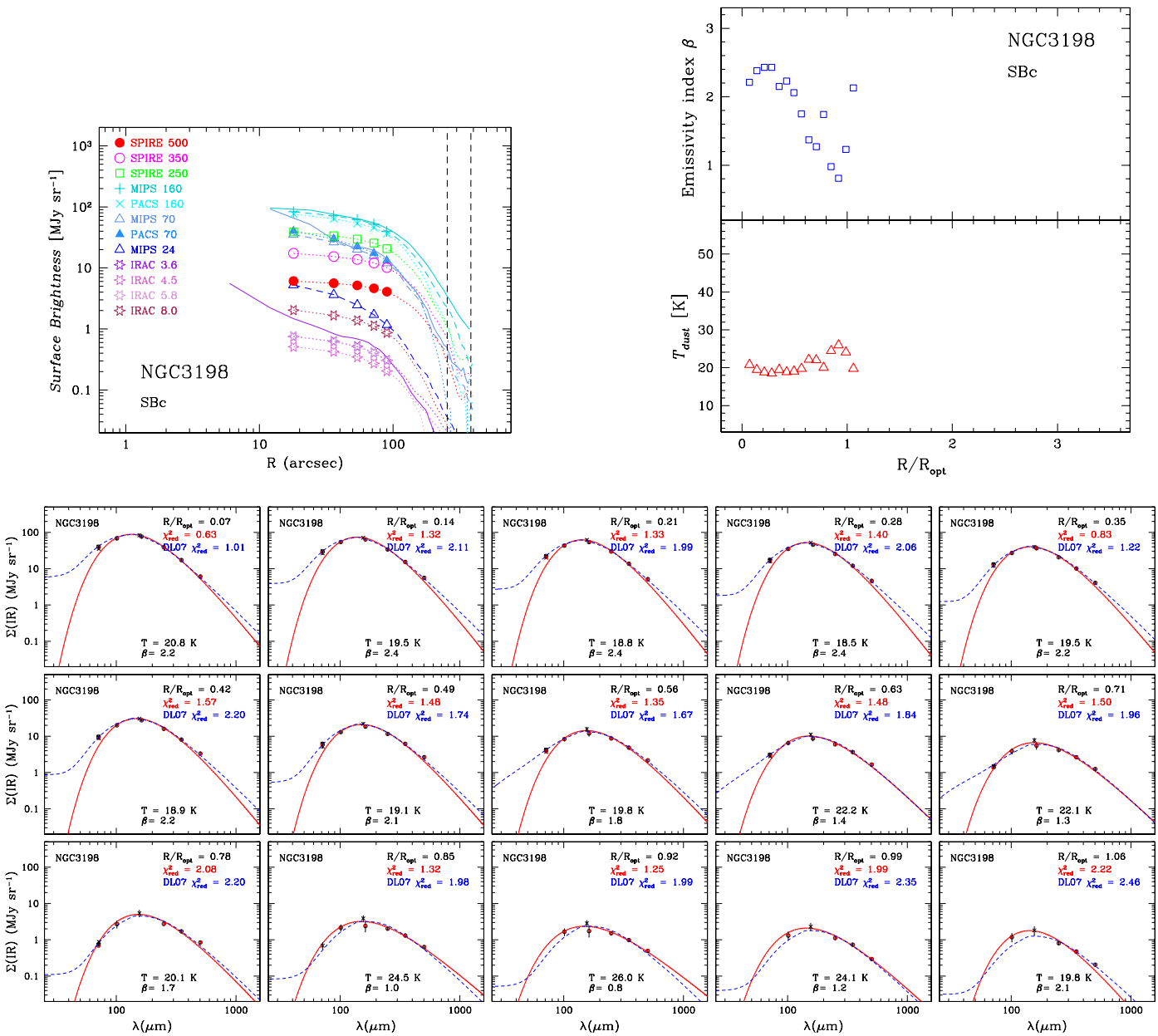

Fig. C.31. *Top left panel*: surface brightness profiles, $\Sigma_{\rm IR}$, for PACS, MIPS, SPIRE, and IRAC 3.6 μm. *Top right panel*: radial temperature trends $T_{\rm dust}$ and emissivity index trends β vs. normalized radii, $R/R_{\rm opt}$. Sets of fluxes are defined over ≥4 wavelengths. The *bottom panels* show each individual SED fit, $\Sigma_{\rm IR}$ vs. wavelength, with best-fit temperature and emissivity index β. The DL07 best-fit models are shown as a (blue) dashed line, and the MBBV fits as a (red) solid one. S/N lower limit = 3.0. The 70 μm (PACS+MIPS) and 500 μm points are excluded from the fits.

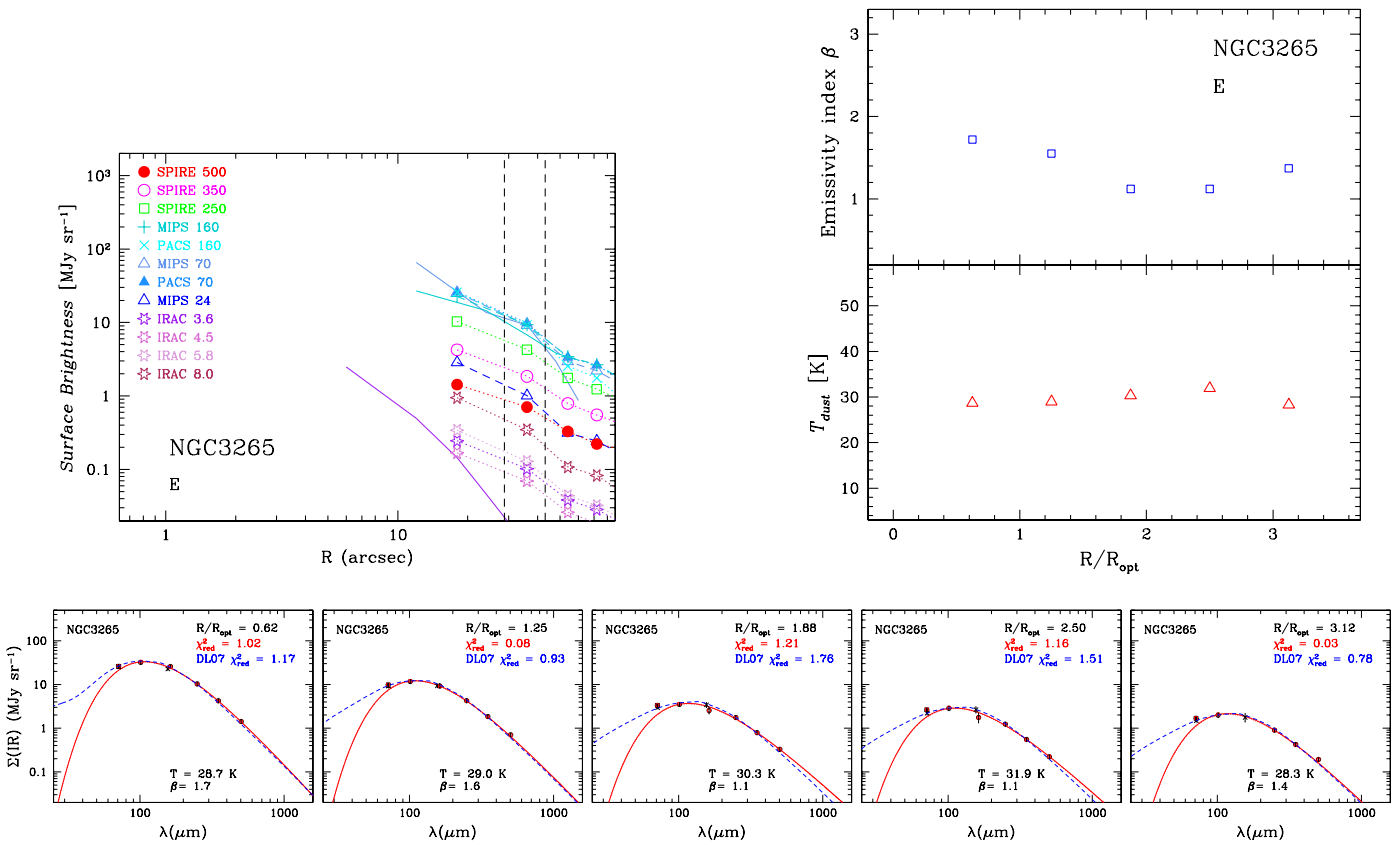

Fig. C.32. *Top left panel*: surface brightness profiles, $\Sigma_{\rm IR}$, for PACS, MIPS, SPIRE, and IRAC 3.6 μm. *Top right panel*: radial temperature trends $T_{\rm dust}$ and emissivity index trends β vs. normalized radii, $R/R_{\rm opt}$. Sets of fluxes are defined over ≥4 wavelengths. The *bottom panels* show each individual SED fit, $\Sigma_{\rm IR}$ vs. wavelength, with best-fit temperature and emissivity index β. The DL07 best-fit models are shown as a (blue) dashed line, and the MBBV fits as a (red) solid one. S/N lower limit = 3.0. The 70 μm (PACS+MIPS) and 500 μm points are excluded from the fits.

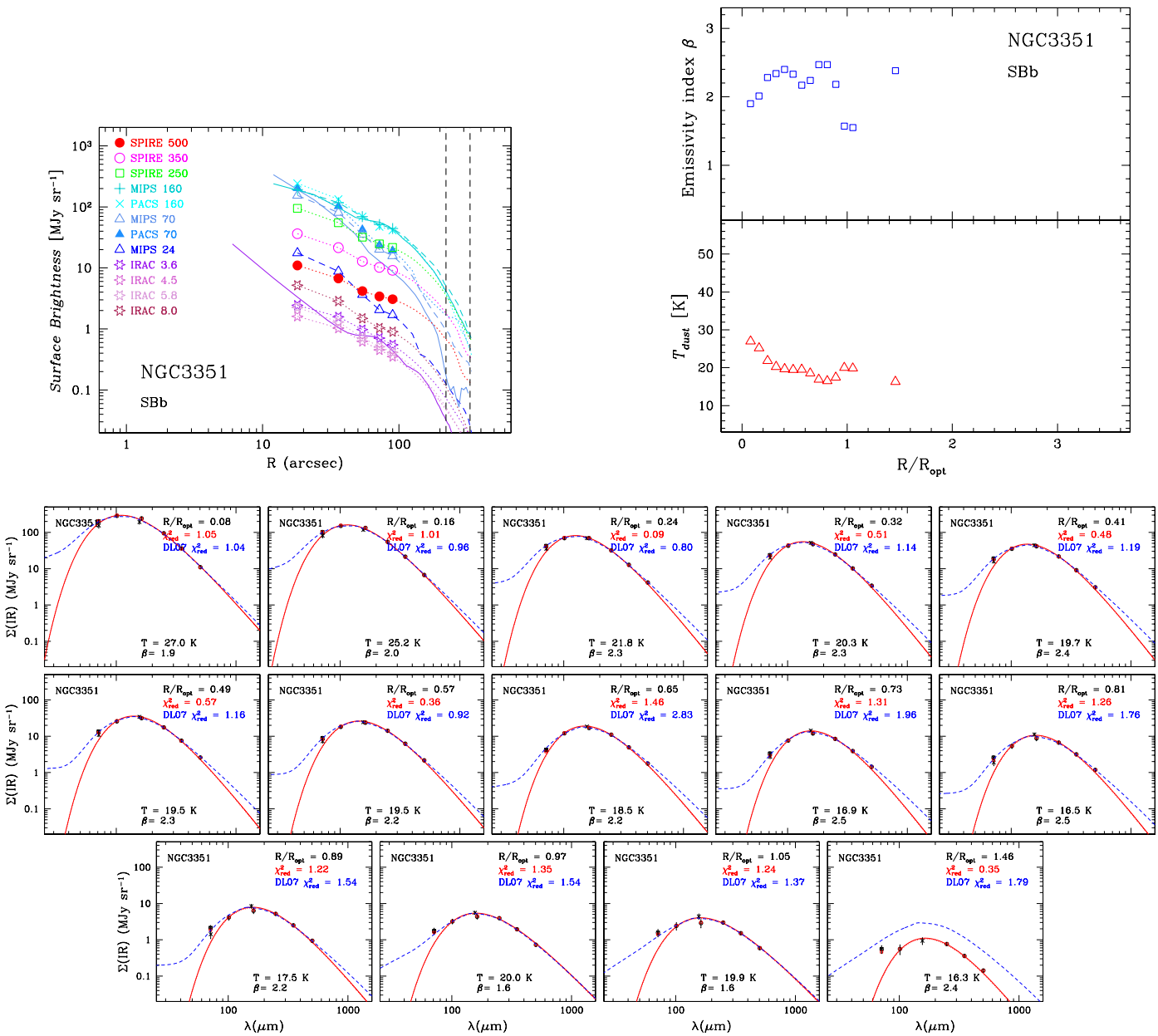

Fig. C.33. *Top left panel*: surface brightness profiles, $\Sigma_{\rm IR}$, for PACS, MIPS, SPIRE, and IRAC 3.6 μm. *Top right panel*: radial temperature trends $T_{\rm dust}$ and emissivity index trends β vs. normalized radii, $R/R_{\rm opt}$. Sets of fluxes are defined over ≥4 wavelengths. The *bottom panels* show each individual SED fit, $\Sigma_{\rm IR}$ vs. wavelength, with best-fit temperature and emissivity index β. The DL07 best-fit models are shown as a (blue) dashed line, and the MBBV fits as a (red) solid one. S/N lower limit = 3.0. The 70 μm (PACS+MIPS) and 500 μm points are excluded from the fits.

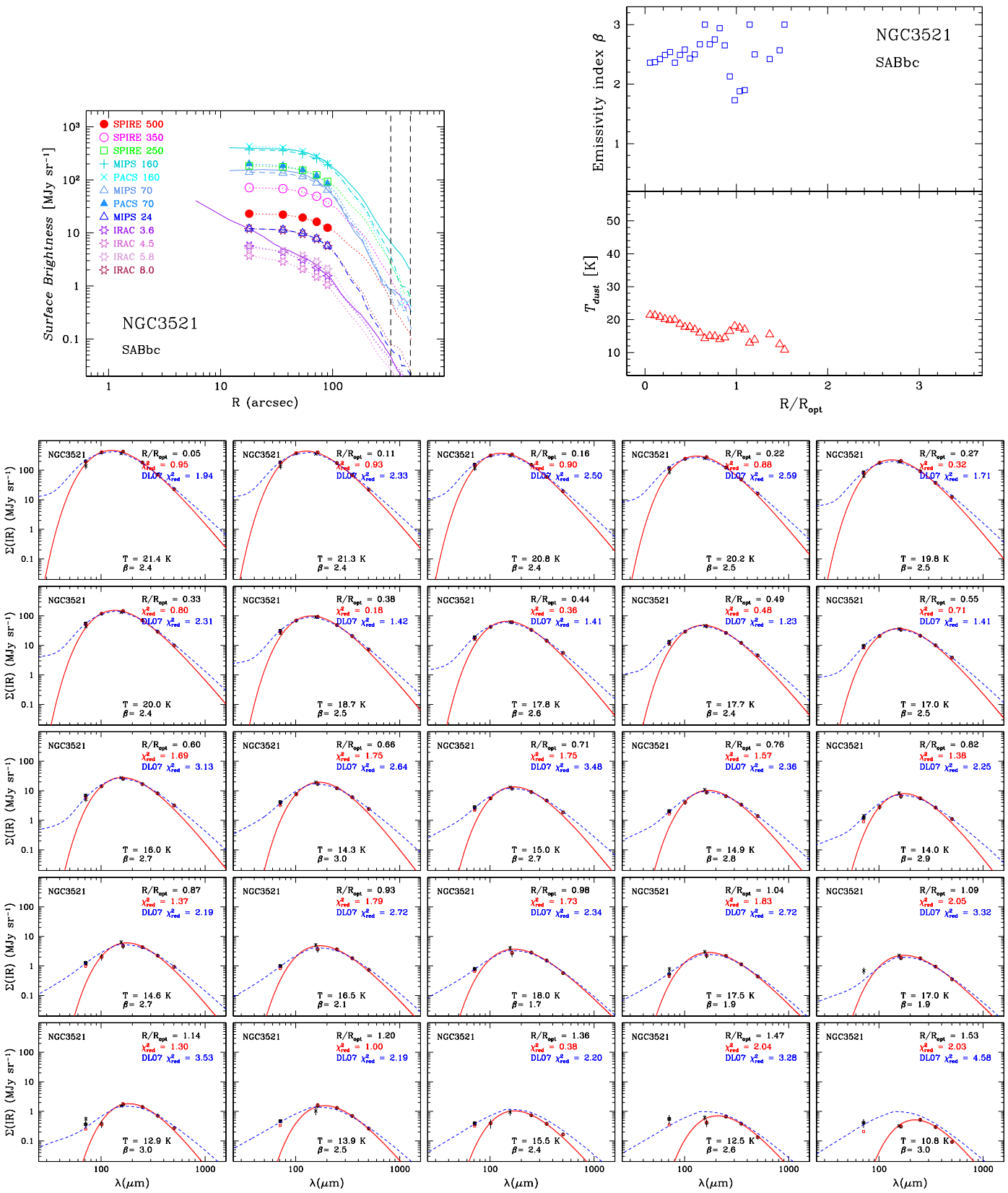

Fig. C.34. *Top left panel*: surface brightness profiles, $\Sigma_{\rm IR}$, for PACS, MIPS, SPIRE, and IRAC 3.6 μm. *Top right panel*: radial temperature trends $T_{\rm dust}$ and emissivity index trends β vs. normalized radii, $R/R_{\rm opt}$. Sets of fluxes are defined over ≥4 wavelengths. The *bottom panels* show each individual SED fit, $\Sigma_{\rm IR}$ vs. wavelength, with best-fit temperature and emissivity index β. The DL07 best-fit models are shown as a (blue) dashed line, and the MBBV fits as a (red) solid one. S/N lower limit = 3.0. The 70 μm (PACS+MIPS) and 500 μm points are excluded from the fits.

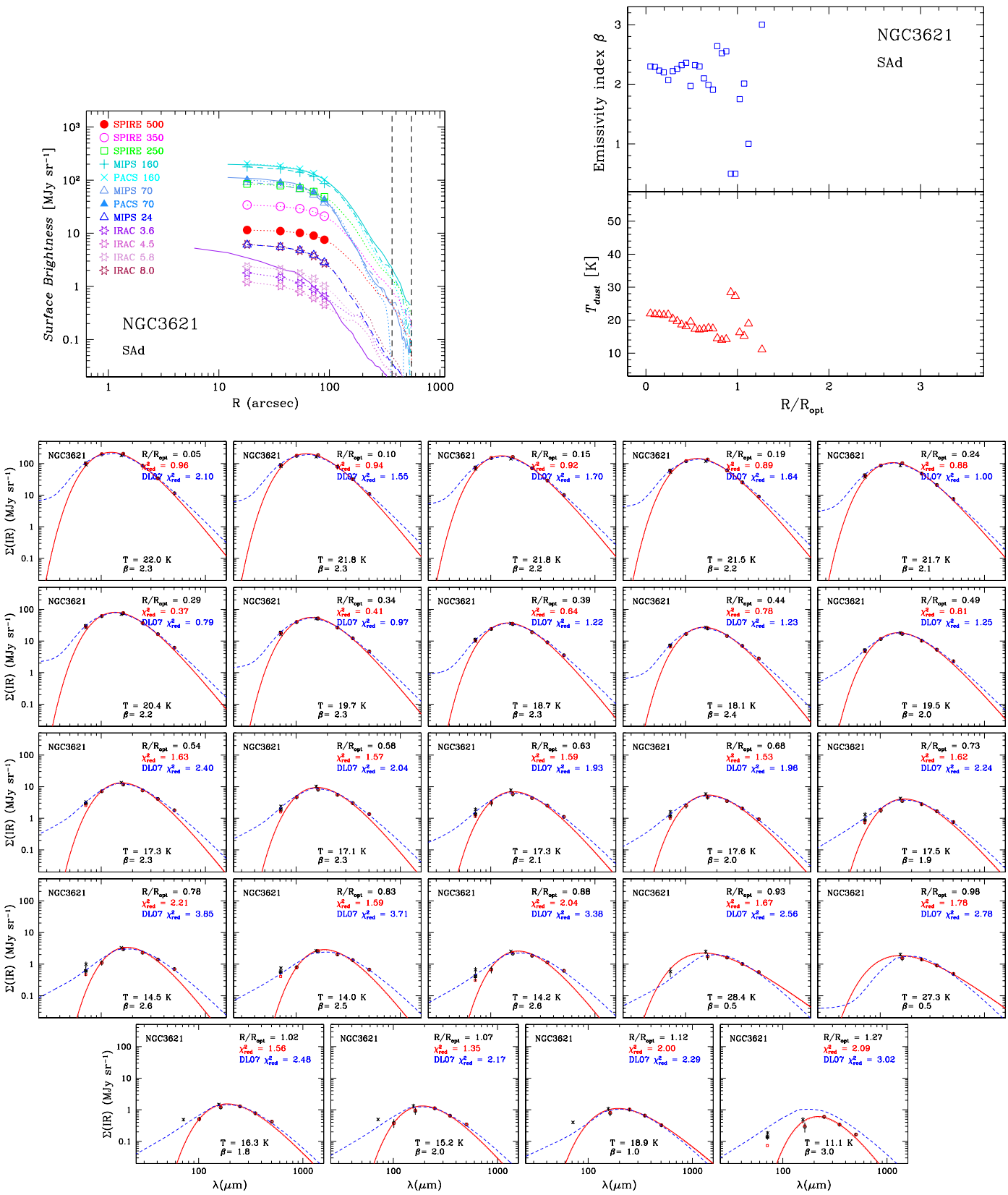

Fig. C.35. *Top left panel*: surface brightness profiles, $\Sigma_{\rm IR}$, for PACS, MIPS, SPIRE, and IRAC 3.6 μm. *Top right panel*: radial temperature trends $T_{\rm dust}$ and emissivity index trends β vs. normalized radii, $R/R_{\rm opt}$. Sets of fluxes are defined over ≥4 wavelengths. The *bottom panels* show each individual SED fit, $\Sigma_{\rm IR}$ vs. wavelength, with best-fit temperature and emissivity index β. The DL07 best-fit models are shown as a (blue) dashed line, and the MBBV fits as a (red) solid one. S/N lower limit = 3.0. The 70 μm (PACS+MIPS) and 500 μm points are excluded from the fits.

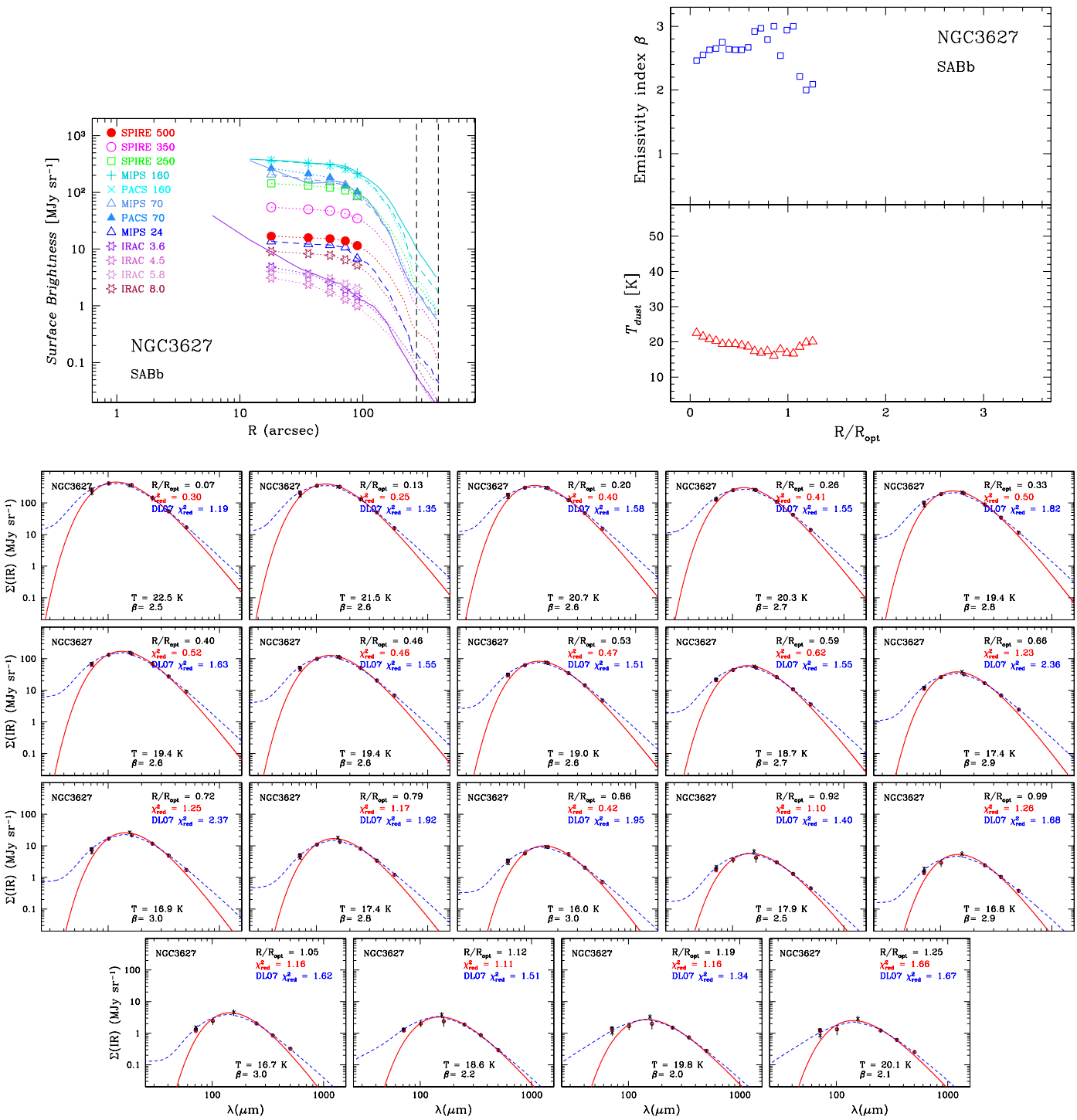

Fig. C.36. *Top left panel*: surface brightness profiles, $\Sigma_{\rm IR}$, for PACS, MIPS, SPIRE, and IRAC 3.6 μm. *Top right panel*: radial temperature trends $T_{\rm dust}$ and emissivity index trends β vs. normalized radii, $R/R_{\rm opt}$. Sets of fluxes are defined over ≥4 wavelengths. The *bottom panels* show each individual SED fit, $\Sigma_{\rm IR}$ vs. wavelength, with best-fit temperature and emissivity index β. The DL07 best-fit models are shown as a (blue) dashed line, and the MBBV fits as a (red) solid one. S/N lower limit = 3.0. The 70 μm (PACS+MIPS) and 500 μm points are excluded from the fits.

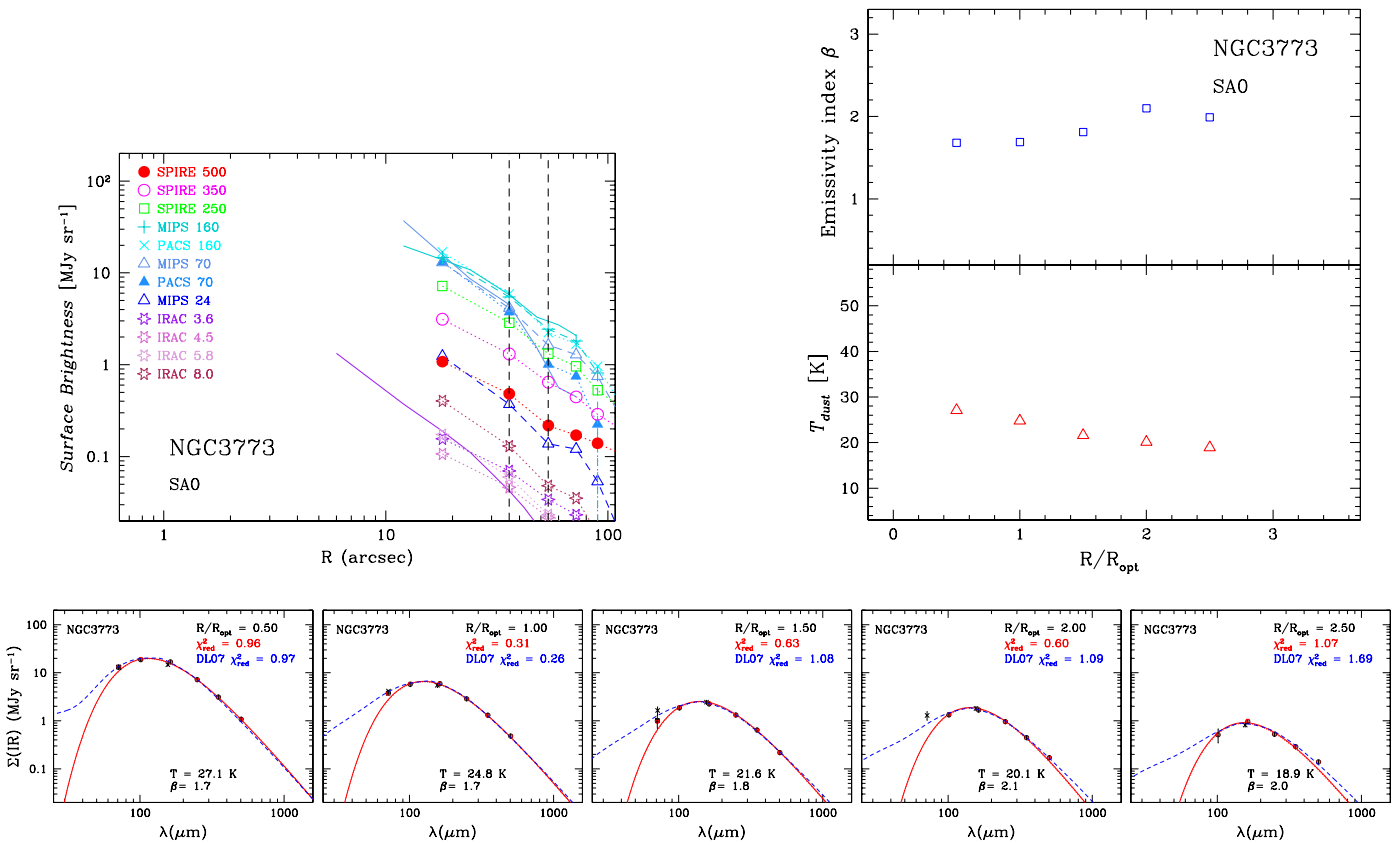

Fig. C.37. *Top left panel*: surface brightness profiles, $\Sigma_{\rm IR}$, for PACS, MIPS, SPIRE, and IRAC 3.6 μm. *Top right panel*: radial temperature trends $T_{\rm dust}$ and emissivity index trends β vs. normalized radii, $R/R_{\rm opt}$. Sets of fluxes are defined over ≥4 wavelengths. The *bottom panels* show each individual SED fit, $\Sigma_{\rm IR}$ vs. wavelength, with best-fit temperature and emissivity index β. The DL07 best-fit models are shown as a (blue) dashed line, and the MBBV fits as a (red) solid one. S/N lower limit = 3.0. The 70 μm (PACS+MIPS) and 500 μm points are excluded from the fits.

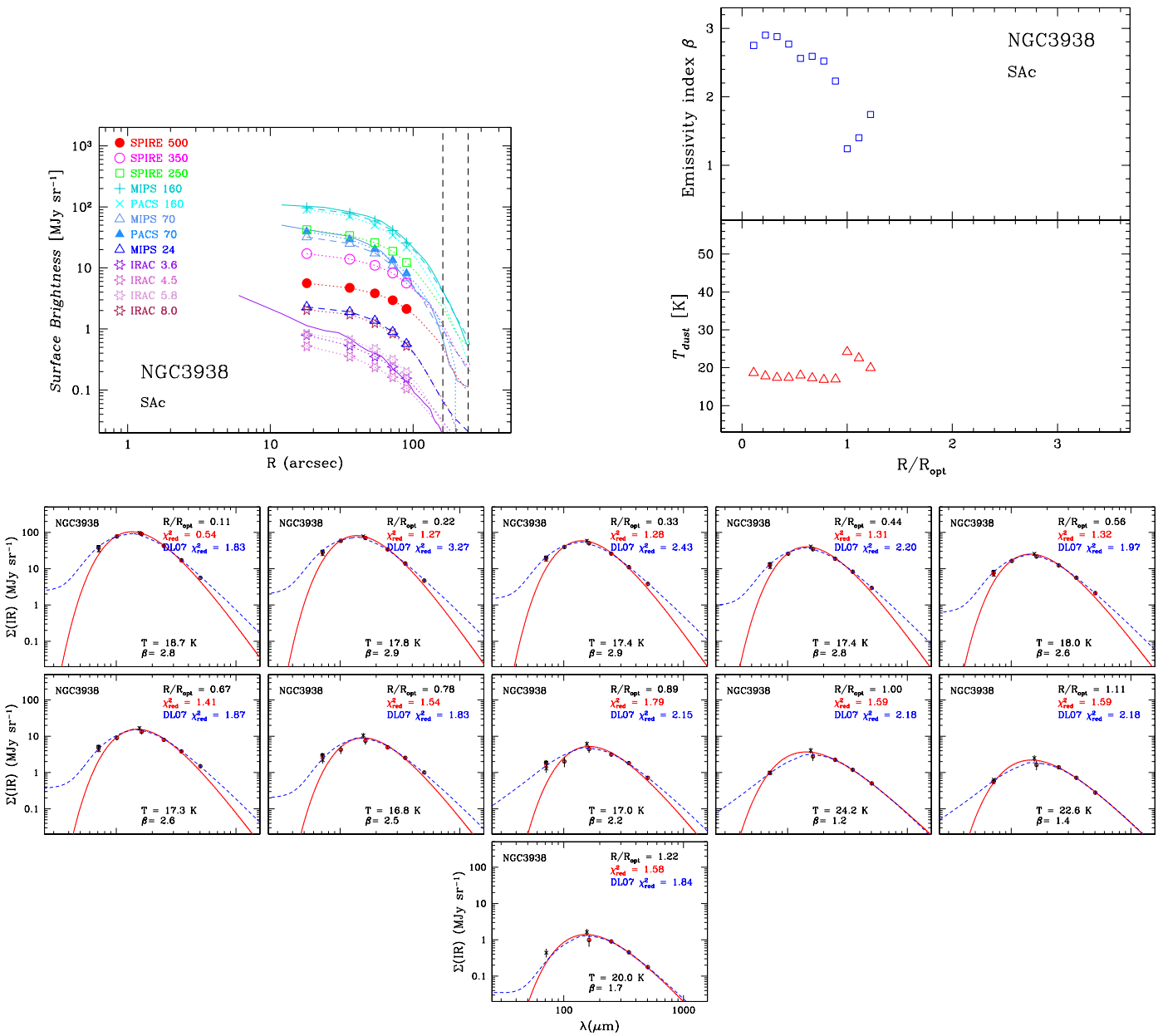

Fig. C.38. *Top left panel*: surface brightness profiles, $\Sigma_{\rm IR}$, for PACS, MIPS, SPIRE, and IRAC 3.6 μm. *Top right panel*: radial temperature trends $T_{\rm dust}$ and emissivity index trends β vs. normalized radii, $R/R_{\rm opt}$. Sets of fluxes are defined over ≥4 wavelengths. The *bottom panels* show each individual SED fit, $\Sigma_{\rm IR}$ vs. wavelength, with best-fit temperature and emissivity index β. The DL07 best-fit models are shown as a (blue) dashed line, and the MBBV fits as a (red) solid one. S/N lower limit = 3.0. The 70 μm (PACS+MIPS) and 500 μm points are excluded from the fits.

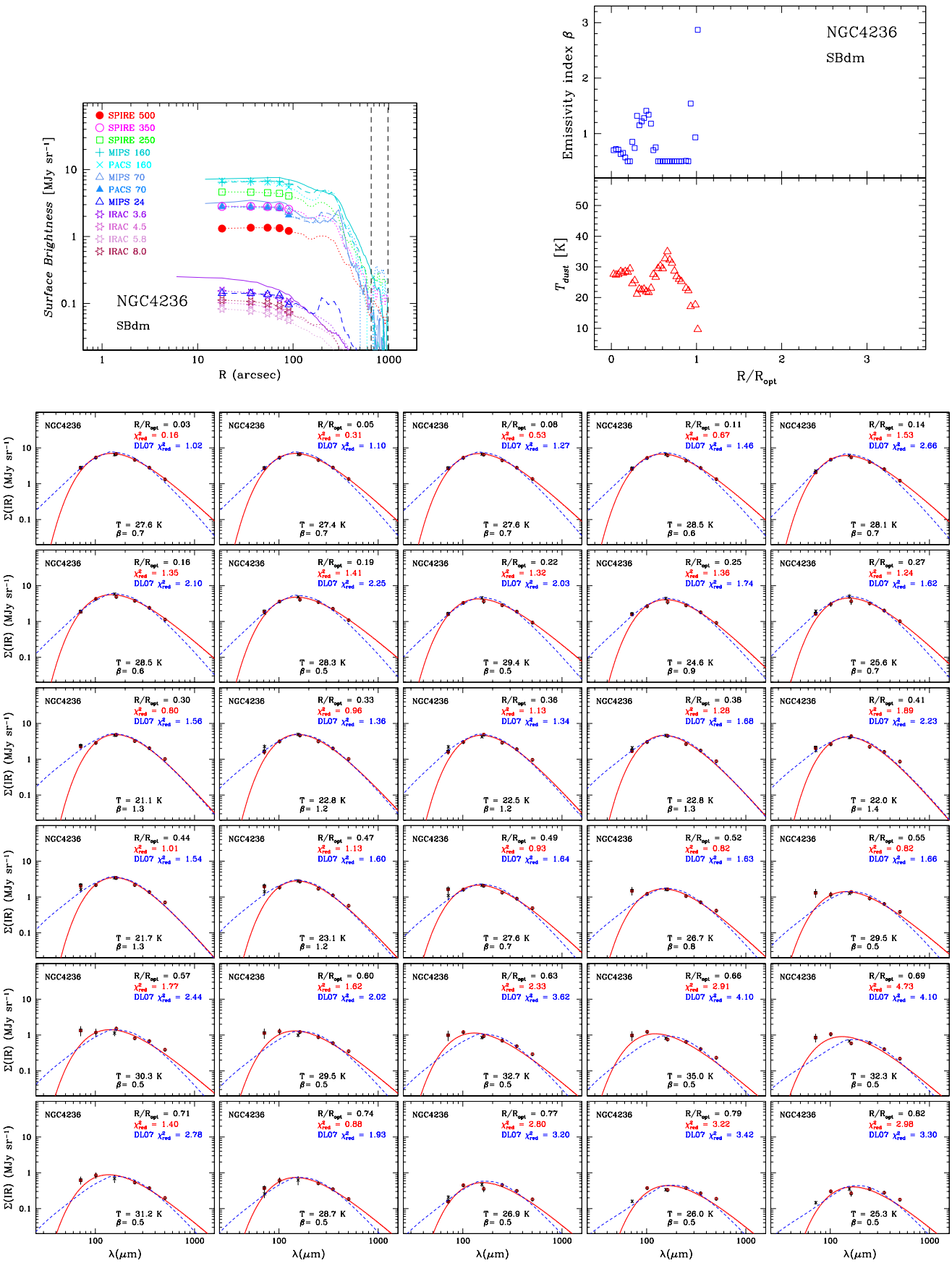

Fig. C.39. *Top left panel*: surface brightness profiles, $\Sigma_{\rm IR}$, for PACS, MIPS, SPIRE, and IRAC 3.6 μm. *Top right panel*: radial temperature trends $T_{\rm dust}$ and emissivity index trends β vs. normalized radii, $R/R_{\rm opt}$. Sets of fluxes are defined over ≥4 wavelengths. The *bottom panels* show each individual SED fit, $\Sigma_{\rm IR}$ vs. wavelength, with best-fit temperature and emissivity index β. The DL07 best-fit models are shown as a (blue) dashed line, and the MBBV fits as a (red) solid one. S/N lower limit = 3.0. The 70 μm (PACS+MIPS) and 500 μm points are excluded from the fits.

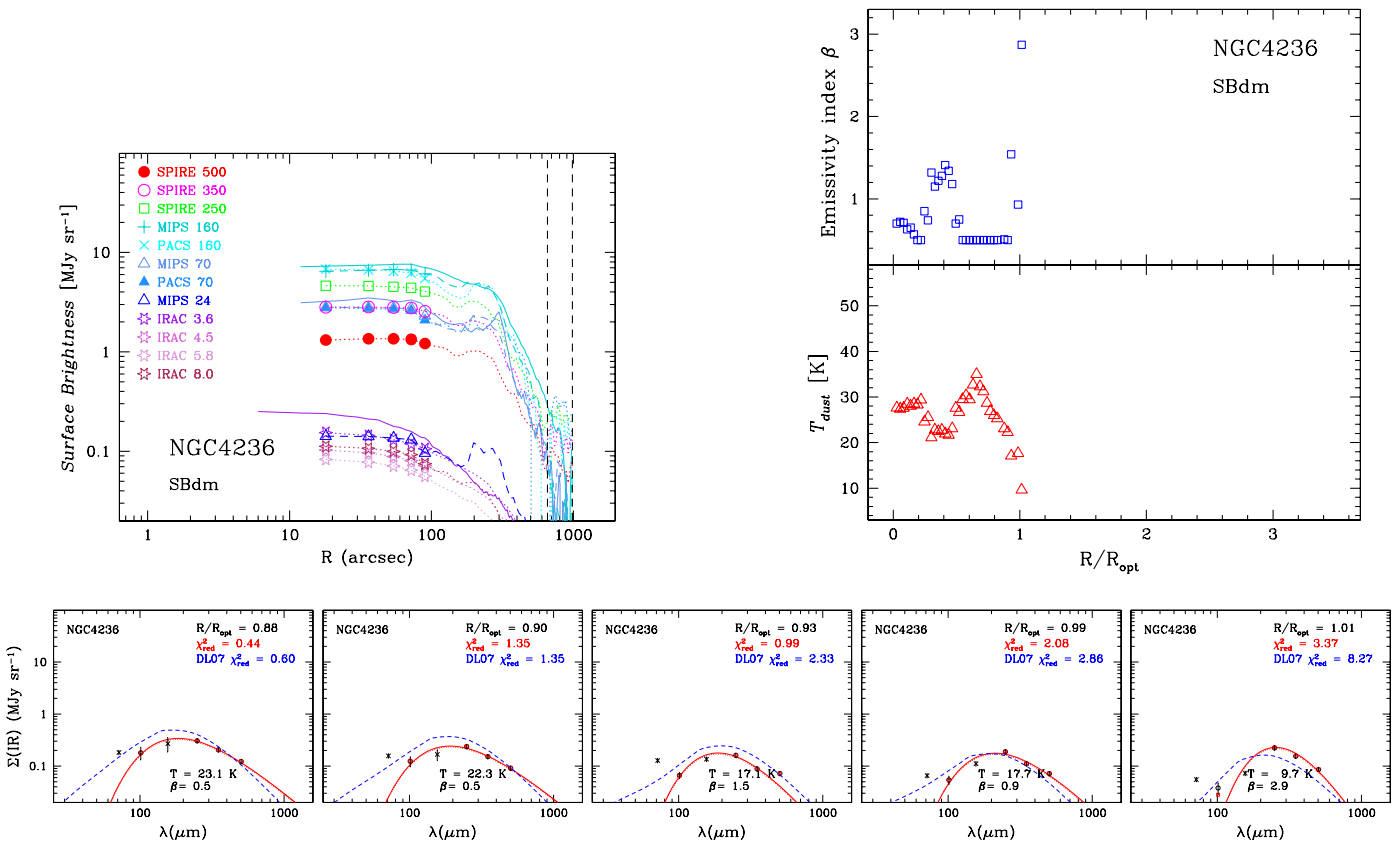

Fig. C.39. continued.

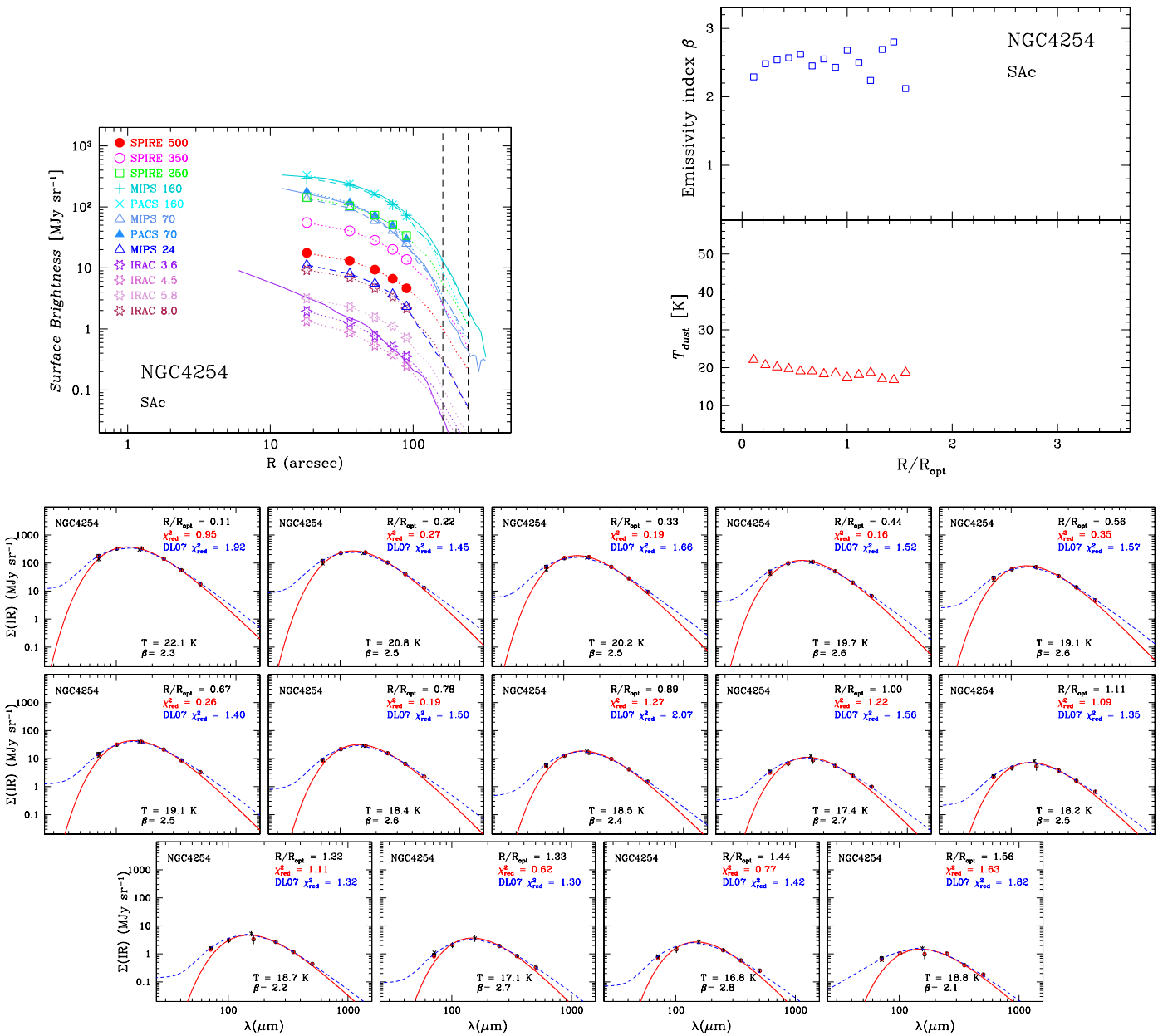

Fig. C.40. *Top left panel*: surface brightness profiles, $\Sigma_{\rm IR}$, for PACS, MIPS, SPIRE, and IRAC 3.6 μm. *Top right panel*: radial temperature trends $T_{\rm dust}$ and emissivity index trends β vs. normalized radii, $R/R_{\rm opt}$. Sets of fluxes are defined over ≥4 wavelengths. The *bottom panels* show each individual SED fit, $\Sigma_{\rm IR}$ vs. wavelength, with best-fit temperature and emissivity index β. The DL07 best-fit models are shown as a (blue) dashed line, and the MBBV fits as a (red) solid one. S/N lower limit = 3.0. The 70 μm (PACS+MIPS) and 500 μm points are excluded from the fits.

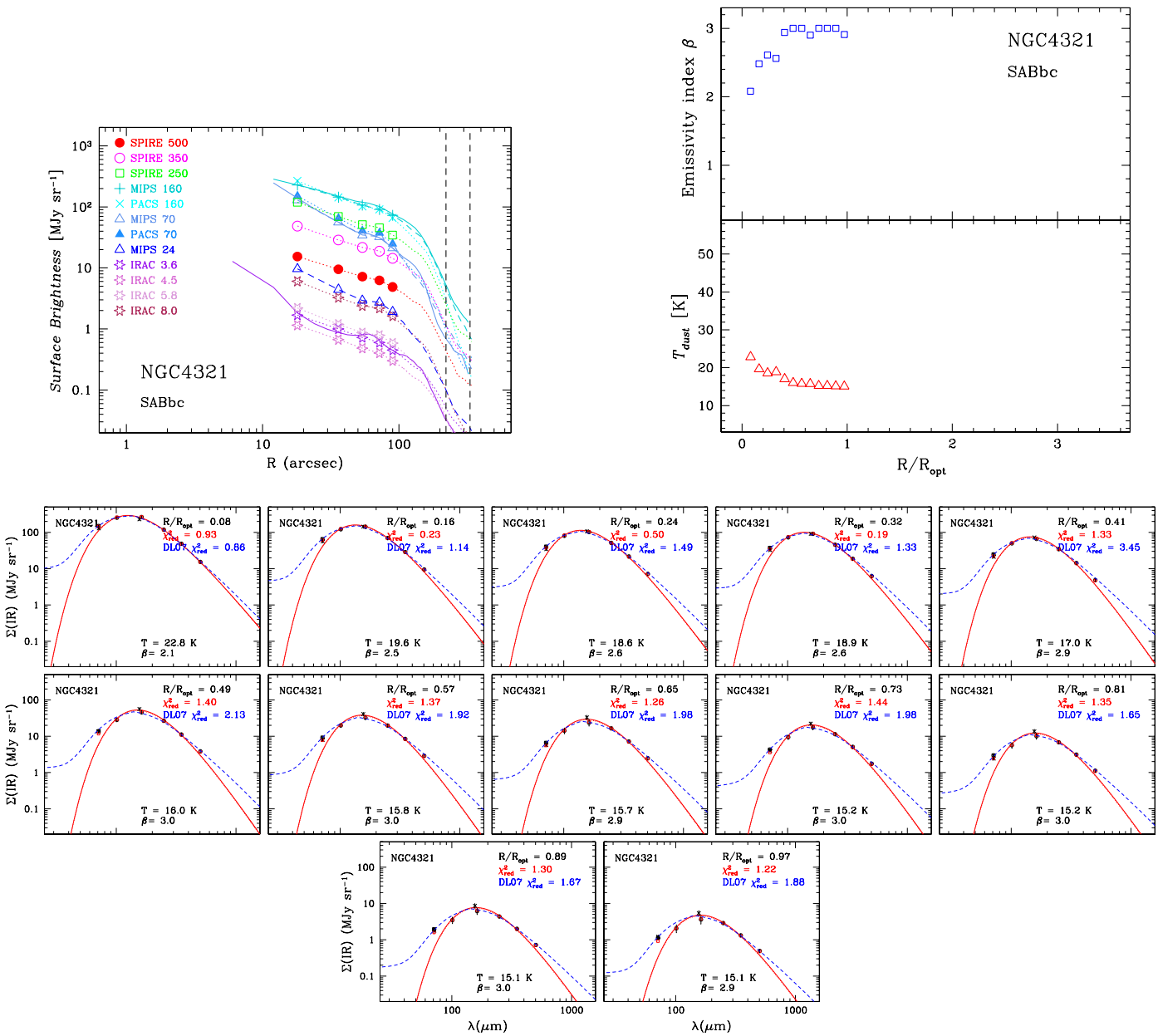

Fig. C.41. *Top left panel*: surface brightness profiles, $\Sigma_{\rm IR}$, for PACS, MIPS, SPIRE, and IRAC 3.6 μm. *Top right panel*: radial temperature trends $T_{\rm dust}$ and emissivity index trends β vs. normalized radii, $R/R_{\rm opt}$. Sets of fluxes are defined over ≥4 wavelengths. The *bottom panels* show each individual SED fit, $\Sigma_{\rm IR}$ vs. wavelength, with best-fit temperature and emissivity index β. The DL07 best-fit models are shown as a (blue) dashed line, and the MBBV fits as a (red) solid one. S/N lower limit = 3.0. The 70 μm (PACS+MIPS) and 500 μm points are excluded from the fits.

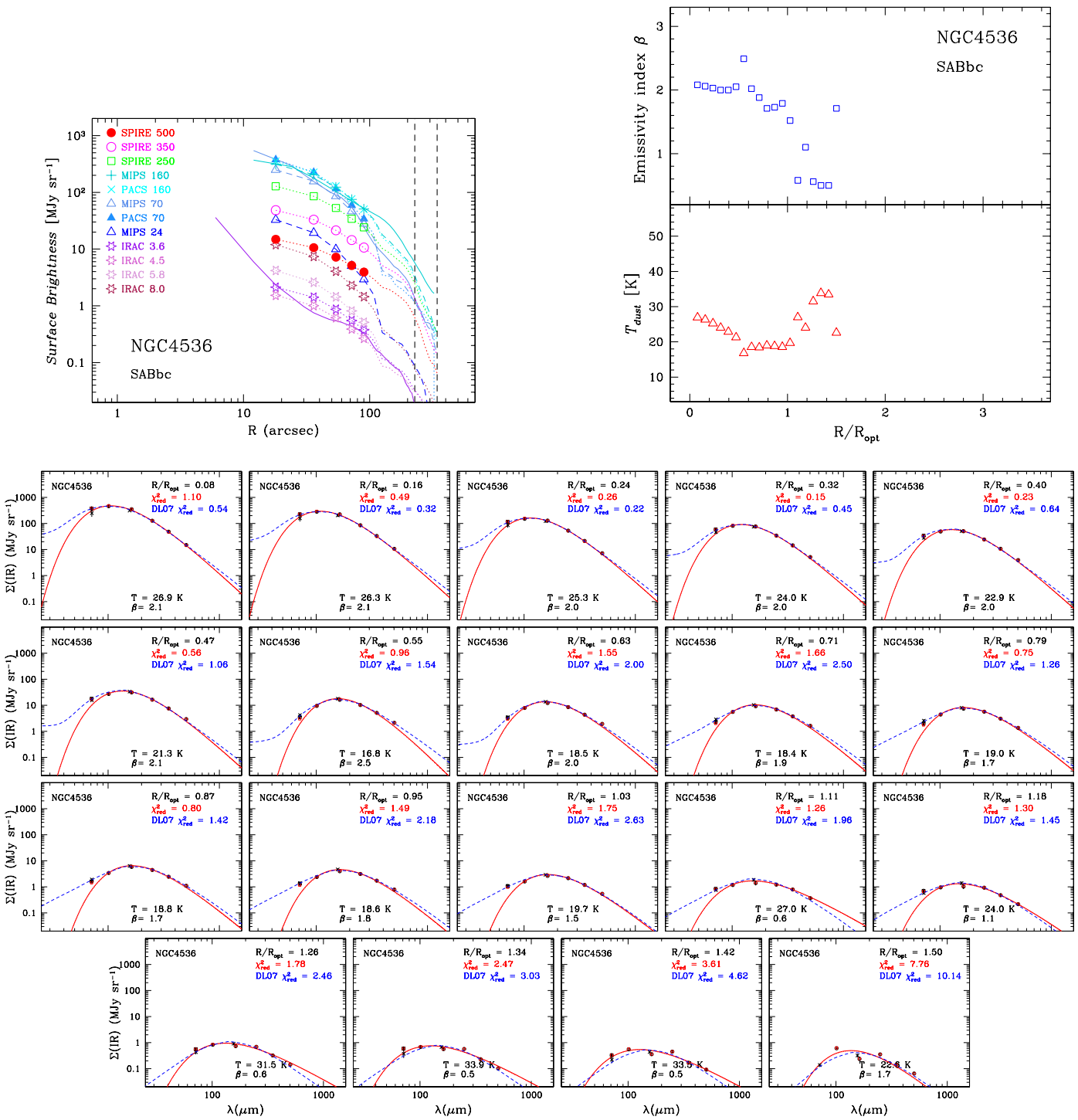

Fig. C.42. *Top left panel*: surface brightness profiles, $\Sigma_{\rm IR}$, for PACS, MIPS, SPIRE, and IRAC 3.6 μm. *Top right panel*: radial temperature trends $T_{\rm dust}$ and emissivity index trends β vs. normalized radii, $R/R_{\rm opt}$. Sets of fluxes are defined over ≥4 wavelengths. The *bottom panels* show each individual SED fit, $\Sigma_{\rm IR}$ vs. wavelength, with best-fit temperature and emissivity index β. The DL07 best-fit models are shown as a (blue) dashed line, and the MBBV fits as a (red) solid one. S/N lower limit = 3.0. The 70 μm (PACS+MIPS) and 500 μm points are excluded from the fits.

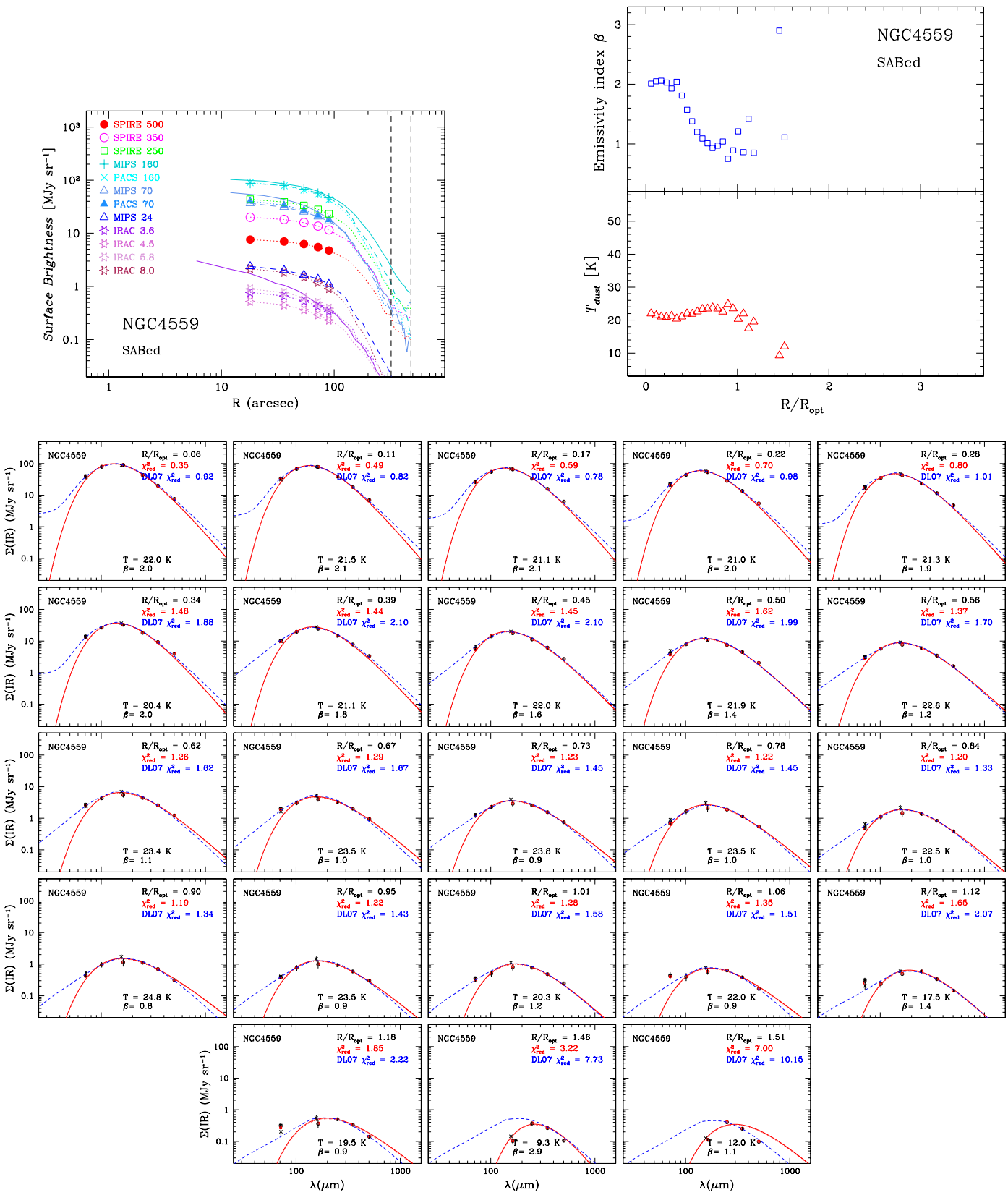

Fig. C.43. *Top left panel*: surface brightness profiles, $\Sigma_{\rm IR}$, for PACS, MIPS, SPIRE, and IRAC 3.6 μm. *Top right panel*: radial temperature trends $T_{\rm dust}$ and emissivity index trends β vs. normalized radii, $R/R_{\rm opt}$. Sets of fluxes are defined over ≥4 wavelengths. The *bottom panels* show each individual SED fit, $\Sigma_{\rm IR}$ vs. wavelength, with best-fit temperature and emissivity index β. The DL07 best-fit models are shown as a (blue) dashed line, and the MBBV fits as a (red) solid one. S/N lower limit = 3.0. The 70 μm (PACS+MIPS) and 500 μm points are excluded from the fits.

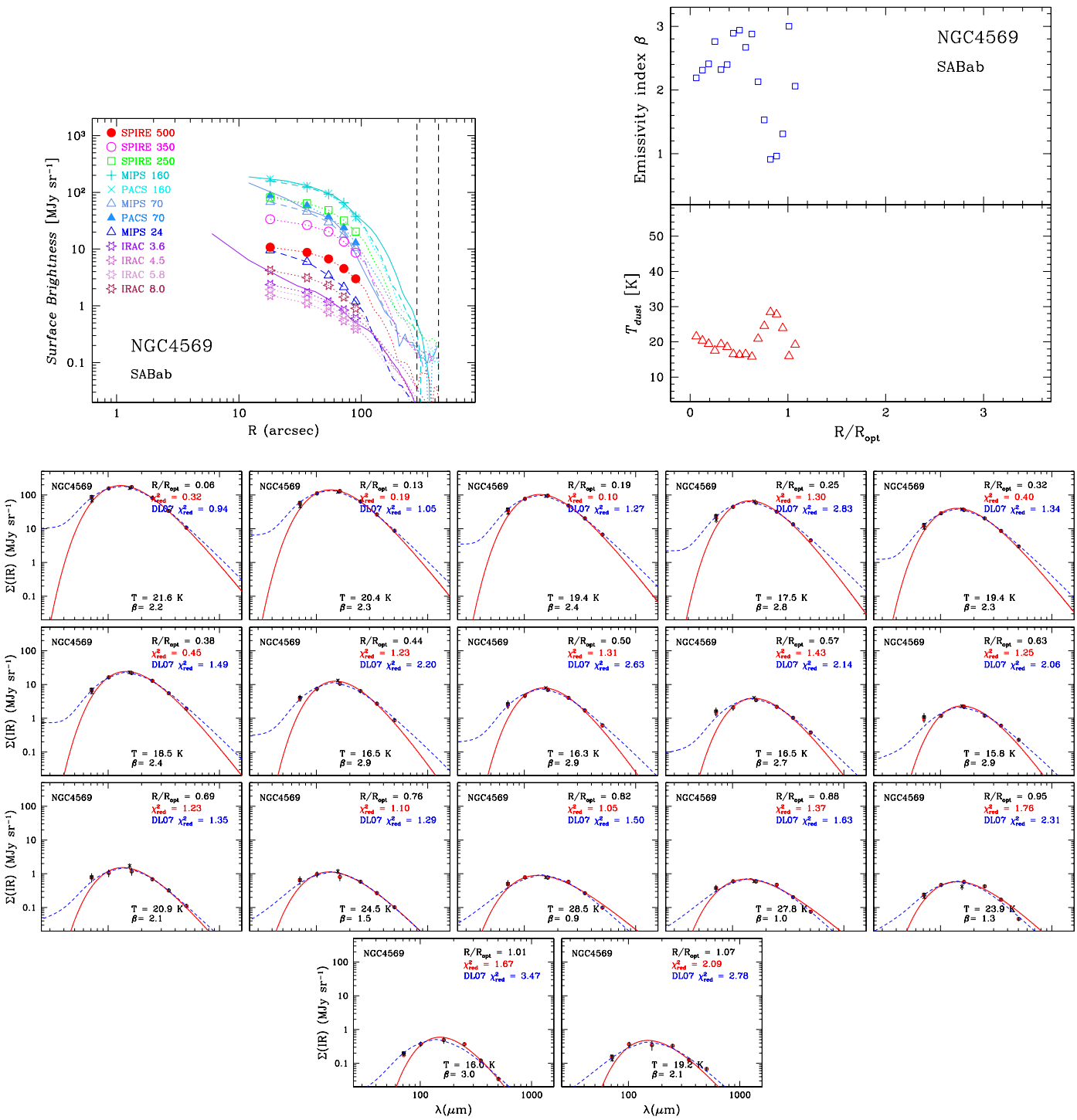

Fig. C.44. *Top left panel*: surface brightness profiles, $\Sigma_{\rm IR}$, for PACS, MIPS, SPIRE, and IRAC 3.6 μm. *Top right panel*: radial temperature trends $T_{\rm dust}$ and emissivity index trends β vs. normalized radii, $R/R_{\rm opt}$. Sets of fluxes are defined over ≥4 wavelengths. The *bottom panels* show each individual SED fit, $\Sigma_{\rm IR}$ vs. wavelength, with best-fit temperature and emissivity index β. The DL07 best-fit models are shown as a (blue) dashed line, and the MBBV fits as a (red) solid one. S/N lower limit = 3.0. The 70 μm (PACS+MIPS) and 500 μm points are excluded from the fits.

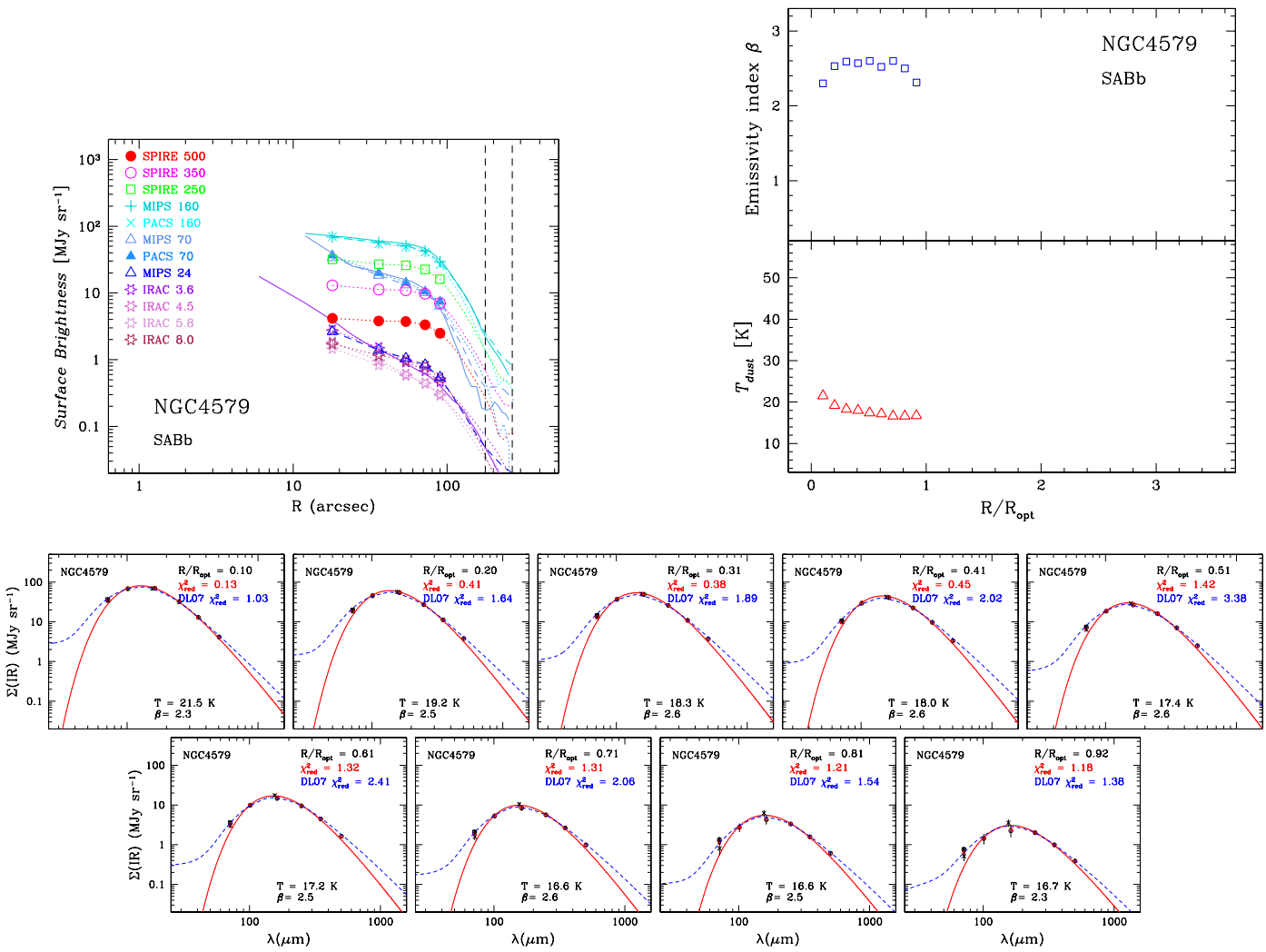

Fig. C.45. *Top left panel*: surface brightness profiles, $\Sigma_{\rm IR}$, for PACS, MIPS, SPIRE, and IRAC 3.6 μm. *Top right panel*: radial temperature trends $T_{\rm dust}$ and emissivity index trends β vs. normalized radii, $R/R_{\rm opt}$. Sets of fluxes are defined over ≥4 wavelengths. The *bottom panels* show each individual SED fit, $\Sigma_{\rm IR}$ vs. wavelength, with best-fit temperature and emissivity index β. The DL07 best-fit models are shown as a (blue) dashed line, and the MBBV fits as a (red) solid one. S/N lower limit = 3.0. The 70 μm (PACS+MIPS) and 500 μm points are excluded from the fits.

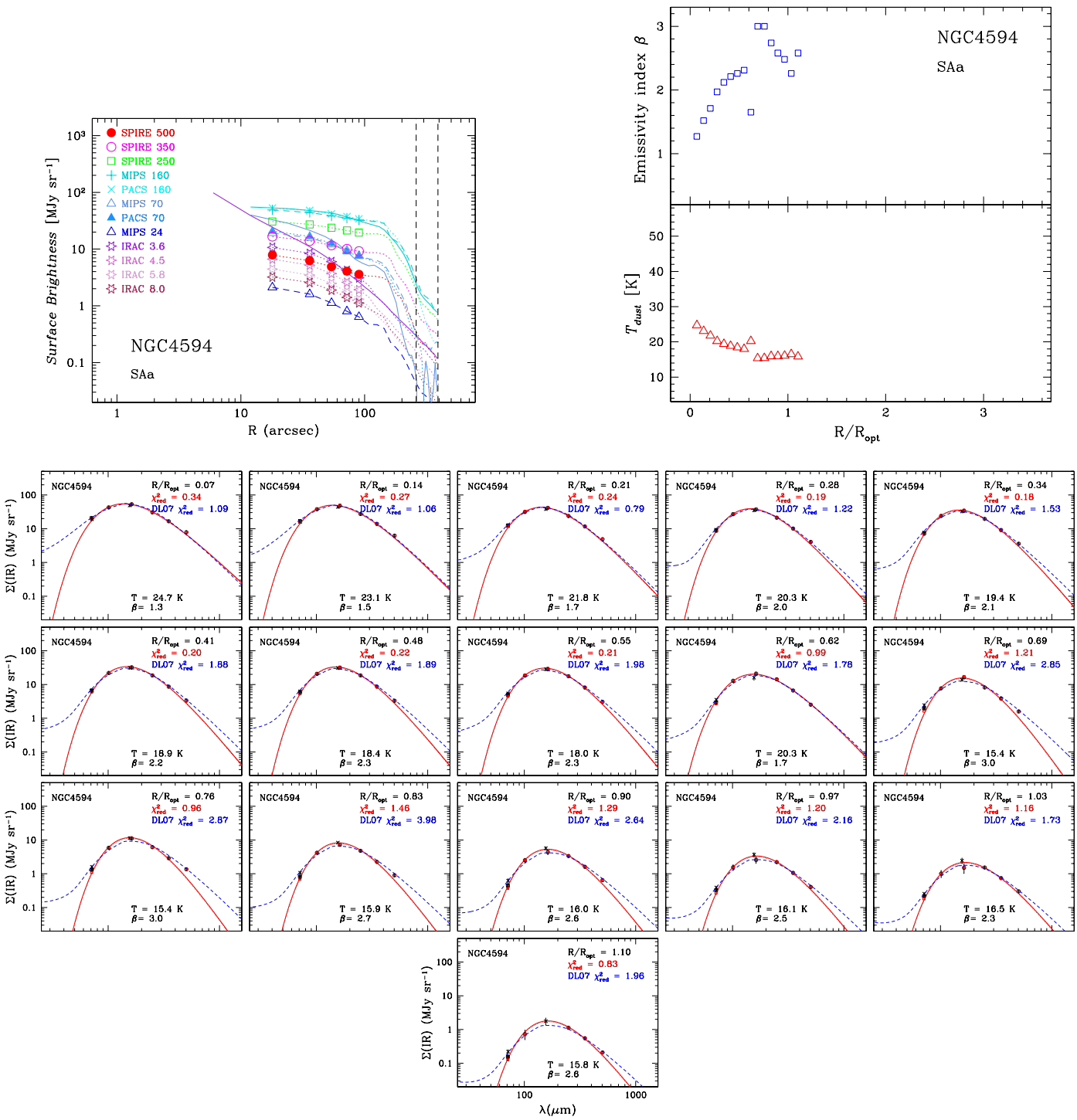

Fig. C.46. *Top left panel*: surface brightness profiles, $\Sigma_{\rm IR}$, for PACS, MIPS, SPIRE, and IRAC 3.6 μm. *Top right panel*: radial temperature trends $T_{\rm dust}$ and emissivity index trends β vs. normalized radii, $R/R_{\rm opt}$. Sets of fluxes are defined over ≥4 wavelengths. The *bottom panels* show each individual SED fit, $\Sigma_{\rm IR}$ vs. wavelength, with best-fit temperature and emissivity index β. The DL07 best-fit models are shown as a (blue) dashed line, and the MBBV fits as a (red) solid one. S/N lower limit = 3.0. The 70 μm (PACS+MIPS) and 500 μm points are excluded from the fits.

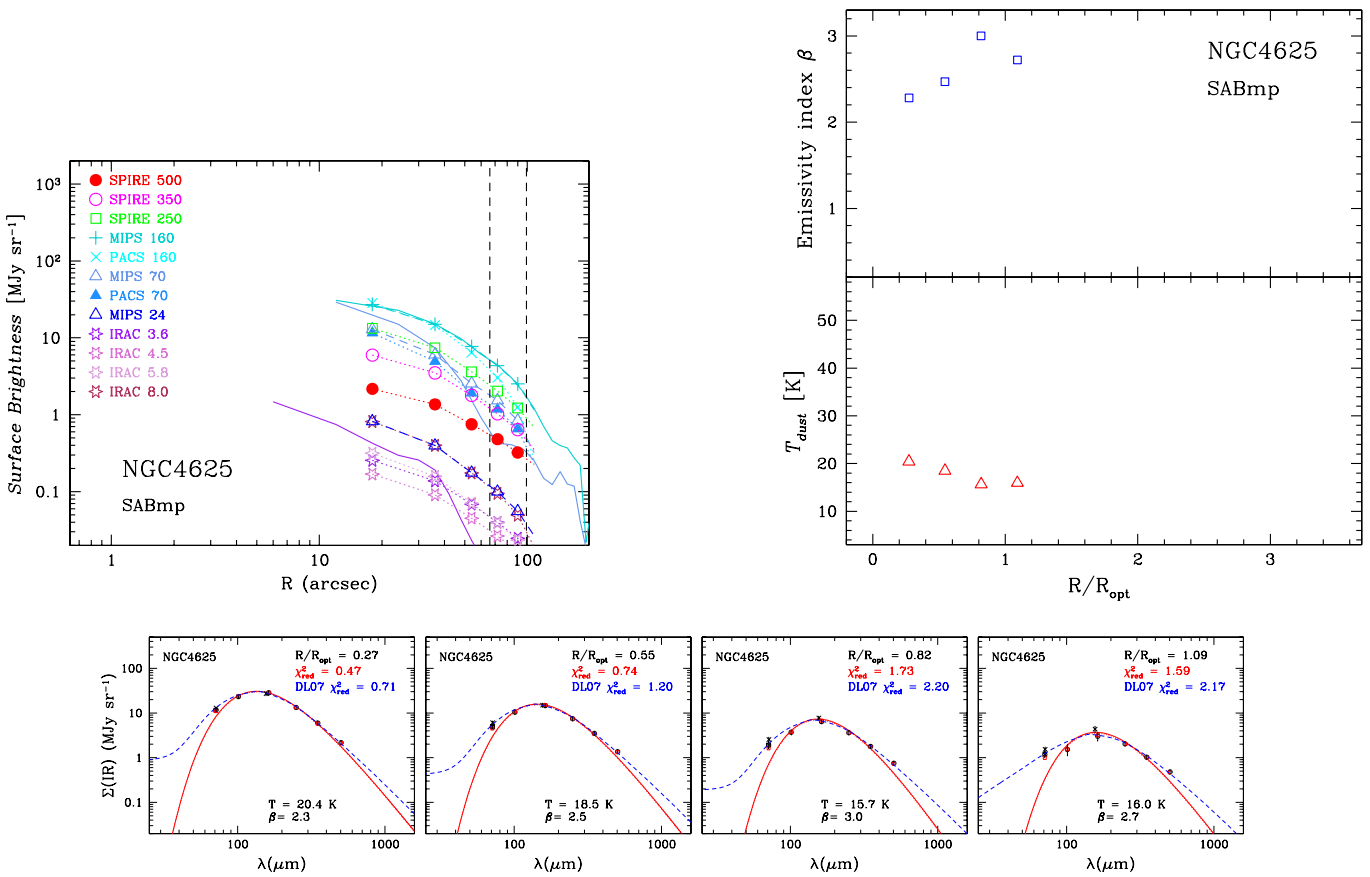

Fig. C.47. *Top left panel*: surface brightness profiles, $\Sigma_{\rm IR}$, for PACS, MIPS, SPIRE, and IRAC 3.6 μm. *Top right panel*: radial temperature trends $T_{\rm dust}$ and emissivity index trends β vs. normalized radii, $R/R_{\rm opt}$. Sets of fluxes are defined over ≥4 wavelengths. The *bottom panels* show each individual SED fit, $\Sigma_{\rm IR}$ vs. wavelength, with best-fit temperature and emissivity index β. The DL07 best-fit models are shown as a (blue) dashed line, and the MBBV fits as a (red) solid one. S/N lower limit = 3.0. The 70 μm (PACS+MIPS) and 500 μm points are excluded from the fits.

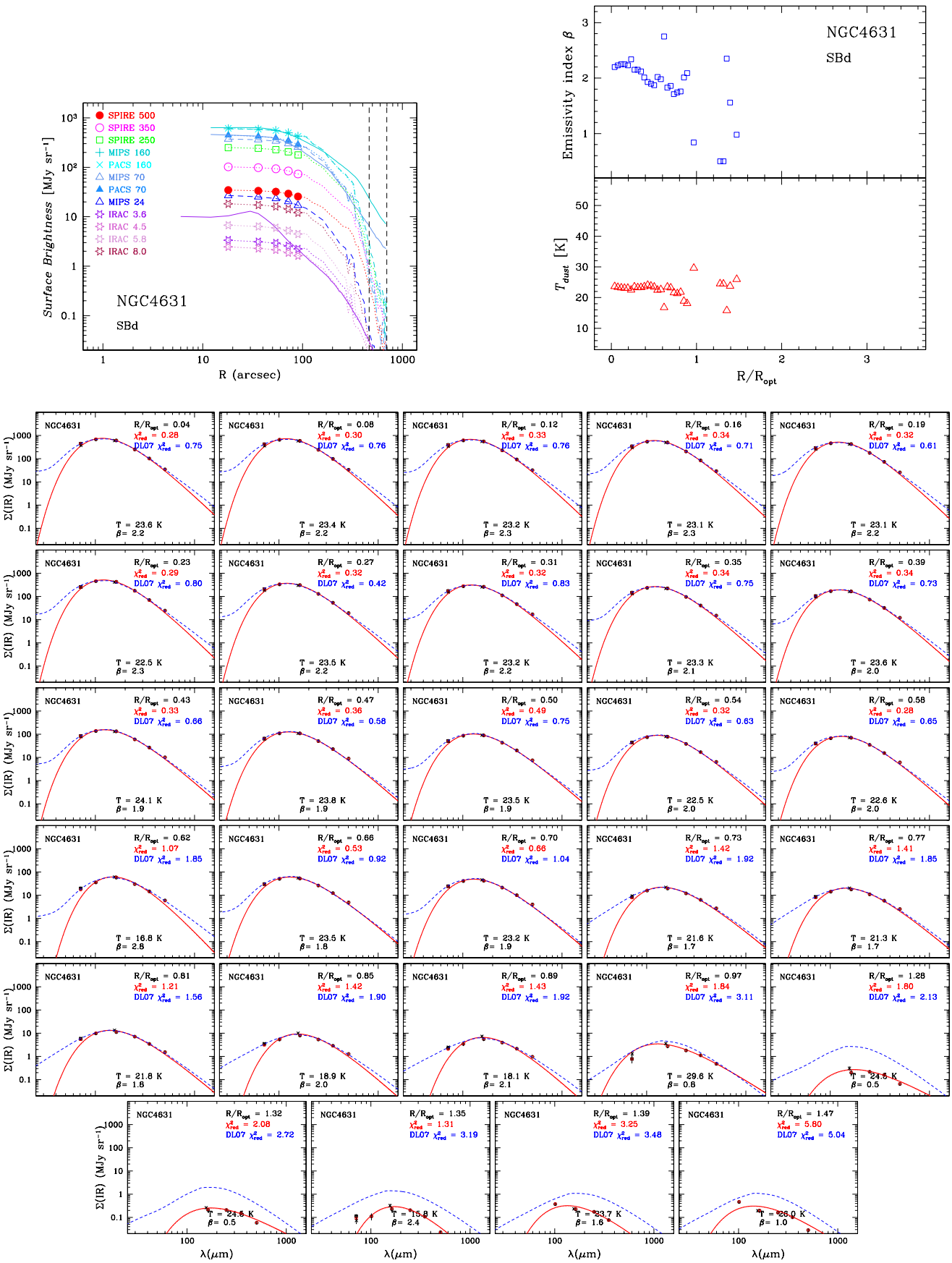

Fig. C.48. *Top left panel*: surface brightness profiles, Σ_{IR}, for PACS, MIPS, SPIRE, and IRAC 3.6 μm. *Top right panel*: radial temperature trends T_{dust} and emissivity index trends β vs. normalized radii, R/R_{opt}. Sets of fluxes are defined over ≥4 wavelengths. The *bottom panels* show each individual SED fit, Σ_{IR} vs. wavelength, with best-fit temperature and emissivity index β. The DL07 best-fit models are shown as a (blue) dashed line, and the MBBV fits as a (red) solid one. S/N lower limit = 3.0. The 70 μm (PACS+MIPS) and 500 μm points are excluded from the fits.

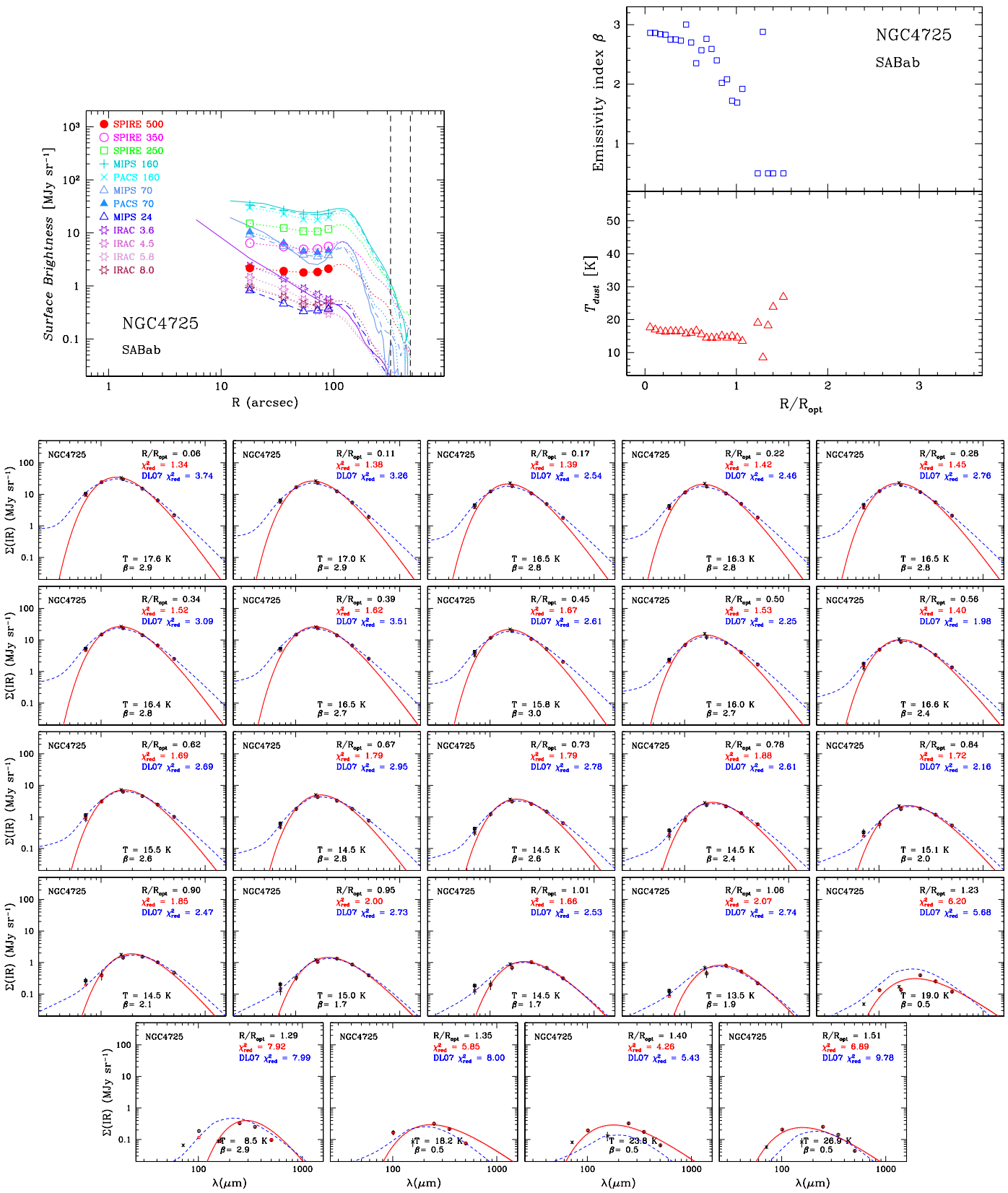

Fig. C.49. *Top left panel*: surface brightness profiles, $\Sigma_{\rm IR}$, for PACS, MIPS, SPIRE, and IRAC 3.6 μm. *Top right panel*: radial temperature trends $T_{\rm dust}$ and emissivity index trends β vs. normalized radii, $R/R_{\rm opt}$. Sets of fluxes are defined over ≥4 wavelengths. The *bottom panels* show each individual SED fit, $\Sigma_{\rm IR}$ vs. wavelength, with best-fit temperature and emissivity index β. The DL07 best-fit models are shown as a (blue) dashed line, and the MBBV fits as a (red) solid one. S/N lower limit = 3.0. The 70 μm (PACS+MIPS) and 500 μm points are excluded from the fits.

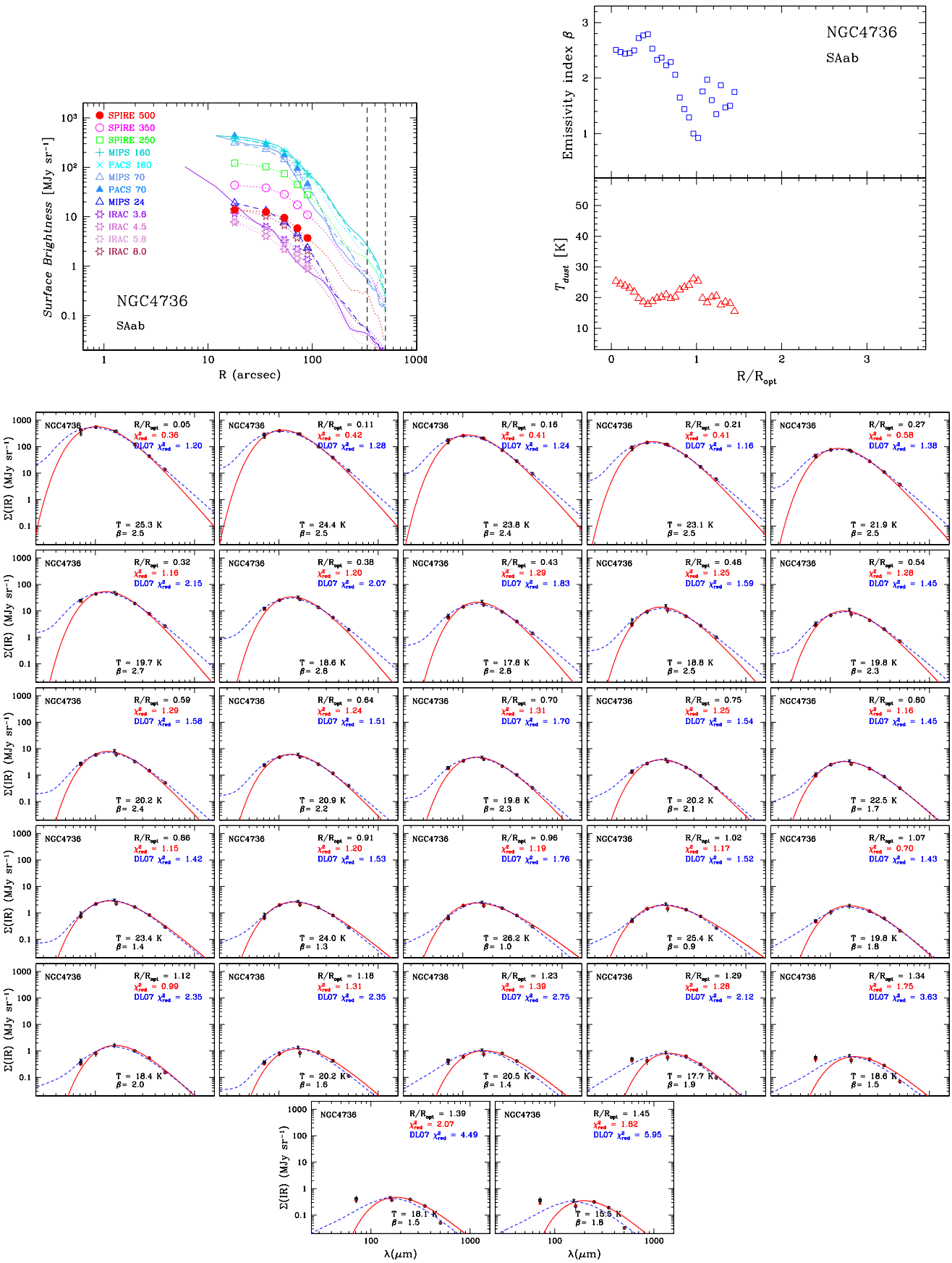

Fig. C.50. *Top left panel*: surface brightness profiles, Σ_{IR}, for PACS, MIPS, SPIRE, and IRAC 3.6 μm. *Top right panel*: radial temperature trends T_{dust} and emissivity index trends β vs. normalized radii, R/R_{opt}. Sets of fluxes are defined over ≥4 wavelengths. The *bottom panels* show each individual SED fit, Σ_{IR} vs. wavelength, with best-fit temperature and emissivity index β. The DL07 best-fit models are shown as a (blue) dashed line, and the MBBV fits as a (red) solid one. S/N lower limit = 3.0. The 70 μm (PACS+MIPS) and 500 μm points are excluded from the fits.

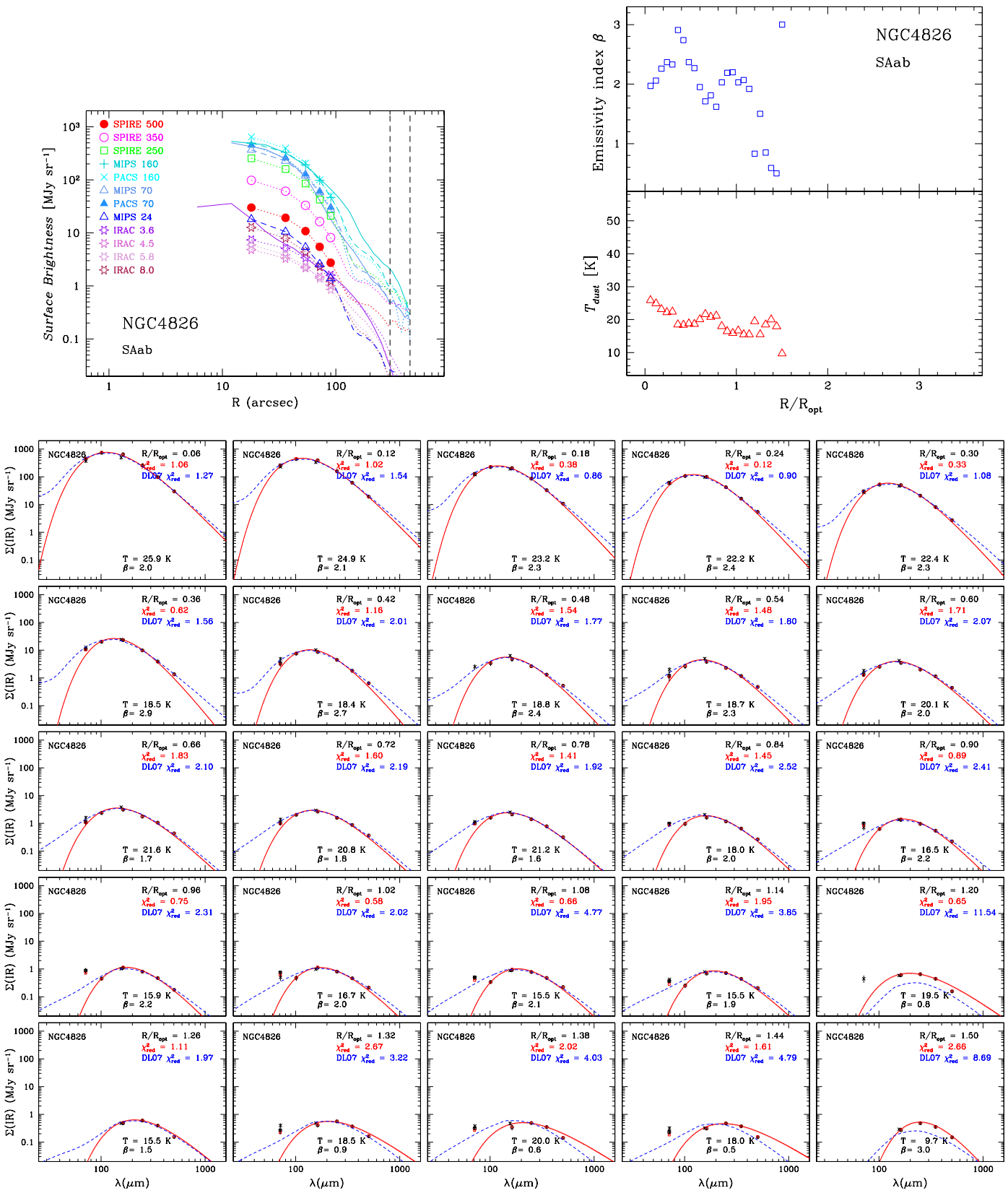

Fig. C.51. *Top left panel*: surface brightness profiles, $\Sigma_{\rm IR}$, for PACS, MIPS, SPIRE, and IRAC 3.6 μm. *Top right panel*: radial temperature trends $T_{\rm dust}$ and emissivity index trends β vs. normalized radii, $R/R_{\rm opt}$. Sets of fluxes are defined over ≥4 wavelengths. The *bottom panels* show each individual SED fit, $\Sigma_{\rm IR}$ vs. wavelength, with best-fit temperature and emissivity index β. The DL07 best-fit models are shown as a (blue) dashed line, and the MBBV fits as a (red) solid one. S/N lower limit = 3.0. The 70 μm (PACS+MIPS) and 500 μm points are excluded from the fits.

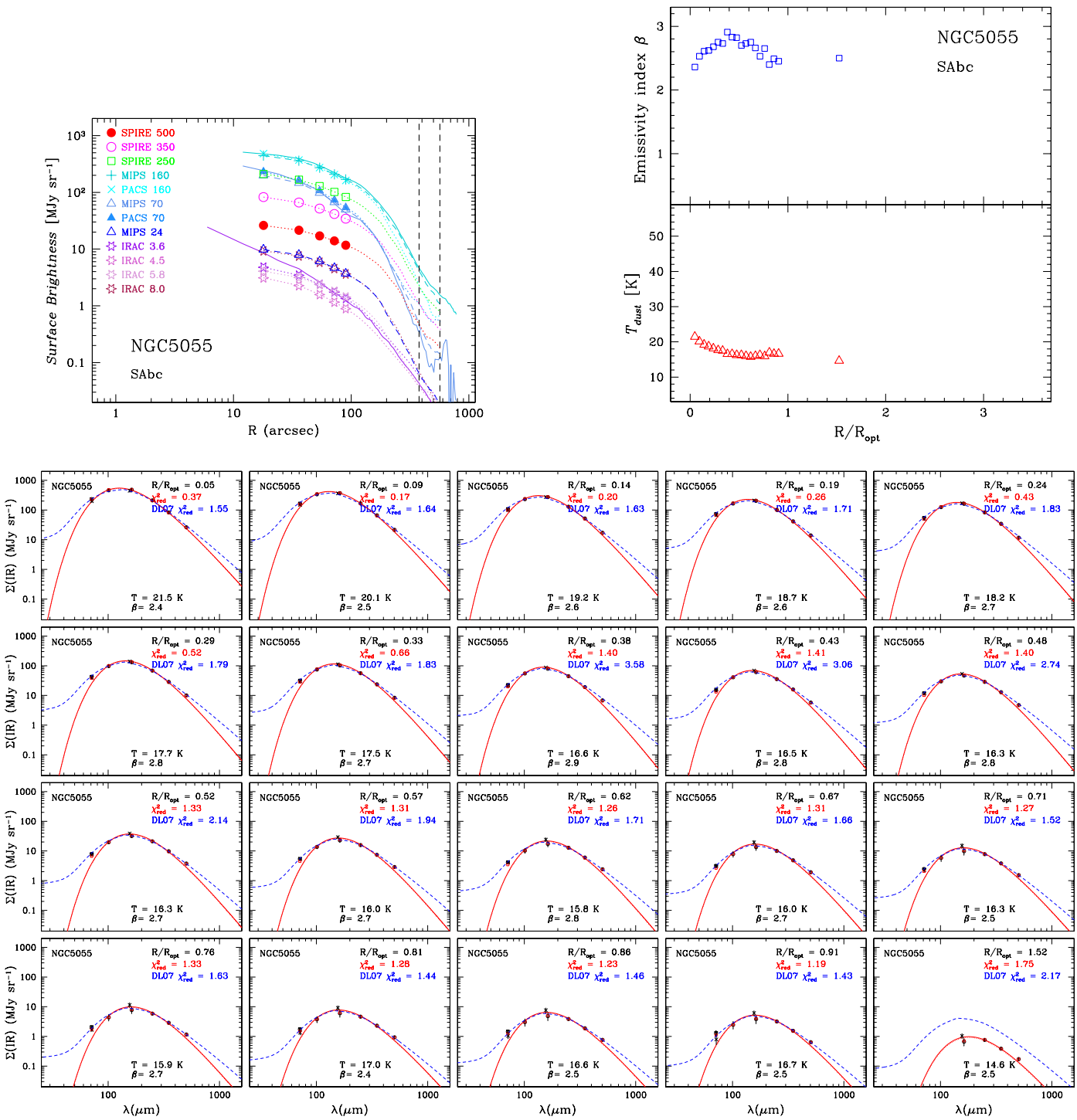

Fig. C.52. *Top left panel*: surface brightness profiles, $\Sigma_{\rm IR}$, for PACS, MIPS, SPIRE, and IRAC 3.6 μm. *Top right panel*: radial temperature trends $T_{\rm dust}$ and emissivity index trends β vs. normalized radii, $R/R_{\rm opt}$. Sets of fluxes are defined over ≥4 wavelengths. The *bottom panels* show each individual SED fit, $\Sigma_{\rm IR}$ vs. wavelength, with best-fit temperature and emissivity index β. The DL07 best-fit models are shown as a (blue) dashed line, and the MBBV fits as a (red) solid one. S/N lower limit = 3.0. The 70 μm (PACS+MIPS) and 500 μm points are excluded from the fits.

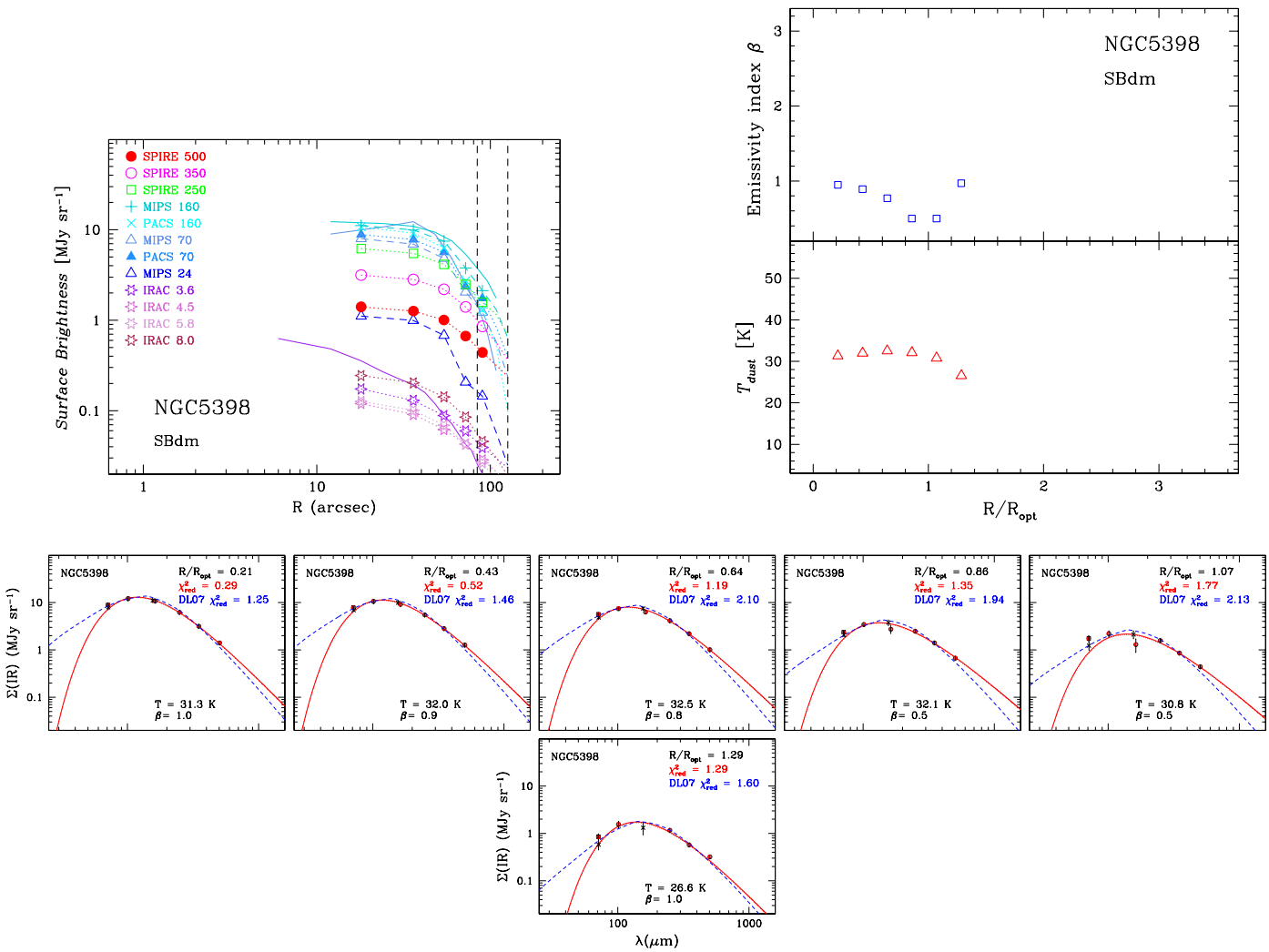

Fig. C.53. *Top left panel*: surface brightness profiles, $\Sigma_{\rm IR}$, for PACS, MIPS, SPIRE, and IRAC 3.6 μm. *Top right panel*: radial temperature trends $T_{\rm dust}$ and emissivity index trends β vs. normalized radii, $R/R_{\rm opt}$. Sets of fluxes are defined over ≥4 wavelengths. The *bottom panels* show each individual SED fit, $\Sigma_{\rm IR}$ vs. wavelength, with best-fit temperature and emissivity index β. The DL07 best-fit models are shown as a (blue) dashed line, and the MBBV fits as a (red) solid one. S/N lower limit = 3.0. The 70 μm (PACS+MIPS) and 500 μm points are excluded from the fits.

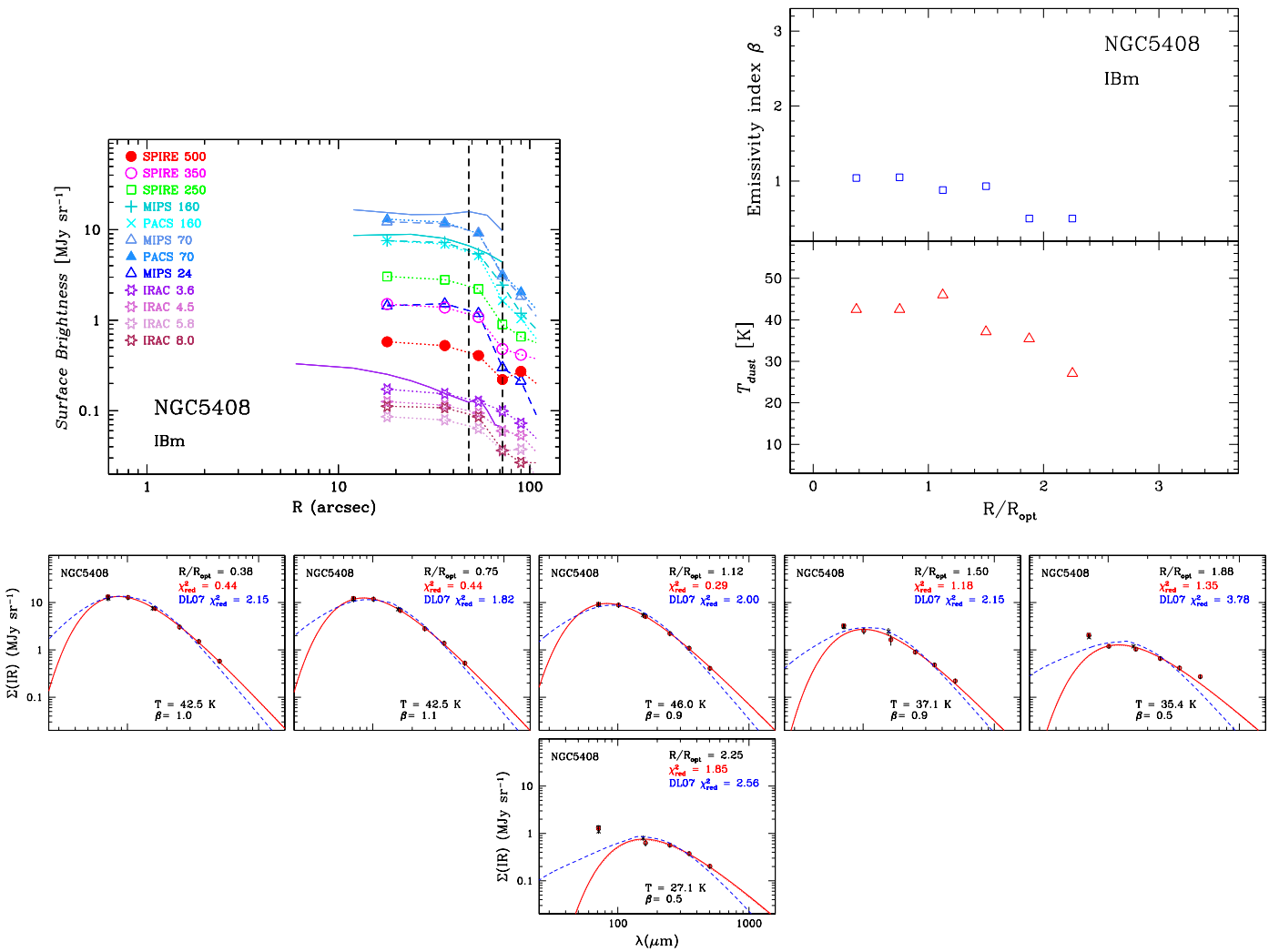

Fig. C.54. *Top left panel*: surface brightness profiles, $\Sigma_{\rm IR}$, for PACS, MIPS, SPIRE, and IRAC 3.6 μm. *Top right panel*: radial temperature trends $T_{\rm dust}$ and emissivity index trends β vs. normalized radii, $R/R_{\rm opt}$. Sets of fluxes are defined over ≥4 wavelengths. The *bottom panels* show each individual SED fit, $\Sigma_{\rm IR}$ vs. wavelength, with best-fit temperature and emissivity index β. The DL07 best-fit models are shown as a (blue) dashed line, and the MBBV fits as a (red) solid one. S/N lower limit = 3.0. The 70 μm (PACS+MIPS) and 500 μm points are excluded from the fits.

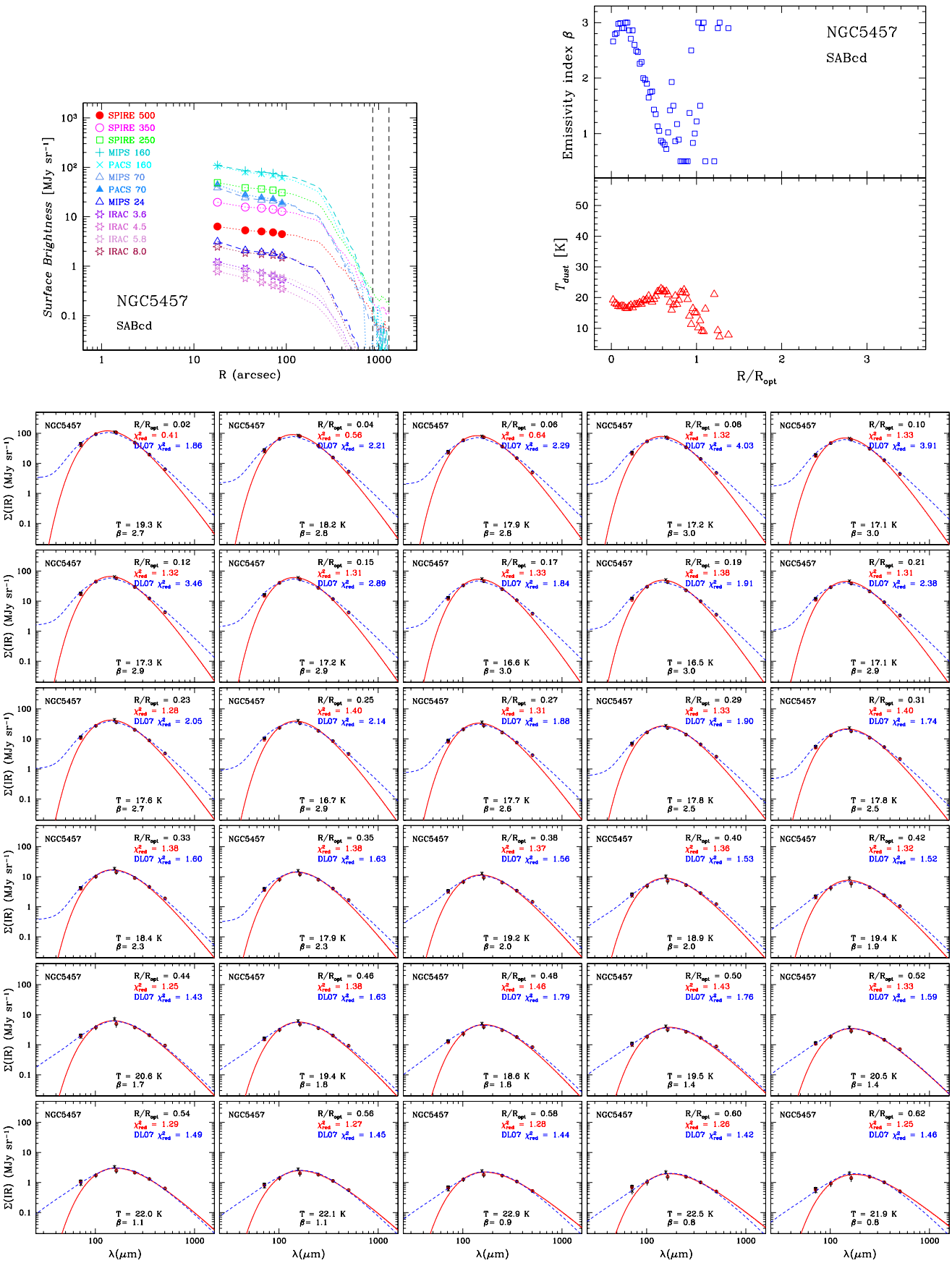

Fig. C.55. *Top left panel*: surface brightness profiles, $\Sigma_{\rm IR}$, for PACS, MIPS, SPIRE, and IRAC 3.6 μm. *Top right panel*: radial temperature trends $T_{\rm dust}$ and emissivity index trends β vs. normalized radii, $R/R_{\rm opt}$. Sets of fluxes are defined over ≥4 wavelengths. The *bottom panels* show each individual SED fit, $\Sigma_{\rm IR}$ vs. wavelength, with best-fit temperature and emissivity index β. The DL07 best-fit models are shown as a (blue) dashed line, and the MBBV fits as a (red) solid one. S/N lower limit = 3.0. The 70 μm (PACS+MIPS) and 500 μm points are excluded from the fits.

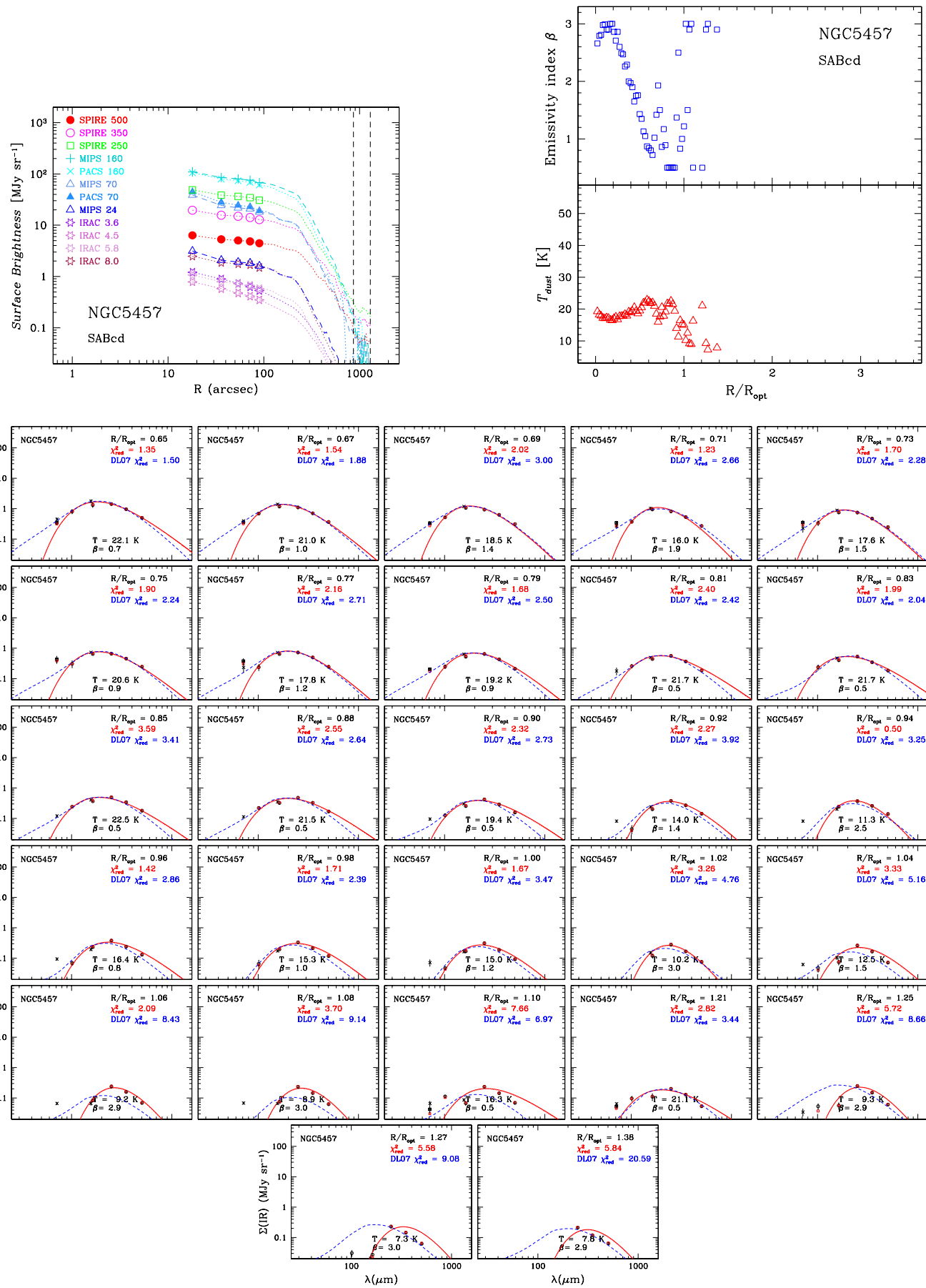

Fig. C.55. continued.

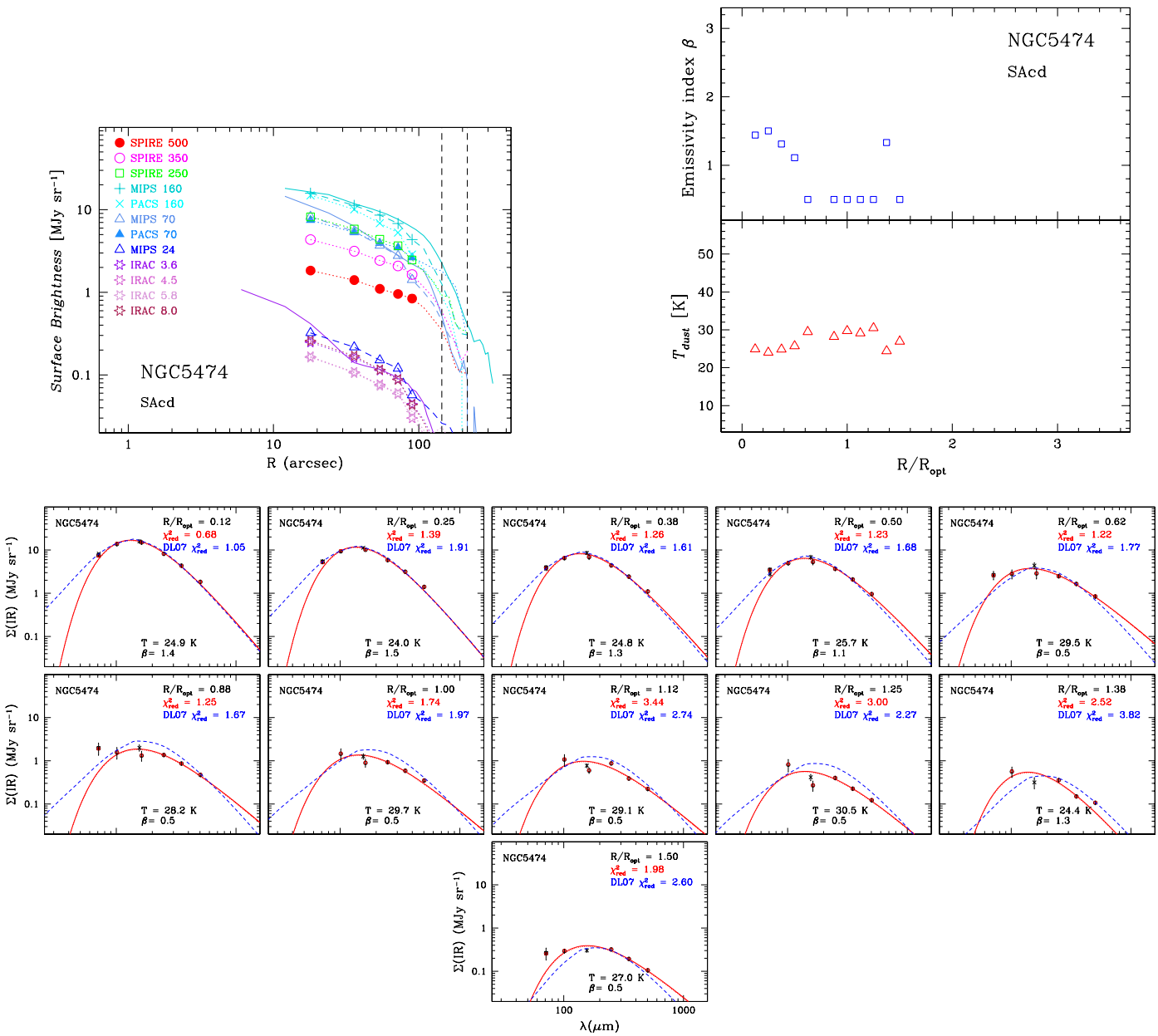

Fig. C.56. *Top left panel*: surface brightness profiles, $\Sigma_{\rm IR}$, for PACS, MIPS, SPIRE, and IRAC 3.6 μm. *Top right panel*: radial temperature trends $T_{\rm dust}$ and emissivity index trends β vs. normalized radii, $R/R_{\rm opt}$. Sets of fluxes are defined over ≥4 wavelengths. The *bottom panels* show each individual SED fit, $\Sigma_{\rm IR}$ vs. wavelength, with best-fit temperature and emissivity index β. The DL07 best-fit models are shown as a (blue) dashed line, and the MBBV fits as a (red) solid one. S/N lower limit = 3.0. The 70 μm (PACS+MIPS) and 500 μm points are excluded from the fits.

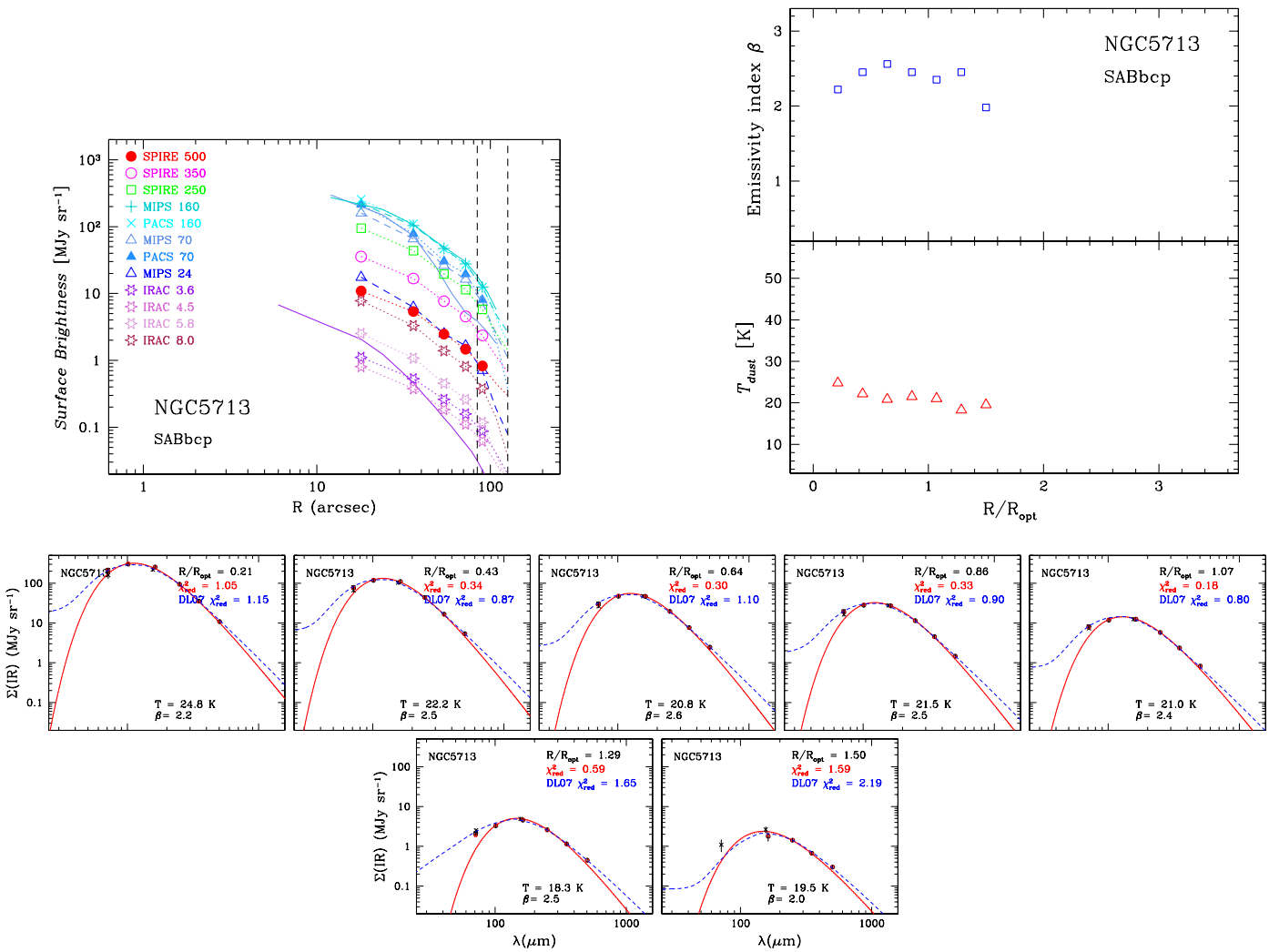

Fig. C.57. *Top left panel*: surface brightness profiles, $\Sigma_{\rm IR}$, for PACS, MIPS, SPIRE, and IRAC 3.6 μm. *Top right panel*: radial temperature trends $T_{\rm dust}$ and emissivity index trends β vs. normalized radii, $R/R_{\rm opt}$. Sets of fluxes are defined over ≥4 wavelengths. The *bottom panels* show each individual SED fit, $\Sigma_{\rm IR}$ vs. wavelength, with best-fit temperature and emissivity index β. The DL07 best-fit models are shown as a (blue) dashed line, and the MBBV fits as a (red) solid one. S/N lower limit = 3.0. The 70 μm (PACS+MIPS) and 500 μm points are excluded from the fits.

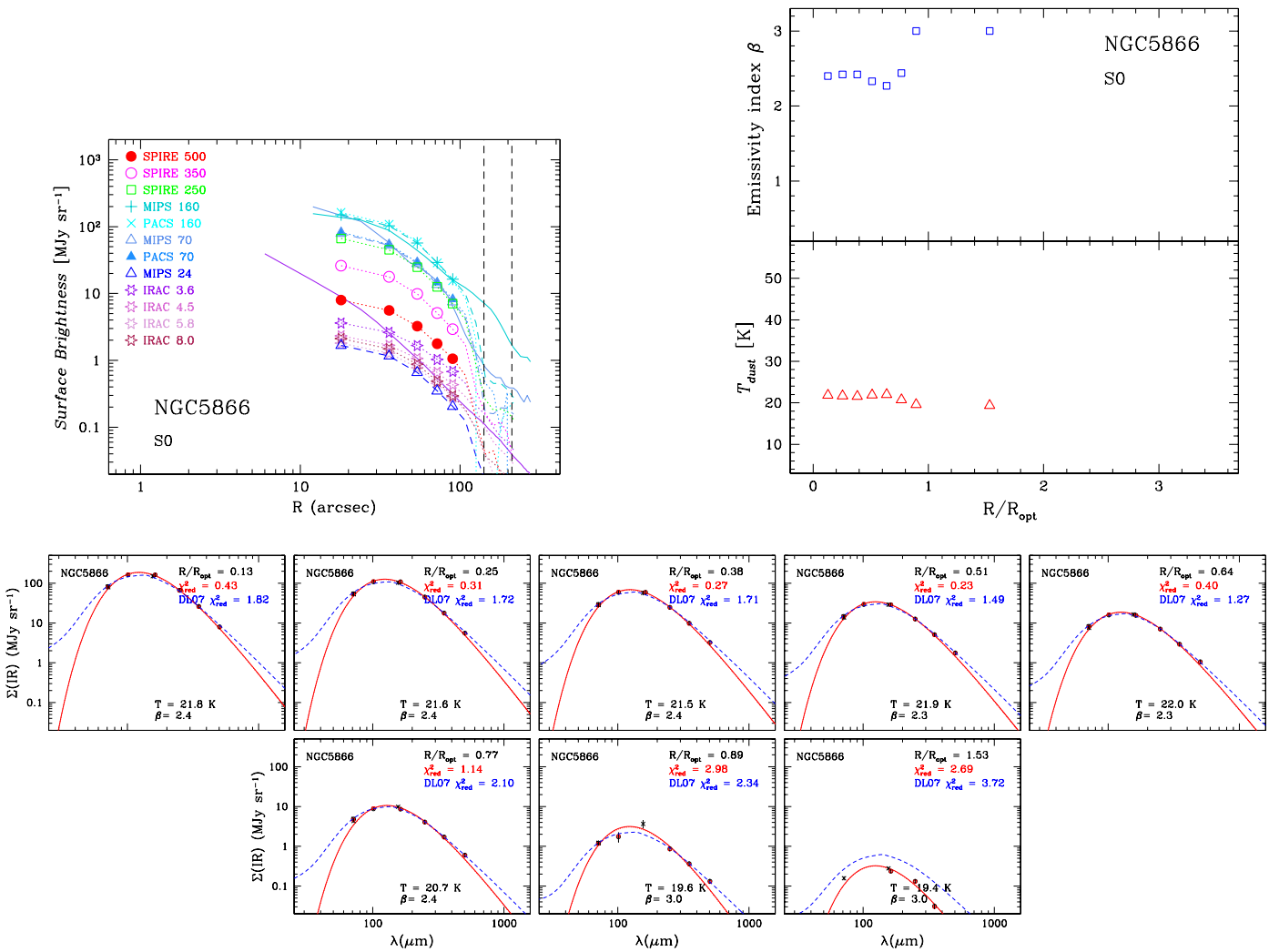

Fig. C.58. *Top left panel*: surface brightness profiles, $\Sigma_{\rm IR}$, for PACS, MIPS, SPIRE, and IRAC 3.6 μm. *Top right panel*: radial temperature trends $T_{\rm dust}$ and emissivity index trends β vs. normalized radii, $R/R_{\rm opt}$. Sets of fluxes are defined over ≥4 wavelengths. The *bottom panels* show each individual SED fit, $\Sigma_{\rm IR}$ vs. wavelength, with best-fit temperature and emissivity index β. The DL07 best-fit models are shown as a (blue) dashed line, and the MBBV fits as a (red) solid one. S/N lower limit = 3.0. The 70 μm (PACS+MIPS) and 500 μm points are excluded from the fits.

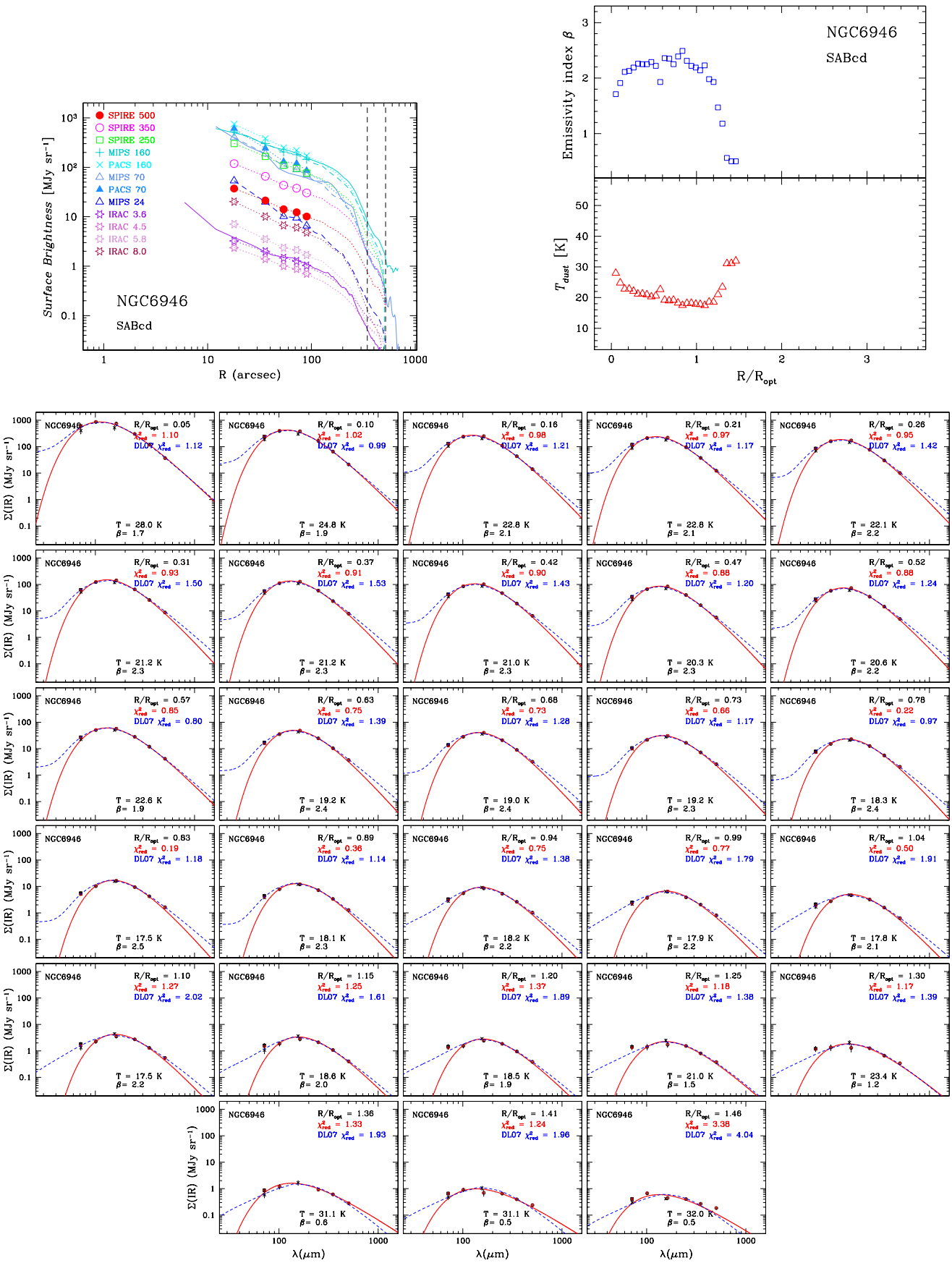

Fig. C.59. *Top left panel*: surface brightness profiles, $\Sigma_{\rm IR}$, for PACS, MIPS, SPIRE, and IRAC 3.6 μm. *Top right panel*: radial temperature trends $T_{\rm dust}$ and emissivity index trends β vs. normalized radii, $R/R_{\rm opt}$. Sets of fluxes are defined over ≥4 wavelengths. The *bottom panels* show each individual SED fit, $\Sigma_{\rm IR}$ vs. wavelength, with best-fit temperature and emissivity index β. The DL07 best-fit models are shown as a (blue) dashed line, and the MBBV fits as a (red) solid one. S/N lower limit = 3.0. The 70 μm (PACS+MIPS) and 500 μm points are excluded from the fits.

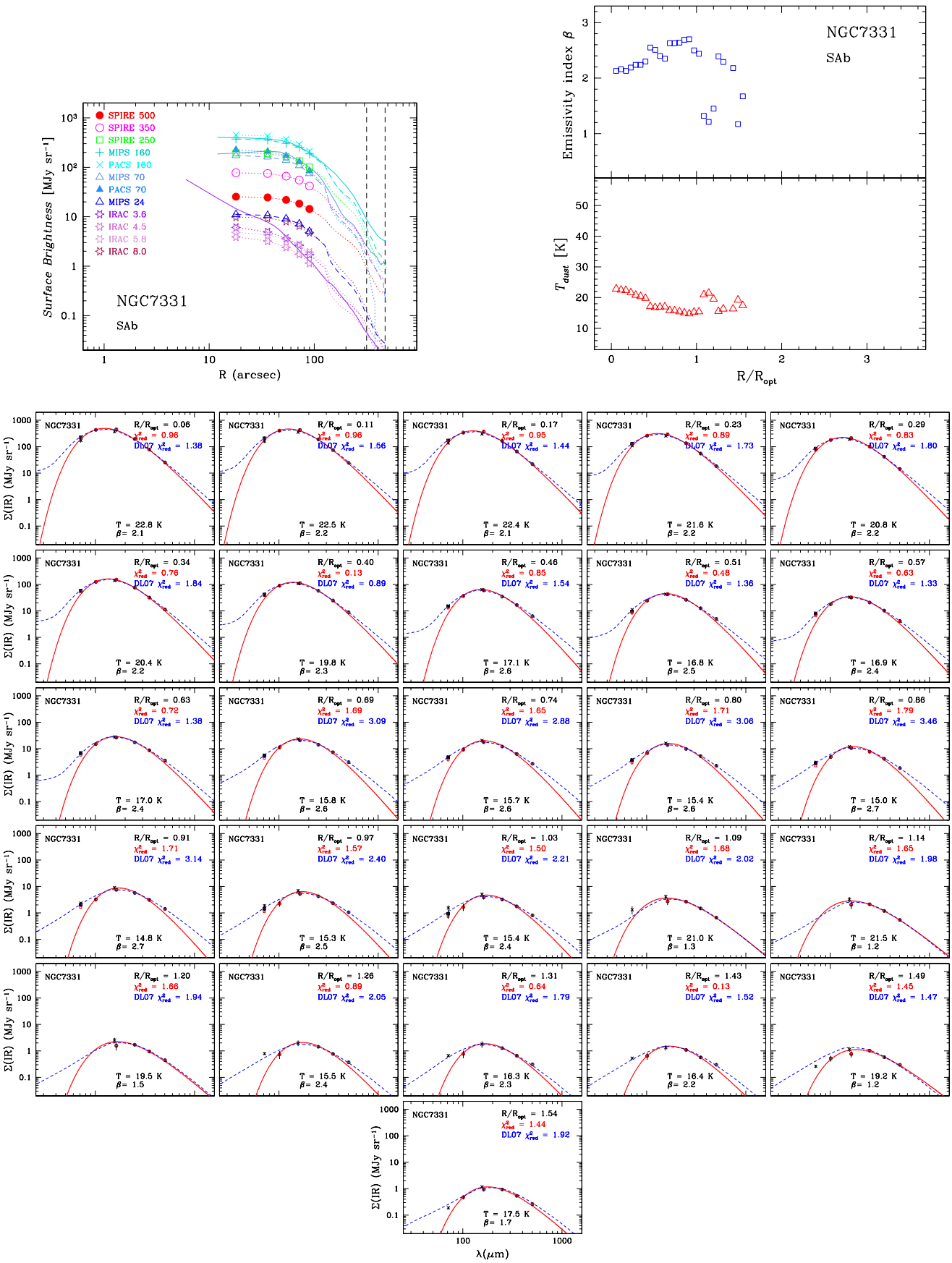

Fig. C.60. *Top left panel*: surface brightness profiles, $\Sigma_{\rm IR}$, for PACS, MIPS, SPIRE, and IRAC 3.6 μm. *Top right panel*: radial temperature trends $T_{\rm dust}$ and emissivity index trends β vs. normalized radii, $R/R_{\rm opt}$. Sets of fluxes are defined over ≥4 wavelengths. The *bottom panels* show each individual SED fit, $\Sigma_{\rm IR}$ vs. wavelength, with best-fit temperature and emissivity index β. The DL07 best-fit models are shown as a (blue) dashed line, and the MBBV fits as a (red) solid one. S/N lower limit = 3.0. The 70 μm (PACS+MIPS) and 500 μm points are excluded from the fits.

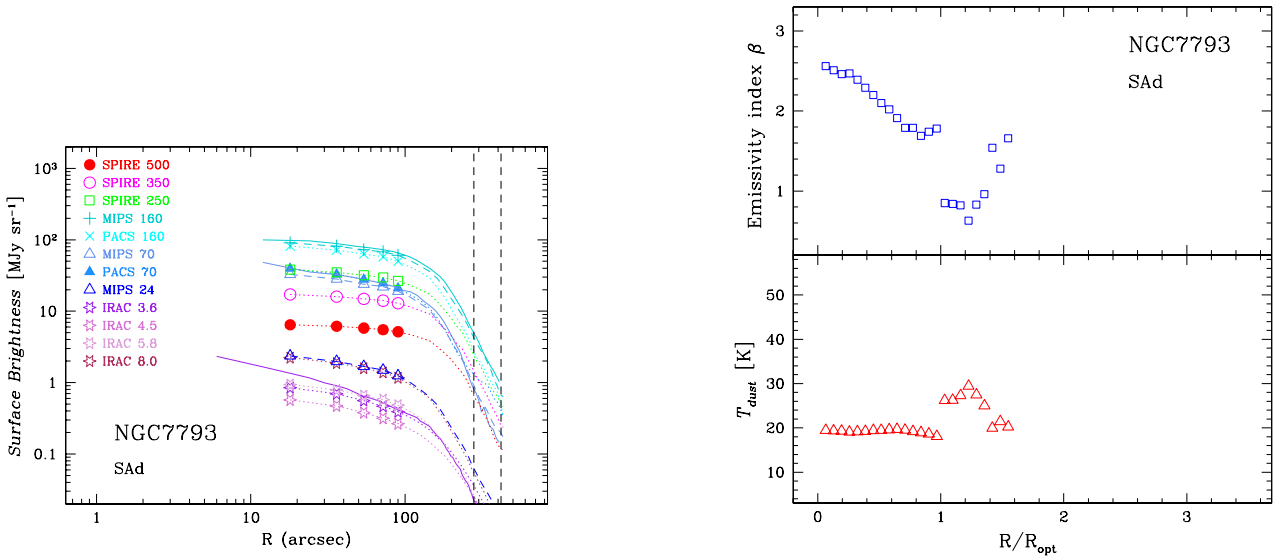

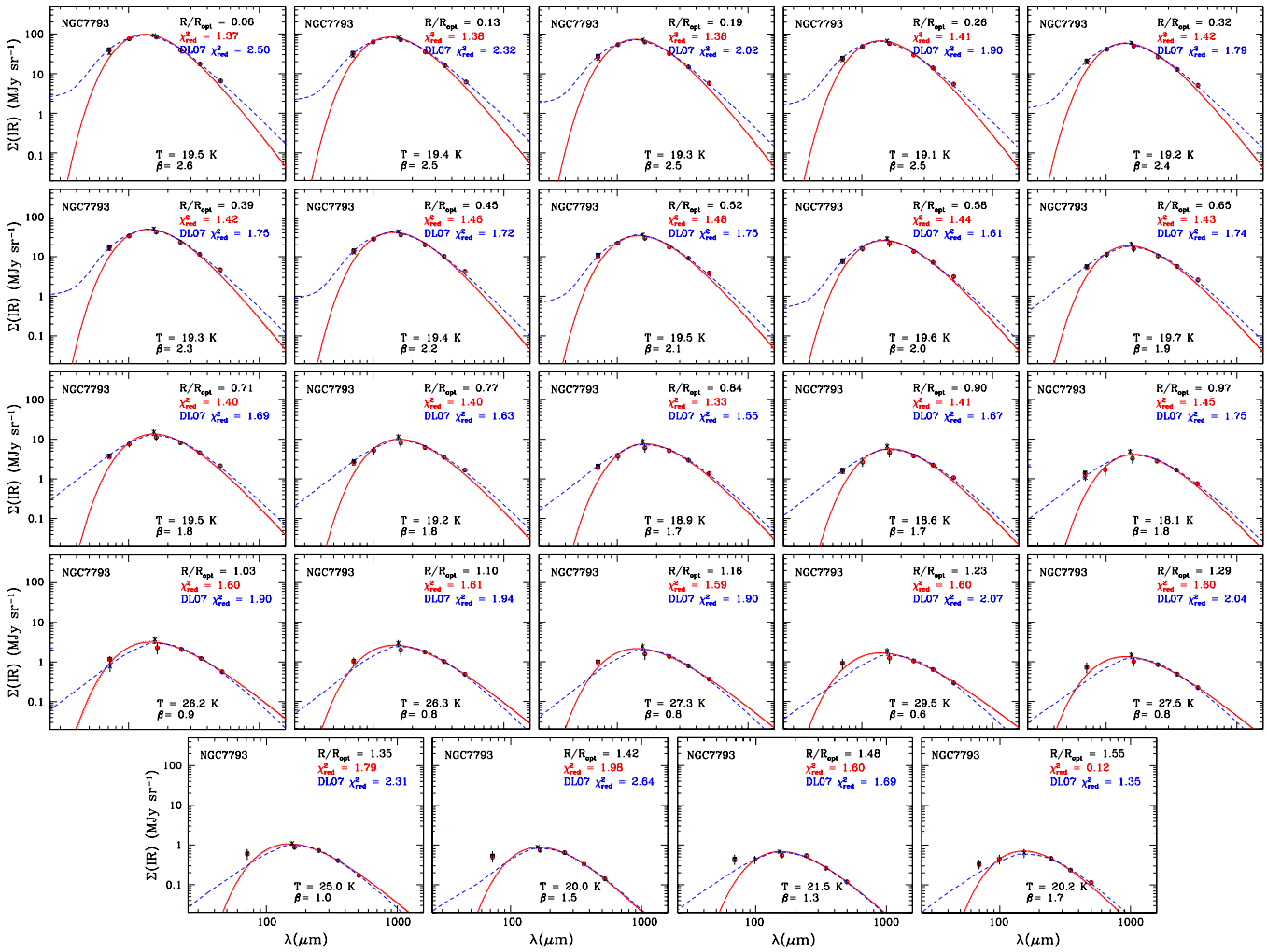

Fig. C.61. *Top left panel*: surface brightness profiles, $\Sigma_{\rm IR}$, for PACS, MIPS, SPIRE, and IRAC 3.6 μm. *Top right panel*: radial temperature trends $T_{\rm dust}$ and emissivity index trends β vs. normalized radii, $R/R_{\rm opt}$. Sets of fluxes are defined over ≥4 wavelengths. The *bottom panels* show each individual SED fit, $\Sigma_{\rm IR}$ vs. wavelength, with best-fit temperature and emissivity index β. The DL07 best-fit models are shown as a (blue) dashed line, and the MBBV fits as a (red) solid one. S/N lower limit = 3.0. The 70 μm (PACS+MIPS) and 500 μm points are excluded from the fits.